UNIVERSIDADE D
COIMBRA

Marta Silva Lapo Pais

Machine Learning Classification in Alzheimer's Disease Based on ^{11}C-Pittsburgh Compound B (PiB) and ^{11}C-(R)-PK11195 (Pk) Pet Imaging Measures and the Correlation Between these two Biomarkers

Thesis submitted to the
University of Coimbra for the degree of
Master in Biomedical Engineering

Supervisors:
Prof. Dr. Miguel Castelo Branco (CIBIT, ICNAS/UC)
Prof. Dr. Francisco Caramelo (IBILI/UC)

Coimbra, 2019

University of Coimbra

Faculty of Sciences and Technology

Master's Degree in Biomedical Engineering

Dissertation

Final Report

Machine Learning Classification in Alzheimer's disease based on ^{11}C-Pittsburgh Compound B (PiB) and ^{11}C-(R)-PK11195 (PK) PET imaging measures and the correlation between these two biomarkers

Marta Lapo Pais

Supervisors:

Prof. Dr. Miguel Castelo Branco (CIBIT, ICNAS/UC)

Prof. Dr. Francisco Caramelo (IBILI/UC)

Coimbra, 2019

1 2 9 0

UNIVERSIDADE D
COIMBRA

This project was developed in collaboration with:

Institute of Nuclear Sciences Applied to Health

Coimbra Institute for Biomedical Imaging and Translational Research

Coimbra Institute for Clinical and Biomedical Research

This project was financial supported by:

Fundação para a Ciência e a Tecnologia

Santa Casa da Misericórdia de Lisboa (Neuroscience Mantero Belard Prize 2015)

ACKNOWLEDGEMENTS

Agradeço em Português, numa língua que me diz muito e onde consigo, mais facilmente, transparecer o que sinto através das palavras que escrevo.

Quero começar por agradecer ao Professor Miguel Castelo Branco por me despertar o gosto pelas neurociências nas aulas teóricas de Visão Computacional e Perceção Biológica. Por me desafiar a fazer este projeto, orientar e confiar nas minhas capacidades, desde o primeiro dia.

Ao Engenheiro Caramelo pelo esclarecimento de todas as dúvidas de última hora e por me colocar questões pertinentes e mostrar outros pontos de vista que foram essenciais para a consolidação de conceitos e para as conclusões finais deste projeto.

Ao Engenheiro Castelhano pela constante disponibilidade e simpatia. Foi a pessoa que recorri no início deste percurso. Um início difícil, onde comecei por duvidar das minhas capacidades. Ensinou-me as bases, auxiliou-me em todas as questões que fui tendo e, acima de tudo, transmitiu-me tranquilidade e segurança pelo o que ia fazendo. E ao restante pessoal do ICNAS que generosamente partilharam o seu conhecimento comigo.

Aos meus amigos, que tiveram uma das tarefas mais difíceis, desligar-me do trabalho. Obrigada por fazerem questão de eu estar presente, por nunca se esquecerem de mim e por me fazerem sentir tão bem, tal e qual como eu sou.

A ti Madrinha. Sem ti nada disto teria sido possível. Obrigada por, mesmo a quilómetros de distância, estares sempre presente. Por me leres e releres a tese vezes e vezes sem conta, por todas as críticas construtivas e pelas palavras de apoio nos momentos de maior insegurança.

Aos meus pais, que, por serem tão diferentes, se complementam tanto. A ti mãe por toda a ajuda psicológica. Pelas tuas chamadas nos momentos mais difíceis. Por estares sempre presente. A ti pai pela tua descontração e calma contagiante. Pela tua prontidão. Sei que te tenho à distância de uma chamada. A vocês os dois por todo o amor e carinho que me deram ao longo destes anos. Por sempre acreditarem nas minhas capacidades. Por todos os valores de humildade, justiça e trabalho. Por me fazerem sonhar sempre mais alto.

Por fim, a ti. Por estares sempre lá, desde, literalmente, o primeiro dia das nossas vidas. Quando olhas para mim sinto-me capaz de tudo. Olha-me nos olhos e vai correr tudo bem.

My father suffered from dementia in the last years of his life, but continued to play guitar. On a visit home I gave him some guitar versions of the Bach cello suites, which he would play for hours a day. On a return visit, he told me that he thought this guy Bach was terrific. I realized that with his memory going, he was rediscovering Bach every day, which was the one consoling consequence of such a horrible condition.

- Martin Chalfie, awarded the 2008 Chemistry Prize

ABSTRACT

Alzheimer's disease (AD) is one of the main neurodegenerative disorders causing dementia. Positron emission tomography (PET) neuroimaging with ^{11}C-Pittsburgh Compound B (PiB) and ^{11}C-(R)-PK11195 (PK) are two of the existing modalities to assess amyloid plaque and activated microglia in human brain, respectively. Since amyloid plaque is the main hallmark of AD and activated microglia is currently found in the brain of AD patients, these imaging biomarkers can be used in diagnostic workup and to achieve early AD diagnosis.

The main goal of the present study is to solve a binary classification problem between healthy controls (HC) and AD patients, by using machine learning (ML) methods based on two PET imaging biomarkers, PiB and PK. Another important goal of this work includes the identification of the brain regions where PiB and PK are most correlated, at both regional and voxel level.

In the present study it was included 41 subjects (20 AD and 21 HC). To understand the impact of the time interval considered in PET image acquisition, the dataset was split in three different groups. Group TOT composed by PiB PET images acquired during the total time of PiB biodistribution, and groups 4070 and 4060, acquired during the characteristic accumulation time of PiB and PK, between minute 40 and 70, and 40 and 60, after administration, respectively. After quantification, pre-processing, feature extraction and selection, PiB and PK PET images were submitted to classification using a support vector machines (SVM) approach. Voxel-wise comparison between AD and HC groups of different quantified PK PET images were performed to understand the impact of distinct reference regions in the normalization of PK PET images and the influence of the quantification method used. Also, voxel-wise and region of interest (ROI) based correlation between standard uptake value ratio (SUVr) PiB and different quantified PK PET images were calculated.

Normalization by cerebellum of PiB PET images of group 4070 yielded the best classification accuracy of AD (accuracy-0.925, sensitivity-1.000, specificity-0.857). Thus, for PiB PET images, cerebellum appears to be the brain region where amyloid accumulation bears the least differences between HC and AD patients, i.e., the best reference region to do the normalization. Also, when using the cerebellum as reference region of PiB PET images, stronger ROI-based correlation with binding

potential (BP) PK PET images in several brain regions was found, compared to normalization based on white matter. Features extracted at regional level from PK PET images did not show improvement, neither in accuracy nor in sensitivity, of the classifier only based on features extracted from PiB PET images. ROI-based correlation results suggest specific binding of PK to cerebellum; thus, supervised cluster analysis algorithm based on four kinetic classes (SVCA4) showed to be the best approach to do the normalization of PK PET images. Both types of quantified PK PET images did not show relevant differences between groups at voxel level. This suggests that PK biodistribution in the brain is not relevant for group differentiation. The reason why is probably related to the fact that activated microglia is associated with neuroinflammation, and this process is quite variable across participants, i.e., it is randomly distributed across brains of AD patients. There were five brain regions where the correlation at voxel level between PK and SUVr PiB PET images agreed the most for all reference regions considered, primary motor cortex, primary visual cortex, somatosensory association cortex, associative visual cortex and premotor cortex. Since, both precuneus (P) and parietal inferior (PI) have important roles in visuospatial processing, ROI-based correlation results are consistent with the ones obtained at voxel level.

Overall, according with the present study, the classifier only based on features extracted from PiB PET images of group 4070, using cerebellum as reference region, was the classifier who solved more accurately the problem proposed, binary classification in AD. Additionally it was also found a positive correlation between PK and PiB in particular in brain regions responsible for motor function and visual processing.

Key words:
Alzheimer's disease (AD), Quantification, Normalization, Classification, Machine Learning (ML), Biomarkers, Positron Emission Tomography (PET), ^{11}C-Pittsburgh Compound B (PiB), ^{11}C-(R)-PK11195 (PK), Correlation

RESUMO

A doença de Alzheimer (AD) é a doença neurodegenerativa responsável pelo maior número de casos de demência. Tomografia por emissão de positrões (PET) com 11C-Pittsburgh Compound B (PiB) e 11C-(R)-PK11195 (PK) são duas modalidades utilizadas na visualização das placas amilóides e da microglia ativada no cérebro humano, respetivamente. Uma vez que as placas amilóides são o principal identificador da AD e que a microglia ativada é também recorrentemente encontrada no cérebro dos doentes de Alzheimer, estes representam dois potenciais biomarcadores imagiológicos que podem ser usados como ferramenta de diagnóstico precoce da doença.

Este trabalho teve como objetivo principal a resolução de um problema de classificação binário, entre controlos saudáveis (HC) e pacientes de Alzheimer, através de métodos de *machine learning* (ML) baseados em dois traçadores imagiológicos de PET: o PiB e o PK. Outro objetivo deste trabalho, incluiu a identificação das regiões cerebrais onde o PiB e o PK apresentam maior correlação, quer a nível do voxel quer a nível regional.

O dataset deste estudo, que incluiu 41 indivíduos (20 doentes de Alzheimer e 21 HC), foi dividido em três grupos por forma a melhor compreender o impacto do intervalo de tempo considerado no protocolo de aquisição da PET. O grupo TOT, composto pelas imagens PET adquiridas durante o tempo total de biodistribuição do PiB, e os grupos 4070 e 4060, compostos por imagens PET adquiridas durante o intervalo de tempo caraterístico de acumulação de cada um destes radiofármacos. Após quantificação, pré-processamento, extração e seleção das características, as características selecionadas das imagens PET, com PiB e com PK, foram utilizadas como variáveis preditoras em classificadores baseados em support vector machines (SVM). Para estudar o impacto das diferentes regiões de referência utilizadas na normalização de imagens PET com PK, e a influência do método de quantificação escolhido, os grupos de AD e HC de diferentes formas de quantificação de imagens PET com PK foram comparados a nível do voxel. Adicionalmente, calculou-se para diferentes regiões cerebrais a correlação existente entre imagens PET com PiB em termos da taxa do valor de captação padronizado (SUVr) e as imagens PET com diferentes formas de quantificação PK.

O classificador com o melhor desempenho foi construído com características extraídas de imagens PET com PiB do grupo 4070 normalizadas pelo cerebelo (exatidão – 0.925, sensibilidade-1.000, especificidade-0.857). Por conseguinte, para imagens PET com PiB, o cerebelo foi a região cerebral onde a diferença na acumulação de amilóide entre os grupos de AD e HC foi a menos significativa, isto é, foi a melhor região de referência. De referir que quando o cerebelo é utilizado como região de referência em imagens PET com PiB, é verificada uma maior correlação a nível regional para com as imagens PET com PK, comparativamente à normalização realizada através da matéria branca. As características extraídas a nível regional de imagens PET com PK não melhoraram nem a exatidão nem a sensibilidade do classificador apenas baseado em características extraídas de imagens PET com PiB. A correlação a nível regional entre imagens PET com PiB e com PK sugere que o cerebelo apresenta uma ligação específica ao PK; consequentemente, o método *supervised cluster analysis algorithm based on four kinetic classes* (SVCA4) relevou ser a melhor abordagem para a normalização de imagens PET com PK. As duas formas de quantificação de imagens PET com PK apresentaram diferenças muito pouco significativas entre os grupos AD e HC a nível do voxel, o que sugere que a biodistribuição do PK no cérebro não permite diferenciar grupos. Esta afirmação apoia a associação que se tem vindo a estabelecer entre a microglia ativada e a neuroinflamação. Como a neuroinflamação é característica de cada indivíduo, isto é, é aleatoriamente distribuída no cérebro dos doentes de Alzheimer, o esperado é a não diferenciação de grupos por parte do PK. Foram encontradas cinco regiões cerebrais onde a correlação a nível do voxel se relevou mais acentuada para quase todas as regiões de referência consideradas, córtex motor primário, córtex visual primário, córtex de associação somatossensorial, córtex visual associativo e córtex pré-motor. Tanto o precuneus (P) como o lóbulo parietal inferior (PI) desempenham funções importantes no processamento visual e espacial. Por conseguinte, é natural que os resultados da correlação a nível regional estejam associados com os obtidos a nível do voxel.

Em suma, de acordo com o estudo realizado, o classificador construído apenas com características extraídas de imagens PET com PiB do grupo 4070, usando o cerebelo como região de referência, foi o classificador que apresentou uma melhor resposta ao problema proposto, classificação binária de indivíduos como AD ou HC.

Adicionalmente, também foi descoberta uma correlação positiva entre o PK e o PiB em regiões cerebrais responsáveis pela função motora e pelo processamento visual.

Palavras-chave:
Doença de Alzheimer (AD), Quantificação, Normalização, Classificação, *Machine Learning* (ML), Biomarcadores, Tomografia por Emissão de Positrões (PET), ^{11}C-Pittsburgh Compound B (PiB), ^{11}C-(R)-PK11195 (PK), Correlação

ABBREVIATIONS

A - amygdala

ACing - anterior cingulate

AD –Alzheimer's disease

APOE - apolipoprotein E

APP - amyloid precursor protein

Aβ –amyloid β

B - brain

BP - binding potential

BPM - biological parametric mapping

C - caudate

CER - cerebellum

CSF –cerebrospinal fluid

DVR - distribution volume ratio

FAD - familial Alzheimer's disease

FDG - ^{18}F- fluorodeoxyglucose

FL - frontal lobe

fMRI - functional MRI

FN – false negative

FP – false positive

FTLD - frontotemporal lobar degenerations

FTS - frontal-temporal space

FWHM - full width at half maximum

GM – grey matter

H - hippocampus

HC - healthy controls

ICNAS – Instituto de Ciências Nucleares Aplicadas à Saúde

IFG - inferior frontal gyrus

IPL - inferior parietal lobule

ITG - inferior temporal gyrus

K-NN - K-nearest neighbor

LOOCV - Leave One Out Cross Validation

MCI - mild cognitive impairment

MFG - middle frontal gyrus

ML – machine learning

MNI - Montreal Neurological Institute

MRI – magnetic resonance imaging

MTC - mesial temporal cortex

MTG - middle temporal gyrus

NINCDS-ADRDA – National Institute of Neurological and Communicative Diseases and Stroke and the Alzheimer's Disease and Related Disorders Association

NFTs - Neurofibrillary tangles

OC - occipital cortex

P - precuneus

PC - prefrontal cortex

PCA - principal component analysis

PCing - posterior cingulate

PET –positron emission tomography

PG - precentral gyrus

PI - parietal inferior

PiB – ^{11}C- Pittsburgh Compound B

PK – ^{11}C-(R)- PK11195

Pmen – putamen

poly – polynomial

PS - parietal superior

PSEN1 - presenilin 1

PSEN2 - presenilin 2

P-tau – phosphorylated tau

rbf – radial basis function

Ref – reference region

RF – random forest

ROI - region of interest

SFG - superior frontal gyrus

sMRI - structural MRI

SPL - superior parietal lobule

SPM - statistical parametric mapping

STG - superior temporal gyrus

SUV - standardized uptake value

SUVr - standard uptake value ratio

SVCA4 - supervised cluster analysis algorithm based on four kinetic classes

SVM - support vector machine

TL - temporal lobe

TN – true negative

TP – true positive

T-tau – total tau

WM – white matter

LIST OF FIGURES

LIST OF TABLES

LIST OF GRAPHICS

CONTENTS

CHAPTER 1 (INTRODUCTION)

BACKGROUND

The human body is made of trillions of cells. The nerve cells, also known as neurons, are the building blocks of the nervous system and represent one of the most important cells of the body. The neurons are specialized cells responsible to pass messages throughout the different parts of the body by an electrochemical process [1, 2].

Neurodegenerative diseases are disorders caused by the progressive death of neurons. Due to the impossibility of reproducing and replacing death neurons, these diseases do not have currently a cure. Some of the most relevant neurodegenerative diseases are Multiple Sclerosis, Alzheimer's disease (AD), Parkinson's disease and Huntington's disease [3].

Even though the progression of these diseases is inevitable, there are treatments that can delay their evolution and treat their symptoms. For example, cognitive stimulation. Naturally, the earlier the diagnosis the most effective these therapeutics can be [3, 4].

In 2019, in the United States more than 55 million people presented a diagnostic of dementia, a number that is expected to increase every year up to 88 million in 2050. Unfortunately, only about half of those are actually diagnosed in the primary care setting [5-7].

1-ALZHEIMER'S DISEASE (AD)

Portugal is an aged country with a predictable increased number of cases of dementia. Due to the lack of epidemiological studies focusing Portugal, the statistics presented herein are a worldwide estimation. Currently, AD is the neurodegenerative disorder responsible for most diagnosed cases of dementia, accounting for 60 to 80 percent of them and representing the sixth leading cause of death in the United States [8-10].

The progressive loss of nerve cells causes neurological and neuropsychological signs and symptoms, such as mobility problems and cognitive dysfunction [3, 4]. When a slight, noticeable and measurable decline in cognitive abilities is detected the mild cognitive impairment (MCI) is often diagnosed. MCI is considered to be a transitional phase between normal aging and AD and, when it is associated with memory loss, there is an increased risk for the patient to develop clinical AD [4, 11, 12].

AD is considered a slowly progressive disorder as its symptoms tend to become worse with time. One of the first symptoms to appear is the loss of memory, which progresses over time in most of the cases, up to the point where one loses the ability to carry on a conversation. On average, patients live eight more years after their first symptoms become noticeable to others. However, since the progression of this disorder depends both on age and other health conditions, the survival range ranges goes from four to twenty years [8, 9].

1.1 – RISK FACTORS

The main risk factors related with Alzheimer's are ageing, decreased reserve capacity of the brain, low mental ability in early life, reduced mental and physical activity during late life, vascular disease, environmental factors, family history and genetics (heredity). Although there are risk factors that cannot be prevented - age, family history and genetics (heredity) – they are not the ones that scientists believe to have the upmost importance in the activation of the disease [6, 9].

From a genetic standpoint, AD is a heterogeneous disorder with two forms, familial Alzheimer's disease (FAD) and sporadic Alzheimer's disease. FAD is very rare and it is caused by mutations in the amyloid precursor protein (APP) gene, located in chromosome 21, and in the highly homologous presenilin 1 (PSEN1) and presenilin 2 (PSEN2) genes, both linked to amyloid β (Aβ) metabolism [6].

In contrast, there are more than 15 million people affected worldwide by sporadic Alzheimer's disease. After several years of research, apolipoprotein E (APOE) ε4 allele has been hypothesised to be the most relevant genetic risk factor in sporadic Alzheimer's disease. However, there might be more genetic factors associated. Since AD is triggered by ageing combined with a complex interaction of

both genetic and environmental risk factors, all the factors that contribute to sporadic Alzheimer's disease as well as their combination remain unknown [6].

1.2- HALLMARKS OF THE DISEASE

Nowadays, it remains unknown what triggers the disease. However, according to the current understanding of molecular pathogenesis, the hallmarks are the **amyloid plaques**, composed of Aβ, the **neurofibrillary tangles** (NFTs), composed of hyperphosphorylated tau, and **neuroinflammation** [13].

Although activated microglia is not a specific pathological hallmark to AD, it is probably related to neuroinflammation and so consistently found in AD patients. According with studies, it may be present years before the clinical and behavioural signs of the disease start to appear. Thus, it can represent another important factor for AD diagnostic [12].

From all the hallmarks of the disease, it is thought that Aβ is the driving force of the disease process, supported by the mutation found in FAD. In line with this, amyloid cascade hypothesis postulate that AD results from an initial imbalance between the production and clearance of Aβ in the brain, followed by neuronal degeneration and ensuing dementia [6, 8, 14].

Figure 1 shows plaques and tangles in the cerebral cortex of an AD patient.

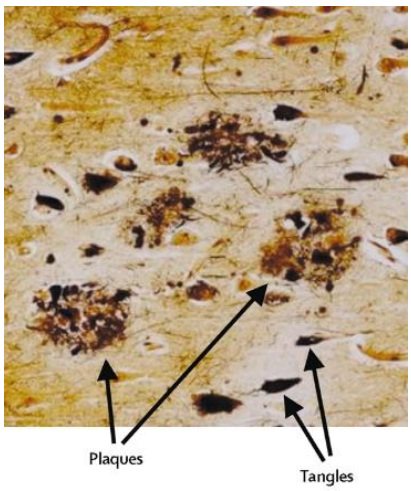

Figure 1 - Plaques and tangles in the cerebral cortex AD. Plaques are extracellular deposits of Aβ whereas tangles are intracellular aggregates composed of a hyperphosphorylated form of the microtubule-associated protein tau. Figure extracted from the book of Blennow, Leon and Zetterberg (2006) – Figure 1 pag. 388 [6]. Copyrights authorized by the author and pending by the The Lancet journal.

2–DIAGNOSIS

AD definitive diagnosis can only be performed *post-mortem* with an autopsy, which allows the confirmation of the presence or absence of amyloid plaques and neurofibrillary tangles [7]. Until recently, clinical diagnosis depended mainly on medical history, together with the clinical, neurological, and psychiatric examination through a 1984's stablished criteria of the National Institute of Neurological and Communicative Diseases and Stroke and the Alzheimer's Disease and Related Disorders Association (NINCDS-ADRDA). Since these criteria for suspected AD largely depended on the exclusion of other dementias, the diagnostic accuracy was relatively low, with sensitivity of around 80% and specificity of 70%. Due to this fact, and to the evidence of other potential biomarkers, NINCDS-ADRDA proposed in 2011 the incorporation of both imaging and molecular biomarkers to the clinical diagnosis of AD [6, 7, 15].

Biomarkers are biological markers able to objectively measure and evaluate some biological state or condition. In this regard, changes that occur at different biological states, corresponding to the evolution of the disorder, can be translated by biomarkers. The currently biomarkers used in AD are the brain scans (imaging biomarkers) and blood tests and measures of cerebrospinal fluid (CSF) (molecular biomarkers) [16-18].

2.1 - MOLECULAR BIOMARKERS

Blood tests and measures of CSF are used to quantify any disease-related marker. Consequently, they can be used in addition to brain scans to verify biological and/or pathogenic changes in the brain [18, 19].

MEASURES OF CEREBROSPINAL FLUID (CSF)

The CSF is the liquid that surrounds the brain and spinal cord. Since CSF is in direct contact with the extracellular space of the brain it can be used as a tracer for the biochemical changes that occur [20].

$A\beta_{42}$ and abnormally phosphorylated (P-tau) and truncated tau proteins have been shown to be the primary components of amyloid plaques and neurofibrillary tangles, respectively. Thus, the levels of these proteins in CSF have been considered as potential AD biomarkers [14, 18].

$A\beta_{42}$ CSF levels in AD patients are a measure of fibrillar $A\beta_{42}$ and plaque load in the brain. $A\beta_{42}$ concentration can be measured in CSF by antibody-based techniques, such enzyme-linked immunosorbent assay (ELISA), and by antibody-independent techniques, such as mass spectrometry. The aggregation of Aβ into plaques results in less Aβ being available to diffuse into the CSF, resulting in **lower levels of this protein in the CSF of AD patients** [14, 18].

In normal conditions, tau is the protein responsible to bind and to stabilise microtubules in neuronal axons, a process that is inhibited when tau becomes phosphorylated. So, patients with **AD are characterized by having high CSF tau levels (total tau (T-tau) and/or P-tau)**. CSF T-tau is increased to around 300% in patients with Alzheimer's disease and, according with several evidences, it reflects the intensity of the neuronal and axonal damage, and degeneration of the brain. Also, patients with high T-tau measures are more likely to have a faster progression from MCI to AD, cognitive decline and higher mortality [6, 14, 18].

Since CSF levels are normal in several other neurodegenerative diseases, abnormal CSF levels allow to discriminate patients with AD from both the cognitively normal elderly and patients with other dementias. However, to improve the diagnosis of AD, a delineation of the temporal changes of core and candidate CSF biomarkers in preclinical AD and the investigation of their association with established and emerging neuroimaging markers as well as with comorbidities and other age-related risk factors is needed [14, 19].

2.2 - IMAGING BIOMARKERS

Brain scans, used to investigate what is happening in the brain of AD patients, can be acquired by different imaging modalities, such as magnetic resonance imaging (MRI) and positron emission tomography (PET). By using these techniques, it is possible to assess biological and pathogenical changes in the brain and, thus, access

disease risk or make prognosis, clinical guidance of diagnosis, and monitorization of therapeutical interventions [6, 18].

IMAGING TECHNIQUES: MAGNETIC RESONANCE IMAGING (MRI)

MRI is a non-invasive imaging technique that uses strong magnetic fields and radio waves to produce 3D detailed anatomical images [21, 22].

There are two types of MRI images, structural MRI (sMRI) and functional MRI (fMRI). Since brain morphometry can be measured by sMRI, this technique has been used to detect secondary effects of AD, such as grey matter atrophy, which is related to the loss of neurons, synapses and dendritic de-arborization; white matter atrophy; and ex vacuo expansion of CSF spaces. Consequently, it represents a powerful indicator of the stage and intensity of the neurodegenerative aspect of AD pathology [13, 23].

According with several studies changes in MRI imaging can be used to successfully separate patients with AD from both healthy aging subjects and MCI patients. However, atrophy in the hippocampal and entorhinal cortex have also been associated to other dementias, such as frontotemporal dementia and vascular dementia; Thus, MRI might bear difficulties on the discrimination of AD patients from patients with other dementias [6].

In the Figure 2 is present an example of a a study using MRI imaging to detect grey matter (GM) atrophy in the brains of AD patients.

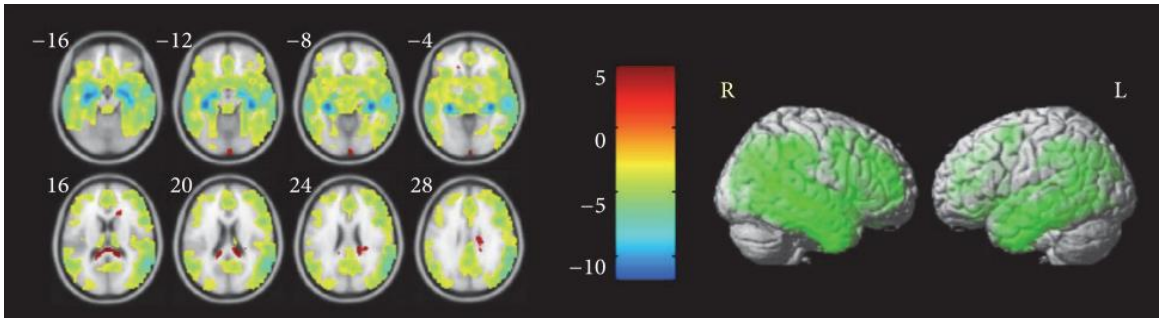

Figure 2 - Grey matter (GM) atrophy. Left part shows the differences of GM between AD and HC. Indicating that AD compared with HC in the hippocampus part present a significant atrophy. From right part, it is possible to see significant regions of GM loss between AD and HC in whole brain. Figure extracted from the article Xiao et al. (2017) – Figure 3 pag.6 [24]. Copyright authorization pending.

IMAGING TECHNIQUES: POSITRON EMISSION TOMOGRAPHY (PET)

Tracers are substances with atomic or nuclear, physical, chemical or biological properties that can help identify, observe or track the behaviour of a variety of biological processes. A tracer is called radiotracer when one or more atoms of its chemical composition are replaced by a radioisotope. Different techniques, such as single photon emission computed tomography (SPECT), PET and computed radioactive particle tracking (CARPT) use radiotracers as visualizing tools [25, 26].

PET is an imaging technique that uses reduced amounts of radioisotopes emitters of positrons to evaluate organ and tissue functions. PET images are formed by mapping the gamma photons that arrive at opposite detectors within a tiny window time. These gamma rays are produced by a process called positron-electron annihilation. In this process, two gamma photons (511keV) are produced when a positron, emitted by the radiotracer, meets an electron inside the patient's body [27, 28].

Due to its capacity to detect changes at the cellular level, PET imaging may access the early onset of disease, even when some changes characteristics of the disease are not identified by other imaging techniques, such MRI, and before the appearance of the first symptoms [27, 29].

^{18}F- FLUORODEOXYGLUCOSE (FDG) PET IMAGES

FDG shows the glucose metabolism, namely its decrease (hypometabolism). Hypometabolism is well established in AD, in cognitively normal individuals at high risk for AD, in cognitively normal individuals with a parent with AD and in patient diagnosed with MCI. Due to this, FDG was one of the first biomarkers used in PET in the diagnosis of AD [30]. It is capable to demonstrate neuronal dysfunction in the temporal, parietal and posterior cingulate cortex, characteristic of AD patients. Also, has the potential to play a predictive role at detecting which normal controls or MCI patients are most likely to convert to AD with high accuracy [6, 30].

An example of longitudinal metabolic reductions on FDG-PET scan is present in the Figure 3.

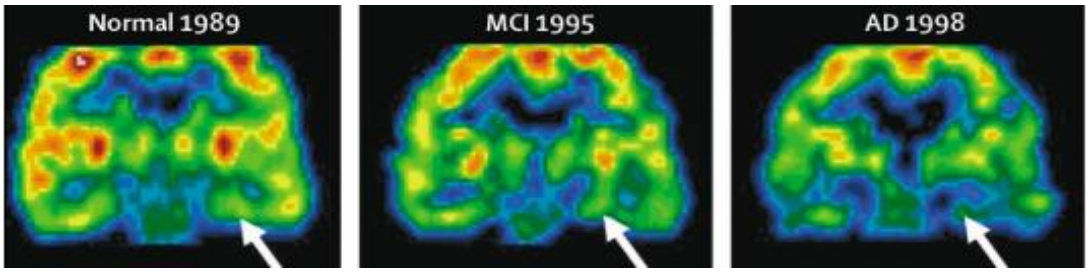

Figure 3 - Longitudinal metabolic reductions on FDG-PET scan. FDG-PET scans in a 71-year-old cognitively normal woman at baseline (1989) and over 9 years. During this observation period the patient declined to MCI and later was diagnosed with AD, which was confirmed at autopsy. Arrows indicates progressive reductions in glucose metabolism. Figure extracted from the book of Blennow et al. (2006) – Figure 6 pag. 394 [6]. Copyrights authorized by the author and pending by the The Lancet journal.

CARBON-11 (^{11}C) RADIOLABELLED MOLECULES FOR PET IMAGING

As aforementioned, the retention of activated microglia and amyloid plaques have been widely reported in pathological examination of AD. Since carbon 11-Labelled Pittsburgh Compound B, know as PiB, and carbon 11- Labelled (R)-PK11195, known as PK, can be used as measure for amyloid plaques and microglia activation, respectively, these two radiopharmaceuticals have been widely used in PET imaging studies as tools for AD diagnosis [31].

RADIONUCLIDE ^{11}C

Since organic compounds contain carbon and ^{11}C is a positron emitter, this radionuclide represents one of the most common tracers used in PET. In fact, until today, more than 200 compounds have been labelled with ^{11}C [32].

The most common radionuclides used in PET images along with their decay characteristics, half-time, decay mode, maximum energy, mean energy and maximum range are present in the Table 1.

Table 1- Common radionuclides used in PET images and their decay characteristics, half-time, decay mode, maximum energy, mean energy and maximum range [32].

Nuclide	Half-life (min)	Decay mode	Maximum energy (Mev)	Mean energy (Mev)	Max. range (mm)
^{11}C	20.4	100% β^+	0.96	0.386	4.1
^{13}N	9.98	100% β^+	1.19	0.492	5.4
^{15}O	2.03	100% β^+	1.7	0.735	8
^{18}F	109.8	97% β^+	0.69	0.25	2.4

PRODUCTION

The production of radioisotopes for use in biomedical procedures, such as diagnostic imaging and/or therapeutic treatments, is made by the conversion of the atoms of one element into another. This conversion, that involves altering the number of protons in the nucleus (target), can be accomplished by nuclear reactions in reactors or by charged particle bombardment in accelerators [32].

The short half-life of ^{11}C ($T_{1/2}$ = 20.4 min) is the main challenge for the synthesis of his labelled tracers. Fortunately, across the years, the improvement of automated techniques for radiosynthesis allowed the development of ^{11}C tracers. ^{11}C is generally produced by charged particle bombardment in cyclotron, in accordance with the nuclear reaction: $^{14}N(p,\alpha)\ ^{11}C$, where ^{14}N (nitrogen-14) is the target, p (positron) the charged particle bombarded and α (alpha) the particle that is emitted by the nuclear reaction [26, 32].

^{11}C-PITTSBURGH COMPOUND B (PIB) PET IMAGES

The development of the PET tracer PiB has made in-vivo imaging of amyloid plaques in human brain possible, which as aforementioned represent a core molecular feature of AD [30].

In line with this, the differences in PiB uptake profile observed in PET imaging between controls and AD patients can be used as a tool for AD diagnosis. AD patients present a higher uptake of PiB on amyloid plaques in cortical areas (amyloid-positive) than normal controls [6, 30, 33].

In general, AD patients are PiB positive and healthy controls PiB negative. PET images of MCI patients, who will eventually convert to AD, should be characterized as positive PiB. However, this characterization is tricky, in most cases. There are at least two distinct explanations for PiB negativity in MCI subjects. Firstly, it is possible that a fraction of MCI subjects is a non-AD process, such as cerebrovascular pathology, medial temporal sclerosis, tauopathy, or other processes. Secondly, PiB-negative MCI subjects may be at earlier stages of the AD process, when prefibrillar amyloid is not yet detected by PiB [34].

Nowadays, the widely used form of PiB is radiolabelled for PET with ^{11}C. Several developments across the years, resulted in the availability of amyloid imaging tracers labelled with longer half-life radioisotopes such as ^{18}F ($T_{1/2}$ = 110 min), florbetapir, florbetaben, and flutemetamol [34, 35].

PiB BEHAVIOUR AFTER ADMINISTRATION

In accordance with standards protocols, subjects are positioned in the scanner, injected with 10 to 15 mCi of PiB, and then scanned using a dynamic acquisition protocol that lasts between 60 to 90 minutes. There are two main options to analyse PET time–activity data, the subjects do or do not arterial cannulation. Arterial cannulation is highly invasive and technical demanding. Due to this PET quantification often relies on alternative methods that do not require arterial cannulation [34, 36].

Perfusion represents the passage of the radiopharmaceutical through the circulatory system. The perfusion of PiB to the brain is fast, occurring between minute 0 and 10, after administration. On the other hand, the uptake of PiB is observed between minute 40 and 70, after administration [33, 37].

The distribution and uptake of PiB in brain has substantial regional specificity and is associated to different brain regions depending if the subject is an AD patient or healthy control (HC). Control subjects show a quickly clearance of the radiotracer from all areas except from the hemispheric white matter and portions of thalamus and brain stem. On the other hand, AD patients tend to retain PiB in the neocortex at levels twofold higher than white matter and present lower binding levels in medial temporal lobe and primary sensorimotor cortex. So, the regions that are

most PiB positive are the association isocortical areas of the medial (precuneus) and lateral parietal, lateral temporal, frontal extending into gyri recti, and the allocortical anterior and posterior cingulate. All the mentioned areas are known to have high levels of amyloid plaques on *post-mortem* examination [34].

In the Figure 4 PiB scans are presented using the (semi)quantification output standard uptake value (SUV) (Figure 4 - A) and the quantification output mean distribution volume ratio (DVR) (Figure 4 – B).

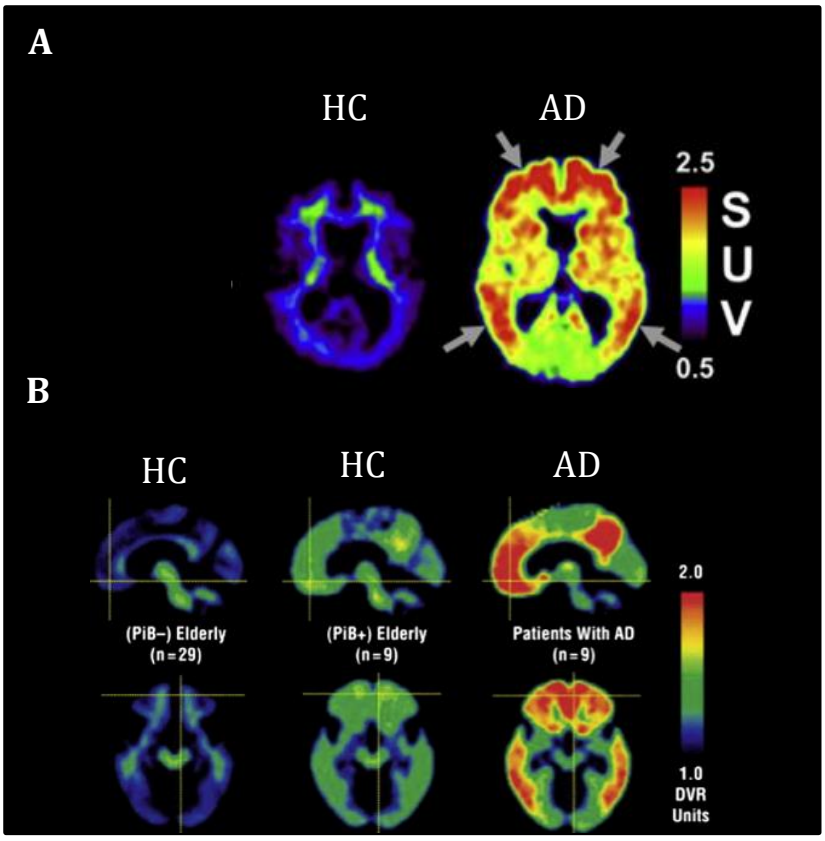

Figure 4 - Representative PiB scans from HC and AD participants using two different quantification outputs. In A using the standard uptake value (SUV) and in B the mean distribution volume ratio (DVR). In A the arrows indicate areas of typical amyloid deposition. In B, PiB- represents the PiB-negative clinically unimpaired participants (left) and PiB+ the PiB-positive clinically unimpaired participants (centre). Figure adapted from two figures of the article of Cohen and Klunk (2014) - Figure 1 pag.118 and Figure 3 pag. 119 [30]. Copyrights authorized by the author.

^{11}C-(R)-PK11195 (PK) PET IMAGES

Inflammatory mechanisms like microglial activation might be involved in the pathogenesis of AD. Due to the capacity of PK to reveal microglial activation this

radiopharmaceutical can be used for *in vivo* imaging of microglial activation in the human brain and can represent a target of AD and MCI [12, 38].

2.3 - COMBINATION OF MULTIPLE BIOMARKER MODALITIES

It is arguably to postulate that the combination of molecular biomarkers, such as measures of cerebrospinal fluid, with imaging biomarkers, using both structural (sMRI) and functional (SPECT/PET) neuroimaging techniques, may potentially increase the diagnostic accuracy as compared with the use of one biomarker alone. This was therefore a goal of the current thesis [14].

3- QUANTIFICATION

PET allows for sequential measurements of *in vivo* distribution of a radioligand after its intravenous administration. Sequential measurements are done over time, and are influenced by several factors, such as blood flow and radioligand clearance from plasma, besides the number of receptors and their affinity. Therefore, clinically or experimentally relevant information is extracted by applying **tracer kinetic models** to PET time–activity data. In PET kinetic modelling the knowledge of the input function, that represents the behaviour of the radiotracer in the blood (or plasma) to a site of interest, is mandatory. This input function can be assessed by **plasma input models** or through **reference tissue input models** [39, 40].

Since **plasma input models** assess the most continuous and noiseless input function, they represent the gold-standard. However, these models require arterial blood sampling, which is laborious and invasive [41].

In contrast, **reference tissue input models** are methods where a reference tissue is used instead of an arterial input function. The input function can be assessed applying compartmental models, multiple-time graphical analyses or by semi-quantitative analysis applying tissue-to-reference tissue ratio. These methods do not require arterial blood sampling, and thus represent an easy choice for routine clinical studies. However, there are evidences that they can be biased due to (specific) binding of the reference region considered to the radioligand injected [34, 42, 43].

In table 2 are present the pros and cons of the two main types of models used in quantitative analysis of PET studies, reference tissue input models and arterial function input models.

Table 2 - Pros and cons of the two models used in quantitative analysis of PET studies: reference tissue input models and arterial plasma input models [43].

	Reference tissue	**Arterial function**
Pros	→Non-invasive; →Can provide binding potential in receptor studies.	→Represents the true input function (gold standard); →Can be corrected for labelled metabolites.
Cons	→Optimal reference tissue is available only for a few radioligands; →Radioactivity spread from adjacent tissues or due to scatter can affect the performance of the model; →Specific analysis models required; →Metabolite analysis is not possible.	→Invasive; →Labour-intensive.

PiB Quantification

After PET image acquisition, the binary diagnostic assessment of PiB is established, i.e., abnormal (amyloid-positive) versus normal (amyloid-negative). This assessment is done in accordance with the values of the tracer uptake in cortical regions of interest by two different approaches: visual assessment and quantification. The second approach, quantitative assessment, allows higher accuracy and more reliable evaluation of PiB [33].

The standardized uptake value ratio method is the most common PiB (semi)quantification approach used in PiB PET images. Using semi-quantitative analysis applying tissue-to-reference tissue ratio this method normalizes the uptake within target regions to that within a reference region. The cerebellum, white matter and grey matter are been widely used as reference region, since its amyloid accumulation has been demonstrated to bear no relevant differences between HC and AD patients [33, 34].

PK QUANTIFICATION

The gold standard for analysis of dynamic PK studies is the two-tissue reversible plasma input model (2T4k). 2T4k model requires accurate invasive arterial blood sampling during the scan, which complicates the procedure, and is prone to errors [42].

Since the pattern of microglial activation is generally unknown, the choice of an anatomical region to be used as reference region may be challenging without appropriate pathological information. Due to this, reference tissue input models for years were not considered trustworthy PK quantification approaches. However, after several efforts, automatic approaches to extract reference tissue kinetics of PK, such as supervised cluster analysis algorithm based on four kinetic classes (SVCA4), have been found and used in the quantification of PK PET data [42].

4- CLASSIFICATION PROBLEM

MACHINE LEARNING

Machine learning (ML) can be broadly defined as computational methods that are able to extract knowledge from data to improve performance or to make accurate predictions. ML is inherently related to areas as artificial intelligence, computer science, data analysis and statistics, so it is also known as predictive analytics or statistical learning [44, 45].

With all the data available today, ML applications have become in recent years abundant in everyday life. From automatic recommendations of which movies to watch, to what food to order, protein function, image recognition, face detection, medical diagnosis and treatment, among others, ML applications are everywhere [44].

As it was mentioned, neuroimaging biomarkers changes are important tools for the diagnosis of AD. These changes can be translated by features and these features can be used as inputs in ML methods for the classification of AD, MCI and HC [46].

UNSUPERVISED AND SUPERVISED MACHINE LEARNING

Supervised and unsupervised are two types of ML. Supervised machine learning is one of the most commonly used and successful type of ML. It can be broadly defined as an efficient and accurate method that predicts a specific outcome from a given input that has never been seen. To achieve that, the algorithm is provided with examples of input/output pairs, that comprise the training set. The two main types of supervised ML problems are **classification** and **regression**. Assign a category to each item represents a classification problem, while the predictions of real value for each item represent regressions tasks. Ranking (order items according to some criteria), clustering (partition items into homogeneous regions) and dimensionality reduction or manifold learning (transform an initial representation of items into a lower-dimensional representation of the same items, while preserving some properties of the initial one) are other examples of learning problems [44, 45].

To build a ML model, the dataset needs to be split into two parts: training set and test set. Supervised learning builds a model on the training data and then make accurate predictions on the new unseen data, that present similar characteristics as the training set used (test set) [44, 45].

A model **generalizes** from the training set to the test set, when makes accurate predictions on unseen data. On the other hand, **overfitting** a model occurs when a model too complex is built for the available information, on the other way, choosing too simple a model is called **underfitting**. The goal is to find a model in between, which allows generalisations as accurately as possible [44].

CROSS VALIDATION

Cross-validation techniques can be used to guarantee that the chosen ML model extracts the correct patterns/information from the given data, and it is not getting up too much noise. So, cross-validation techniques are used to assess the classification performance of ML models on unseen data. Moreover, since, in practice, the amount of labelled data available could not be enough to set aside two different samples, one for validation and other for training, cross-validation techniques are used to exploit the labelled data for both model validation and training [45, 47, 48].

In conclusion, cross-validation is a resampling procedure used to evaluate ML models on a limited data sample [45, 47, 48].

Supervised machine learning algorithms

As expected, the success of the chosen learning algorithm depends both on the dataset and the classification problem. Therefore, the first and most important thing to do before building the model is to become familiar with the data and to understand how it relates to the task to be solved [44, 45].

K-nearest-neighbours (K-NN), support vector machines (SVM), Naïve Bayes, ensembles of decisions trees and neural networks are the most used supervised ML algorithms. The strengths, weakness and some observations of these supervised ML algorithms are presented in Table 3 [44, 45].

K-nearest-neighbours (K-NN)

K-NN is a ML algorithm used for both classification and regression problems. To predict to which class belongs a new data point the algorithm finds the next lying k examples. The class to which most of the neighbours belong is assumed to be the class of the new example. In line with this, there are two important parameters in K-NN classifier, the number of neighbours (K) and how the distance between data points is measured. By default, Euclidean distance is used for quantitative variables. For two class classification problem this algorithm only considers exactly one nearest neighbour, which is the closest training data point to the new data point [44].

Naïve Bayes classifiers

The Naïve Bayes classifier technique is a simple classifier based on the so-called Bayesian theorem and is particularly suitable when the dimensionality of the inputs is high. According with Bayesian theorem, there is a strong independence between the features (in the dataset); thus, it is possible to update the probabilities of hypotheses when some evidences are given. In line with this, Naïve Bayes learn

parameters by looking at each feature individually and collect simple per-class statistics from each feature to do the prediction [44, 49-51].

DECISIONS TREES

Decision trees are widely used models for both classification and regression tasks. Essentially, they learn a hierarchy of if/else questions, leading to a decision. Decision tree is an easy to follow and understand method [44].

SUPPORT VECTOR MACHINES (SVM)

SVM is a powerful classifier, appropriate to high dimensional problems. The objective of SVM is mapping the non-linear separable data points into a higher-dimensional feature space where linear separation is possible. To avoid the explicit mapping needed to get linear learning algorithms to learn a nonlinear function or decision boundary, kernel methods are performed. Kernel methods represent the data only through a set of pairwise similarity comparisons between the original dataset. In line with this, the linear separation problem is solved by the addition of nonlinear features (kernel functions) to the dataset. There are three kernel functions commonly used in SVM: the linear kernel, the polynomial kernel (poly) and the radial basis function (rbf) kernel [4, 44, 52].

During training, the SVM learns the importance of each training data points in the decision boundary between the two classes. Typically, only the ones that lie on the border between the classes have importance for the decision. These are called support vectors and give the support vector machine its name [44].

To make a prediction for a new point, the distance to each of the support vectors is measured. The class of the new point is based on that distances and on the importance of the support vectors learned during training [33, 44].

NEURAL NETWORKS

Neural networks are a biologically-inspired programming algorithm which enables a computer to learn from observational data. It can be viewed as a

generalization of linear models that perform multiple stages of processing to reach a decision. Given enough computation time, data and careful tuning of the parameters, neural networks often present better results than other ML algorithms in many problems, such as image recognition, speech recognition and natural language processing [44].

ENSEMBLES CLASSIFIER

Although the large majority of the existing techniques rely on a single classifier there are several methods that combine the outputs of multiple ML models to create more powerful ones. These methods are called ensemble methods and are used to increase performance, by exploring the diversity of the base classifiers in terms of features or examples, which are usually randomly selected. Gradient Boosted Decision Trees and Random Forests (RF) are the two most common ensemble methods [4, 44].

Table 3 - Strengths, weakness and some applications of the most relevant supervised ML algorithms [44, 53].

Algorithms	Strengths	Weakness	Applications
k-NN	→Model easy to understand and fast to build; →Reasonable performance; →Good for small datasets; →Good as a baseline.	→Slow predictions when the training set is large; →Does not perform well on dataset with many features; →Pre-process of data is needed.	→Industrial applications (look for similarity of items in comparison to others); →Handwriting detection; →Image/video recognition.
Naïve Bayes	→Good for very large data sets and high-dimensional data; →Great as baseline model.	→Only for classification.	→Classification without manually processing of web pages, forum posts, blog snippets, and tweets.
Decisions trees	→Easily visualized and understood by nonexperts; →Work well for features in different scales; →No pre-processing is needed.	→Tend to overfit and provide poor generalization performance.	→Data exploration; →Pattern recognition; →Medical diagnosis (disease identification); → Risk trends.
SVM	→Powerful for medium-sized datasets of features with similar meaning; →Allow complex decision boundaries, i.e., guarantees optimal separation.	→It can be difficult to understand; →Require careful pre-processing and scaling of the data and tuning of the parameters.	→ Business applications (comparison of stocks performance); →Medical data.
Neural Networks	→Able to capture information contained in large amounts of data; →Builds incredibly complex models;	→Long time to train; →Careful pre-processing of the data and tuning of the parameters;	→Image and speech recognition; →Natural language processing.

STATE OF THE ART

In this section, will be presented several studies using molecular and/or imaging biomarkers of AD. It will be evidenced the relevance of the changes of these biomarkers in the brain of AD patients and the diagnosis of this disease. Also, the most pertinent quantification and ML methods that have been use in AD classification problems are addressed.

1.1 – MOLECULAR BIOMARKERS

According with various studies on consecutive patients, classification of AD made by T-tau and $A\beta_{42}$ CSF measures presented an average sensitivity of 84% and 89%, respectively, while the specificity against cognitively normal elderly people was 91% and 90% [6].

Other studies have also demonstrated high sensitivity and specificity of CSF measures as biomarkers in discriminating AD from both cognitively normal elderly people and from patients with other dementias, such as frontotemporal, Lewy body and vascular [14].

1.2 – IMAGING BIOMARKERS

MAGNETIC RESONANCE IMAGING (MRI)

The medial temporal lobe, including the hippocampus and entorhinal cortex are the first affected regions in the brain of AD patients. Several studies using MRI have demonstrated that hippocampal atrophy is capable to distinguish AD from cognitively normal elderly people, with 80–90% accuracy. However, only a few studies using MRI have addressed the differentiation of AD from other dementias [6].

In 2016 R. Gad performed a study using MRI images of 120 individuals (40 AD, 40 MCI and 40 HC). The classification of the groups was performed using two different methods, KNN and SVM. After filtering and normalization, the features were extracted

and the ones with highest accuracy were selected to build the classifier. SVM polynomial order three provided the best average accuracy (97.92%) [46].

A different study carried out in 2018 by Lee et al used a total of 1342 individuals (869 HC and 473 patients with probable AD). This study proposed a new ML method to quantify the similarity between the cortical atrophy pattern of an individual subject and the one of a representative AD patient cohort. Simultaneously, a longitudinal validation study was done, using 79 patients with MCI and 27 patients with probable AD dementia. Surface-based morphometry yielded a sensitivity and specificity of 87.1% and 93.3%, respectively. In the longitudinal validation study, both MCI-converts and AD patients with faster decline presented higher atrophy similarity at both baseline and first year visits, in comparison to non-converters [54].

A different study using T1-weighted MR scans from pathologically proven AD patients and cognitively normal elderly individuals was used to classify the grey matter segment. Linear SVM approach classified 96% of pathologically verified AD patients and 89% of mild, clinically probable AD patients [7].

POSITRON EMISSION TOMOGRAPHY (PET)

Ensemble methods are well established in ML studies using PET images. These methods increased the performance of the classifier by the analysis and exploration of the diversity of the base classifiers in terms of features or examples [4].

^{18}F- fluorodeoxyglucose (FDG)

In three class classification problem (HC, MCI and AD) RF and SVM are the favourite ensembles methods used to classify FDG PET brain images. To test that, voxel intensities were extracted from 177 FDG PET volumes and used as inputs of the classifier. The classification was performed using ensemble method of classifiers where each base classifier (both SVM and RF) in the ensemble had its own optimized feature subset. Ensemble methods outperformed the base classifiers with the best accuracy of 66.78% being obtained by the SVM ensemble [4].

Another study using FDG PET volumes consists of 164 subjects (42 HC, 27 MCI patients who had not converted to AD within 5 years (nc-MCI) and 95 MCI patients

who converted to AD within 5 years (MCI-AD)). In this study, FDG uptake values of 26 volumes of interest were submitted to ANCOVA and SVM analyses. Lower FDG uptake values were found in the temporoparietal area of individuals in the MCI-AD group. HC and nc-MCI revealed similar FDG uptake values, higher uptake values comparing with MCI-AD group. The best discrimination of nc-MCI from MCI-AD patients was obtained using SVM, with an accuracy of 89%, correctly detecting 93% of the nc-MCI patients [55].

The low accuracy of FDG PET evidenced by these studies is probably caused by the reflection of hypometabolism and neurodegeneration in non-AD syndromes, such as frontotemporal lobar degenerations (FTLD) [56].

^{11}C-Pittsburgh Compound B (PiB)

PiB has been studied in several research settings, with the goal of determining whether a positive amyloid PET imaging can be used to predict imminent decline in MCI individuals, and whether amyloid PET imaging can be used to follow and explore the performance of emerging antiamyloid therapeutic agents [34].

PIB: in vivo imaging of amyloid plaques

Post-mortem tissue studies have shown that in the brain of patients with AD, PiB binds specifically to amyloid-laden portions, and in cognitively normal elderly control brains there is a nonspecific level of PiB retention in the cortex [34].

Braak and Braak (1990), Brilliant et al. (1997), Suenaga et al. (1990) and Wolf et al. (1999) studied the pattern of PiB retention in the brain. In AD, PiB retention was mainly observed in a brain region commonly associated with amyloid plaques accumulation, the frontal cortex. It was also observed a retention of PiB in precuneus/posterior cingulate and parietal, occipital and temporal cortices, with a relative sparing of PiB retention in the mesial temporal areas. Previous reports also show extensive Aβ deposition in the striatum, the striped mass of white and grey matter located in front of the thalamus [56, 57].

PiB imaging in MCI patients

A longitudinal study made by Forsberg and colleagues (2007) suggests that MCI subjects with high PiB retention have a higher tendency to convert into AD patients, comparing with subjects with low PiB retention. This tendency has also been observed in several subsequent studies performed by Koivunen et al., (2011), Villemagne et al. (2011) and Wolk et al. (2009) [56].

Several studies regarding amyloid deposition in prodromal AD found that 50% to 60% of MCI individuals are PiB positive. In a different study Nordberg et al. reported that 62% of the studied MCI subjects were PiB positive, and approximately 24% of them had converted into a clinical diagnosis of AD during the initial follow-up period [34].

These results raise the possibility of PiB PET amyloid imaging playing a role in the identification of MCI subjects and in the identification of those whom are more likely to convert to AD [34].

PiB imaging in normal older subjects

Aizenstein et al. (2008), Jack et al. (2008), Kantarci et al. (2012), Klunk et al. (2004), Mintun et al. (2006), Mormino et al. (2009), Mormino et al. (2011) Pike et al. (2007), Reiman et al. (2009), Rowe et al. (2010) and Villemagne et al. (2008) found considerable PiB retention in normal elderly subjects, ranged from a proportion of 10 to 30 percent [56].

Other studies showed cortical PiB retention in approximately 15% to 20% of apparently cognitively normal subjects. This finding supports the theory of why amyloid plaques are recurrently found in the brains of older nondemented individuals at autopsy. PiB-positive older subjects are probably capable of tolerating a certain amount of amyloid due to the existing reserve of cognition [34].

PiB and MRI

Archer et al. (2006) found a correlation between the PiB binding and the rate of decline in whole-brain volume, among a group of patients with a clinical diagnosis of AD. According to this study, amyloid deposition was associated with higher rates of atrophy, which supports a primary role for amyloid in AD. Two PiB-negative subjects studied, identified clinically as AD, presented very small atrophy in brain volume. They did not show evidence of decline after a year, which leads to the conclusion that they may have another disease other than AD [34].

PiB and CSF

Fagan et al. (2006) compared the levels of CSF $A\beta_{1-42}$ and other CSF measures to PiB binding using 24 subjects (18 HC, 3 very mild, 2 mild and 1 moderate dementia). In general, the subjects were separated in two non-overlapping groups, a group of PiB positive subjects, with low CSF Aβ levels, and a group composed by the PiB-negative subjects, with higher levels of Aβ. Three PiB positive of the 18 cognitively normal subjects presented low levels of CSF $A\beta_{1-42}$. [34].

A different study consisting of 243 individuals (AD, HC, MCI and other dementias) used PiB PET images and CSF concentrations of $A\beta_{38}$, $A\beta_{40}$ and $A\beta_{42}$ to solve the AD classification problem. The classifier was constructed using a SVM approach. SUVr PiB PET images normalized by cerebellar grey matter and pons produced a similar classifier performance (accuracy-96%, sensitivity-96%, specificity-95%), outperforming both classifiers using the CSF multiple Aβ concentrations features (best accuracy 91%) and SUVr PiB PET images normalized by white-matter. In conclusion, this study found pons to be the best reference region to normalized PiB PET images, since vaster differences were observed at voxel level between the groups and a stronger correlation between the several CSF Aβ concentrations were found. Even though there were misclassified cases found using the cerebellar grey matter or pons as reference region, both approaches outperformed the visual assessment (accuracy -92.0%, sensitivity-92.6%, specificity -90%) [33].

PiB and FDG

Across the years several studies have investigated the association between PiB and FDG PET images in AD. A study done by Ng et al. (2007) found PiB more accurate than FDG using both visual assessment (accuracy, 90% vs. 70%) and receiver operating characteristic (ROC) analysis (95% vs. 83%). Similar results were obtained by Rabinovici et al., where PiB showed a higher inter-rater agreement between visual and quantitative classifications, when compared to FDG [56].

Li et al. (2008) found 94% of agreement between PiB and FDG in differentiating AD from normal controls, and just 54% in classifying MCI subjects. In addition, Lowe et al. demonstrated in 2009, using PiB and FDG images of AD and MCI subjects, that while PiB and FDG displayed similar AD diagnostic accuracy, PiB was significantly better in the classification of MCI subtypes [56].

In 2011 Rabinovici et al. performed a study using 107 subjects (62 AD and 45 FTLD) to test the diagnostical performance of PiB and FDG in the classification of clinically diagnosed AD and FTLD patients. Better sensitivity results were found using PiB in visual assessment (89.5%), when compared to FDG reads (77.5%). Similar specificity values were obtained using PiB and FDG reads, 83% and 84%, respectively [56].

Buckner et al. postulated the association of amyloid deposition to hypometabolism (brain dysfunction) as a measure by FDG metabolism. Even though DeKosky et al. (2002) and Ikonomovic et al. (2007) found an inverse correlation between PiB retention and glucose metabolism in several cortical areas, PiB retention and glucose metabolism did not correlate in the frontal cortex. Since the frontal cortex is a specific region of PiB binding these findings suggest that probable Aβ deposition is not able to reduce cerebral metabolism locally. Another study done in 2006 by Edison et al. found an inverse correlation, reduced by 20%, between PiB retention and regional glucose metabolism in temporal and parietal cortices [34, 56].

PiB and PK

Parbo et al. (2017) studied PiB and PK PET images of a total of 57 patients (42 MCI and 15 HC) to determine the amyloid retention and to detect the extension of

neuroinflammation (microglial activation) in MCI cases. In PiB PET images amyloid-positivity was defined for a PiB retention of 1.5 above the retention of this radiopharmaceutical in the reference region. On the other hand, for PK PET images parametric maps of binding potential (BP) were generated using supervised cluster analysis. 62% of MCI cases presented an higher amyloid retention in cortical areas and 85% of them an increased microglial activation, comparing to HC. Voxel-wise analysis found a positive correlation between levels of amyloid retention and PK binding potentials within subregions of frontal, parietal and temporal cortices. In general, PK PET reveals increased inflammation in cortical areas accompanying the amyloid deposition of amyloid positive MCI cases [58].

A study performed to verify the differences between the retention of PiB and PK in the brain of AD patients consisted of 17 subjects (5 HC, 6 MCI and 6 mild to moderate AD). No differences of PK retention between the groups or the presence or absence of β-amyloid were found. According to these results it can be assumed that either microglial activation is limited to severe stages of AD or PK is unable to detect microglial activation in initial phases of AD. This study also showed significantly greater levels of PiB retention in subjects with a clinical diagnosis of probable AD, compared to HC. MCI cases crossed a range from control-like to AD-like levels of PiB retention. Two HC exhibited high PiB retention in specific regions of amyloid plaques accumulation in AD; thus, they probably represent prodromal cases of AD. The quantification of PiB radiotracer was done using regional standardized uptake value (SUV) method, normalized to the cerebellar SUV determined over the minute 40 and 90, after administration. For PK, 2 methods of quantification were applied: 1) reference tissue model using the whole cerebellum; 2) and tissue ratio method through the sum, over the minute 10 and 60, after administration, of regional radioactivity concentration and normalized using subcortical white matter as reference region [31].

^{11}C- (R) - PK11195 (PK)

PK: in vivo imaging of microglial activation

PET with PK is one of the modalities used for *in vivo* imaging of microglial activation in the human brain. The potential of PK to reveal microglial activation was confirmed in 2013 by studies using Zymosan-Treated Rats with induced microglial activation [38, 56].

As it was mentioned before, inflammatory mechanisms like microglial activation are probably involved in the pathogenesis of AD. Thus, PK can be used as a tool of AD diagnosis. In line with this, a study using 50 subjects (19 patients with probable AD, 10 MCI cases, and 21 HC) was carried by Schuitemaker et al. (2013) to investigate if increased PK binding potential is present in AD and MCI individuals. The quantification of PK binding potential (BP) were done using receptor parametric mapping (RPM), with supervised cluster analysis. Comparisons between groups were performed at voxel level using mixed model analysis. The occipital lobe presented small differences between the groups of PK BP, showing a slightly increased PK BP in the occipital lobe of AD patients. Results from regions of interest (ROI)-based analyses show no differences between the groups of PK BP. **These non-consensual results suggest that microglial activation is probably an indirect phenomenon occurring in AD patients** [12].

PK quantification

To verify which data analysis method is the best one to quantify BP of PK PET images a study using 25 individuals tested different approaches. From the 25 studied individuals, 18 were HC (12 HC with arterial blood sampling and 6 without blood sampling), 3 patients had Huntington's disease and 4 AD. Data were analysed using arterial input function and predefined kinetic classes. Predefined kinetic classes extracted the grey matter without specific tracer binding and used it as reference tissue. BP was estimated using rank-shaping exponential spectral analysis. Since both quantification approaches were in excellent agreement and highly correlated, this study showed that **supervised reference tissue extraction may represent a**

robust and reproducible quantitative method to assess PK in the human brain [38].

Another study, consisting of 34 subjects (9 young controls, 8 old controls, 9 MCI and 8 AD), used two different methods to quantify dynamic PK PET images: 1) supervised cluster analysis (SVCA) algorithms based on either four (SVCA4) and six (SVCA6) kinetic classes; 2) and manually defined cerebellum. Data were analysed using arterial input function and reference tissue model with and without vascular correction. The best reference regions, i.e., the reference region with the lowest specific bind to PK, was given by SVCA4. Also, higher differences between groups in specific binding were observed using SVCA (4 or 6). Data analysed by reference tissue model with vascular correction improved both parametric images and PK binding potential differences between groups. In general, SVCA combined with reference tissue model with vascular correction presented the best assessment of binding potential PK PET images [42].

MOTIVATION AND OBJECTIVES

Nowadays, the diagnosis of AD makes use of clinical, biological and imaging criteria, however most of times the diagnose only occurs when symptoms become manifest. Nevertheless, characteristic neurodegenerative changes in the brain of AD patients, plaque and tangle load and neurodegeneration, start earlier. Even though the progression of AD is inevitable, late diagnosis is a factor that reduces the potential of causal disease-modifying therapeutic approaches, which in turn delays the evolution of the disease or symptomatic treatment [59].

The main goal of current clinical workup is to find a new method to change the standard timeline of Alzheimer's disease diagnostic, depicted in Figure 5 - a), to the timeline b) presented in Figure 5 - b). However, to achieve an early diagnosis of AD, more studies with imaging and biochemical biomarkers, and their correlation, evidencing their relevance in the diagnostic of AD, need to be performed. Therefore, the aim of the present study is to solve a binary classification problem of HC and AD patients using ML methods based on two PET imaging biomarkers, PiB and PK and to study the putative correlation between these two radiopharmaceuticals.

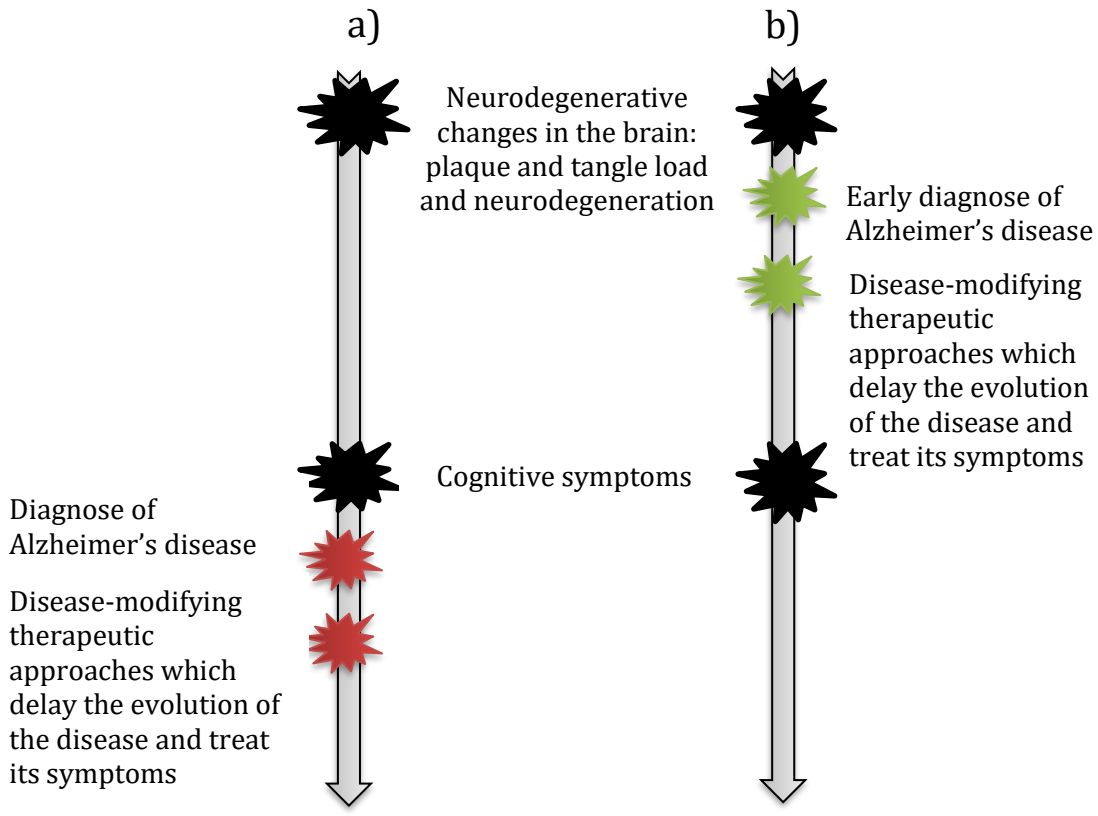

Figure 5 - Timeline for AD diagnosis: a) standard and b) desirable.

CHAPTER 2 (MATERIALS, METHODS AND RESULTS)

INTRODUCTION

The main goal of the present study is to set up an automatic binary classifier to predict whether a patient has AD or not. To achieve the intended output, different groups of PET images acquired using two different radiopharmaceuticals, PiB and PK, were utilised as classifiers inputs.

Other goals of this work include:

1) Understanding the impact of:

1.1) The distinct reference regions used in the normalization of PET images;

1.2) The time interval considered in PET images acquisition;

1.3) The method of quantification used;

2) The investigation of the correlation between PiB and PK PET images, in different brain regions.

1- DATASET

The dataset used in this study consists of 41 subjects (20 AD and 21 HC). All HC patients had both PiB and PK PET images. 18 subjects of AD have both PiB and PK PET images. One of the remaining has just PiB PET image and the other one just PK PET image. If there was high PiB retention in cortical regions PiB PET images were classified as PiB positive (abnormal), otherwise, they were classified as PiB negative (normal) [33].

To understand the impact of the acquisition time interval considered in PET images acquisition, the dataset was split in three different groups. For PiB two groups of images were considered: a group composed by the PET images acquired during the total time of PiB biodistribution (group TOT); and a group composed just by the images acquired during the characteristic accumulation time of this radiopharmaceutical, between minute 40 and 70, after administration (group 4070). For PK only PET images acquired during the characteristic accumulation time of PK

were considered, between minute 40 and 60, after administration (group 4060). Group TOT includes 35 subjects (14 AD and 21 HC) and both group 4070 and 4060 have 40 subjects (19 AD and 21 HC).

2-MATERIALS

2.1- 2DSLICESTIMEFRAMESTO3D

The conversion of all raw data (PET images) from their initial DICOM format (*.dcm*) to NIfTI format (*.nii)* was achieved by using the *2DslicesTimeFramesTo3D* executable. This executable, provided by the Institute of Nuclear Sciences Applied to Health (ICNAS), allowed the concatenation of thousands of dynamic DICOM PET images in just two files: one with all PET images in NIfTI format acquired during the total time of the radiopharmaceutical biodistribution, i.e., with all the PET images of group TOT; and another one with the information regarding the time frames.

2.2- BP_KINETICMODEL

Another computer routine, also provided by the ICNAS, was used to quantify PET images acquired during the radiopharmaceutical characteristic accumulation time: between minute 40 and 70 (group 4070), and minute 40 and 60 (group 4060), after administration, for PiB and PK, respectively.

Unlike 2DslicesTimeFramesTo3D, this executable contains step for selection of a reference region. Therefore, all the features extracted from PET images of group 4070 and 4060 could be directly used and compared between each other.

2.3- MANGO

Mango is a free software composed by several tools for image analysis and a user interface that allows to navigate in the image volumes [60]. This software was firstly used in the co-registration of all PET images to the template Montreal

Neurological Institute (MNI) T1 MRI. After co-registration, it was used in feature extraction.

2.4- STATISTICAL PARAMETRIC MAPPING

Statistical parametric mapping (SPM) is a free software package designed for the analysis of brain imaging data sequences. The sequences can be a series of images from different cohorts, or time-series from the same subject. The current release, SPM12, can be used for the analysis of fMRI, PET, SPECT, electroencephalography (EEG) and magnetoencephalography (MEG) images [61, 62].

SPM12, was used in the pre-processing, to smooth all co-registered images with a 8 mm full width at half maximum (FWHM) Gaussian filter and to do the voxel-wise comparison between groups of different quantified PK PET images. To visualize the voxel-wise correlation between PK PET images and SUVr PiB PET images it was used an older release of SPM, SPM5.

2.5- BIOLOGICAL PARAMETRIC MAPPING (BPM) – A STATISTICAL TOOLBOX FOR MULTI-MODALITY BRAIN IMAGE ANALYSIS

Biological parametric mapping (BPM) is a toolbox developed in MATLAB for multimodal image analysis based on a voxel-wise use of the general linear model. This toolbox includes a user-friendly interface for performing analyses, including voxel-wise multimodal correlation, ANCOVA, and multiple regression. It depends of SPM software for visualization and statistical inference [63].

BPM was used to do the voxel-wise correlation between PK and PiB PET images.

2.6- RSTUDIO

RStudio, an integrated development environment for R, is a free software environment for statistical computing and graphics [64, 65].

In this work, R-3.5.3 and RStudio 1.1.463 were firstly used to select the features to build the classifier. The independent two sample T-test as well as principal

component analysis (PCA) technique were used as feature selection approaches. RStudio 1.1.463 was also used to investigate the correlation of several brain regions at regional level between PiB and PK PET images.

2.7- MATLAB

MATLAB is a programming language that includes matrix algebra and a large network for data processing and plotting. Since this language is easy for beginners, my ML task involved imaging processing through SPM, a free software package designed to work in MATLAB, and I had free license given by the University of Coimbra to use it, MATLAB R2019a was the chosen software to build the binary classifier. To run the BPM toolbox it was used an older release of MATLAB, MATLAB R2011a [66, 67].

3-METHODS AND RESULTS

It is possible to summarize the methods of this work in three main steps:

1) Conversion of all raw data (PET images) from their initial DICOM format (*.dcm*) to NIfTI format (*.nii*);
2) Quantification and pre-processing (co-register and smoothing);
3)
    - 3.1) Voxel Based Analysis
        - 3.1.1) Voxel-wise comparison between AD and HC groups of different quantified PK PET images;
        - 3.1.2) Voxel-wise correlation between PK and PiB PET images.
    - 3.2) Region Based Analysis
        - 3.2.1) Feature extraction of co-registered and smoothed PET images using different brain regions of interest (ROI);
        - 3.2.2) Feature selection (independent two sample T-test and PCA);
        - 3.2.3) Classification;
        - 3.2.4) ROI based correlation between BP PK of group 4060 and SUVr PiB of group 4070 PET images.

3.1- STEP 1: DICOM TO NIFTI

To make medical imaging information interoperable and image-acquisition devices integrated, an international standard image format called DICOM (Digital Imaging and Communications in Medicine) was created [68]. Consequently, all raw PET images presented in this study were coded in DICOM format. However, image analysis software, such SPM and Mango, require data in NIfTI format (*.nii*). So, it was required the conversion of all raw data between these two formats. This task was done using the *2DslicesTimeFramesTo3D* executable.

3.2- STEP 2: QUANTIFICATION AND PRE-PROCESSING

Several quantification methods were performed by the executables *2DSLICESTIMEFRAMESTO3D* and *BP_KineticModel* to quantify and (semi)quantify PiB and PK PET images. All the methods used are reference based methods, i.e., are methods that used reference tissue input models instead of arterial input function models.

PiB PET images quantification

For group TOT, the quantification of PiB PET images was done in terms of Sum. Sum was given by the executable *2DSLICESTIMEFRAMESTO3D* and is equivalent to the sum of all PiB PET images acquired during the total time of PiB biodistribution. Due to physiological differences, such as weight and height, to make the individuals of the group TOT comparable, Sum was represented in terms of standard uptake value ratio (SUVr) using three different reference regions, cerebellum (CER), grey matter (GM) and white matter (WM).

On the other hand, for group 4070, the (semi)quantification of PiB PET images was given directly in terms of SUVr by the executable *BP_KineticModel* through the standardized uptake value (SUV) method. This method was performed for two different reference regions, CER and WM.

Summing up, PiB PET images were quantified according to different reference regions in: 1) $SUVr_{TOT\text{-}CER}$; 2) $SUVr_{4070\text{-}CER}$; 3) $SUVr_{TOT\text{-}GM}$; 4) $SUVr_{TOT\text{-}WM}$ and 5)

$SUVr_{4070\text{-}WM}$. Where in $XX_{YY\text{-}ZZ}$, XX represents the quantification output; yy the group of PET images considered; and zz the reference region used to do the normalization.

PK PET images quantification

As it was mentioned, the quantification of dynamic PK PET images was done using the executable *BP_KineticModel*. This executable quantified PK PET images acquired during the characteristic accumulation time of PK using two different approaches: 1) supervised cluster analysis (SVCA) algorithm based on four (SVCA4) kinetic classes; and 2) CER as reference region. For each one of these approaches, it was used the SUV method to (semi)quantify PK PET images of group 4060 in terms of SUVr and the Logan Plot and the MRTM2 methods to quantify PK PET images of group 4060 in terms of distribution volume ratio (DVR) and binding potential (BP), respectively. In line with this, PK PET images were quantified in six different ways: 1) $SUVr_{4060\text{-}CER}$; 2) $SUVr_{4060\text{-}SVCA4}$; 3) $BP_{4060\text{-}CER}$; 4) $BP_{4060\text{-}SVCA4}$; 5) $DVR_{4060\text{-}CER}$ and 6) $DVR_{4060\text{-}SVCA4}$.

Logan Plot is a reference based graphical method. It can be applied to both reversible and irreversibly binding tracers and simplify the quantification task by converting the model equations into linear plots [69]. On the other hand, MRTM2 method is a linearized reference tissue model. This method quantifies PK PET images in terms of BP according with the model equation 3) present in the article written by Ichise et al. (2003) [70].

PiB and PK pre-processing

To be able to correctly analyse subsequent quantitative images, co-registration needs to be performed. Image co-registration is the process that allows to spatially align two or more images, i.e., allows the identical indexation and assessment of voxel values from different sequences and different post-processing approaches, from two distinct matrices [71, 72].

In line with this, before further processing, all quantified PET images were co-registered (linear spatial normalized) to Montreal Neurological Institute (MNI) T1 MRI template. This task was done using the tool Register Brain (FLIRT) available in

Mango software. The MNI template used was the ICBM152, since it exhibits the best resolution and detail to date. This template is equivalent to the average of 152 normal MRI scans matched to the first MNI template available (MNI305) using a 9-parameter affine transform [73, 74].

After co-registration, with the goal to remove high frequencies of the signal, a spatial smoothing with a 8 mm FWHM Gaussian filter using SPM12 was applied. The exclusion of high frequencies of the signal make the distribution of the intensities more normal which can be very helpful for the validity of the statistical tests [75].

3.3-STEP 3

3.3.1- VOXEL BASED ANALYSIS

Once the image has been quantified, co-registered (realigned) and smoothed the next step is to statistically analyse the data. To compare the two groups (AD and HC) of subjects in a "random effect analysis" (with one scan per subject), it was defined in the "Basic Models" of SPM12 the design two sample T-test. A design matrix, where columns represents the number of groups and lines the number of subjects, was automatically generated by SPM12. This matrix is responsible to solve the estimation problem; and thus, tries to interpret correctly the defined contrast vector, for this case [1 -1], and estimate their global main effect according with the design defined in the "Basic Models", the two sample T-test [76].

In the Figure 6 are presented the sequential scheme of voxel based analysis – comparison between AD and HC groups.

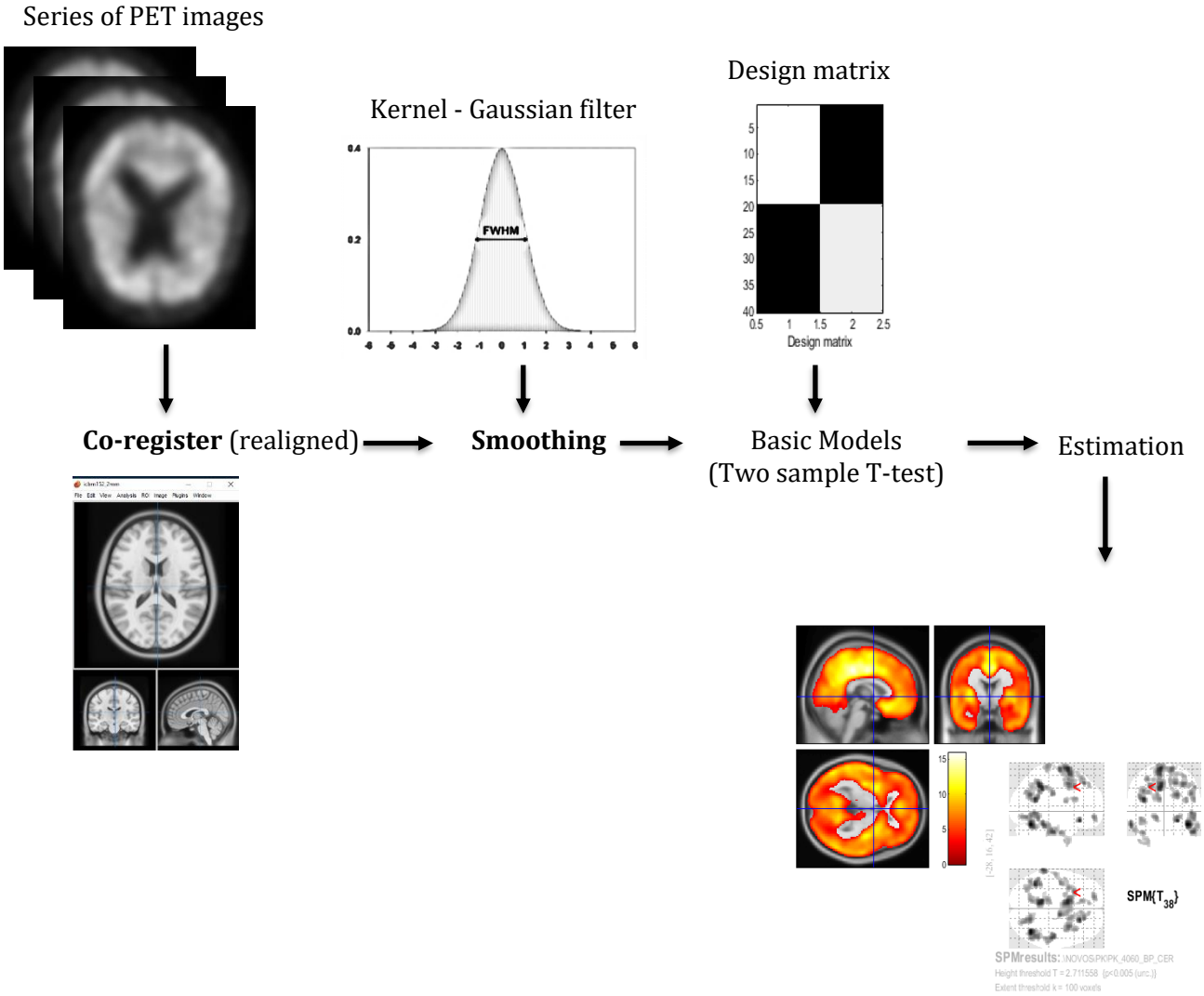

Figure 6 – Sequential scheme of voxel based analysis – comparison between AD and HC groups [75].

PK - COMPARISON BETWEEN AD AND HC GROUPS AT THE VOXEL LEVEL

Comparison between AD and HC groups of different quantified PK PET images at the voxel level was done using the SPM12 (Figures 7-11).

This comparison was performed to understand the impact of distinct reference regions in the normalization of PK PET images and the influence of the quantification method used. In addition this comparison was also performed to verify if the characteristics brain regions of PiB positive PET images (prefrontal cortex (PC), occipital cortex (OC), mesial temporal cortex (MTC), parietal inferior (PI), parietal superior (PS), anterior cingulate (ACing), caudate (C), posterior cingulate (PCing),

precuneus (P), putamen (Pmen) and a mask of the whole brain (B)) presented differences at the voxel level between AD and HC groups of PK PET images. And to identify the brain regions with the most relevant differences at the voxel level between groups of PK PET images. To discover those brain regions, it was found the coordinates of the clusters with the most differences at voxel level, between AD and HC groups of PK PET images (Tables 4-8).

The coordinates of the clusters found, considering CER and SVCA4, as reference region, and the correspondent brain regions are presented in the Tables 4 to 8.

SUVr PK PET images (p-value<0.005 and 100 voxels)

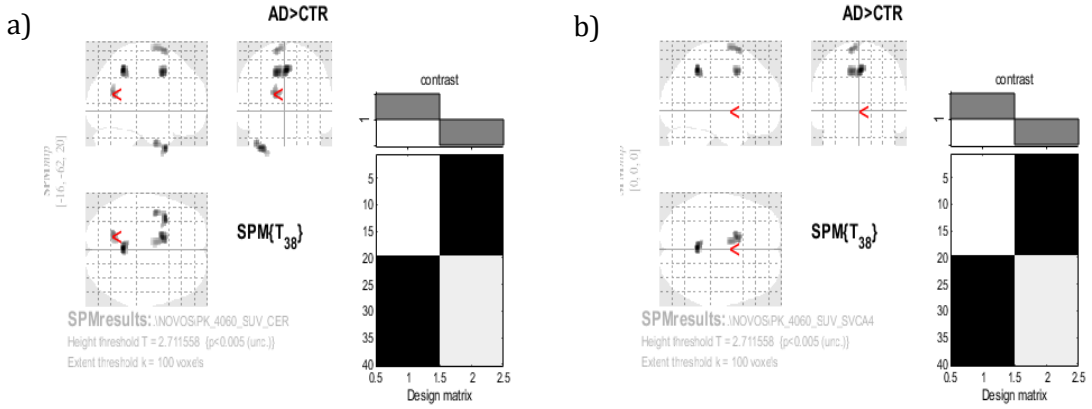

Figure 7 - Comparison between AD and HC groups of SUVr PK PET images at the voxel level considering CER (Figure 7a)) and SVCA4 (Figure 7b)) as reference regions. This comparison was performed for a p-value < 0.005 and 100 voxels as extent threshold.

Table 4 - Correspondence between the coordinates of the found clusters in SUVr PK PET images and the brain regions [77, 78].

Cluster's coordinates	Brain Region
(-12; 8; 44)	Outside defined Brodmann's Areas (BAs)
(-34; 10; -46)	
(-12; 10; 70)	
(0; -48; 46)	**Left – BA31(Dorsal Posterior Cingulate)**
(-16; -62; 20)	**Right – BA11 (Orbitofrontal Cortex)**

BP PK PET images (p-value<0.005 and 100 voxels)

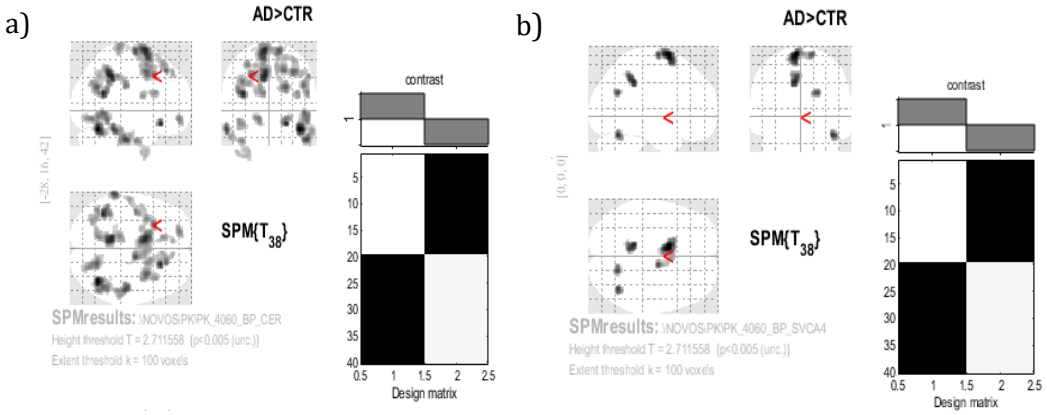

Figure 8 - Comparison between AD and HC groups of BP PK PET images at the voxel level considering CER (Figure 8a)) and SVCA4 (Figure 8b)) as reference regions. This comparison was performed for a p-value < 0.005 and 100 voxels as extent threshold.

Table 5 - Correspondence between the coordinates of the found clusters in BP PK PET images and the brain regions [77, 78].

Cluster's coordinates	Brain Region
(42; -62; -24)	Outside defined Brodmann's Areas (BAs)
(50; -22; -36)	
(-28; 16; 42)	
(-8; -46; 42)	**Left – BA31 (Dorsal Posterior Cingulate)**
(-10; -42; 38)	
(-8; 4; 70)	**Left – BA6 (Premotor Cortex)**
(48; -56; -4)	Right Fusiform (37)
(22; 26; -18)	**Right – BA11 (Orbitofrontal Cortex)**
(-62; -38; -24)	Left – BA21 Middle Temporal Gyrus
(20; -64; 26)	**Right – BA31 (Dorsal Posterior Cingulate)**
(20; -62; 26)	
(48; -22; 28)	Right-PrimSensory (1)

BP PK PET images (p-value<0.001 and 100 voxels)

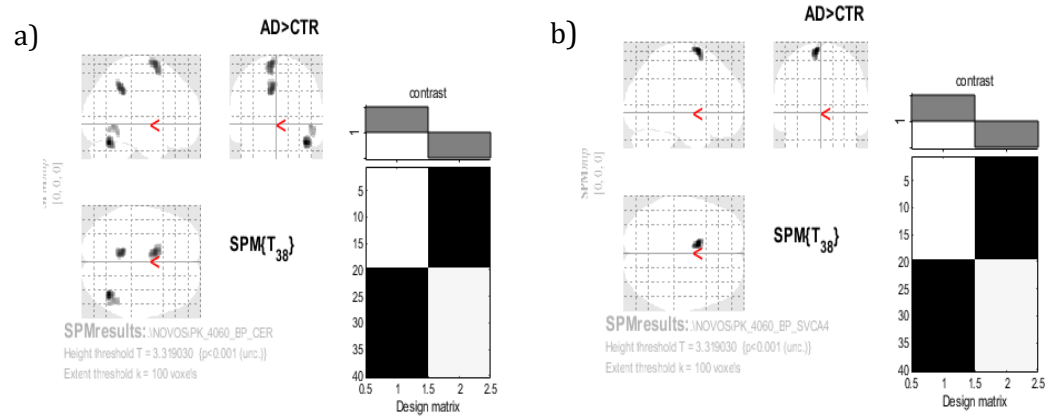

Figure 9 - Comparison between AD and HC groups of BP PK PET images at the voxel level considering CER (Figure9a)) and SVCA4 (Figure9b)) as reference regions. This comparison was performed for a p-value < 0.001 and 100 voxels as extent threshold.

These results were obtained for a p-value less than 0.001, more conservative than the case before (Figure 8 and Table 5).

Table 6 - Correspondence between the coordinates of the found clusters in BP PK PET images and the brain regions [77, 78].

Cluster's coordinates	Brain Region
(42; -62; -24)	Outside defined Brodmann's Areas (BAs)
(-8; -46; 42)	**Left – BA31 (Dorsal Posterior Cingulate)**
(-8; 4; 70)	**Left – BA6 (Premotor Cortex)**
(48; -56; -4)	Right Fusiform (37)

DVR PK PET images (p-value<0.005 and 100 voxels)

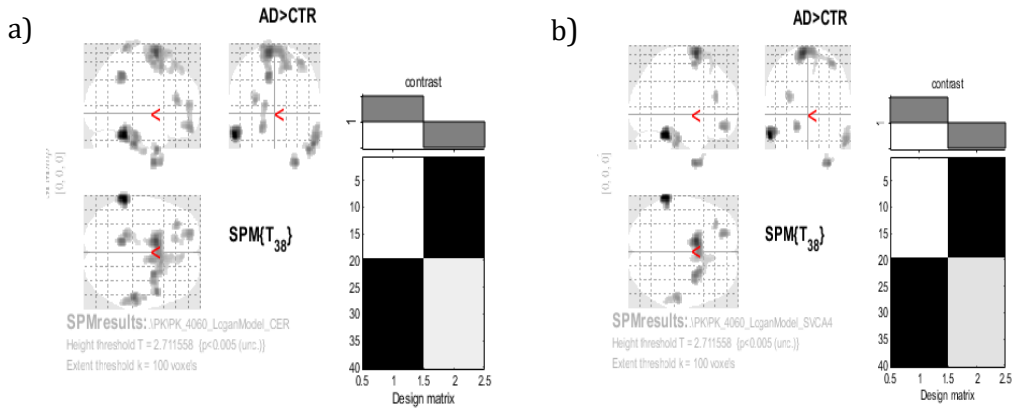

Figure 10 - Comparison between AD and HC groups of DVR PK PET images at the voxel level considering CER (Figure10a)) and SVCA4 (Figure10b)) as reference regions. This comparison was performed for a p-value < 0.005 and 100 voxels as extent threshold.

Table 7 - Correspondence between the coordinates of the found clusters in DVR PK PET images and the brain regions [77, 78].

Cluster's coordinates	Brain Region
(-60; -42; -28)	Outside defined Brodmann's Areas (BAs)
(56; -28; -38)	
(28; 2; -60)	
(-62; -42; -26)	
(-30; 2; -60)	
(-32; 36; 20)	
(-30; 36; 14)	
(-10; -46; 44)	**Left – BA31 (Dorsal Posterior Cingulate)**
(-10; 4; 72)	**Left – BA6 (Premotor Cortex)**
(36; 0; 58)	**Right – BA6 (Premotor Cortex)**
(-20; 54; -18)	**Left – BA11 (Orbitofrontal Cortex)**
(-20; 48; -16)	
(48; 6; -44)	Right – BA20 (Inferior Temporal Gy)
(58; -24; -30)	
(-14; 32; 56)	BA8 (Frontal Cortex)
(-18; -40; 76)	Left – PrimSensory (1)

DVR PK PET images (p-value<0.001 and 100 voxels)

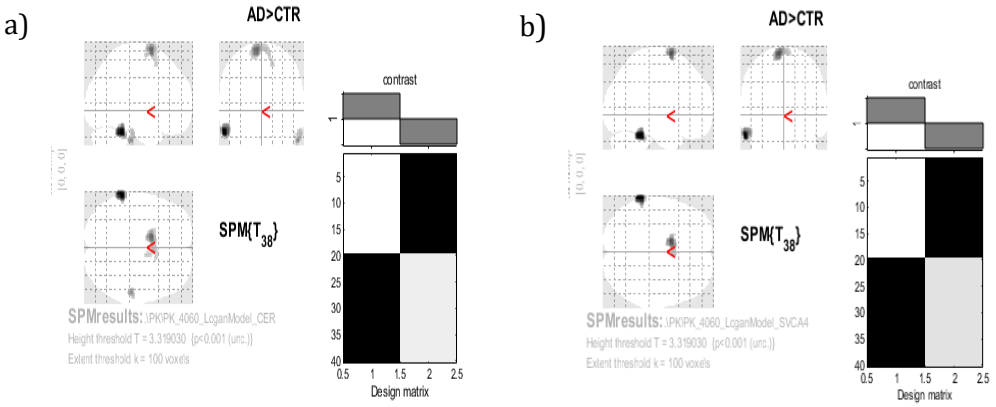

Figure 11 - Comparison between AD and HC of DVR PK PET images at the voxel level considering CER (Figure11a)) and SVCA4 (Figure11b)) as reference regions. This comparison was performed for a p-value < 0.001 and 100 voxels as extent threshold.

These results were obtained for a p-value less than 0.001, more conservative than the case before (Figure 10 and Table 7).

Table 8 - Correspondence between the coordinates of the found clusters in DVR PK PET images and the brain regions [77, 78].

Cluster's coordinates	**Brain Region**
(-60; -42; -28)	Outside defined Brodmann's Areas (BAs)
(56; -28; -38)	
(-62; -42; -26)	
(-10; 4; 72)	**Left – BA6 (Premotor Cortex)**

The comparison between AD and HC groups of SUVr PiB PET images of group 4070 (Figure 12a)), BP (Figure 12b)) and DVR (Figure 12c)) PK PET images, using CER as reference region, for a p-value less than 0.001 and 100 voxels as extent threshold, are displayed using colour scale in Figure 12.

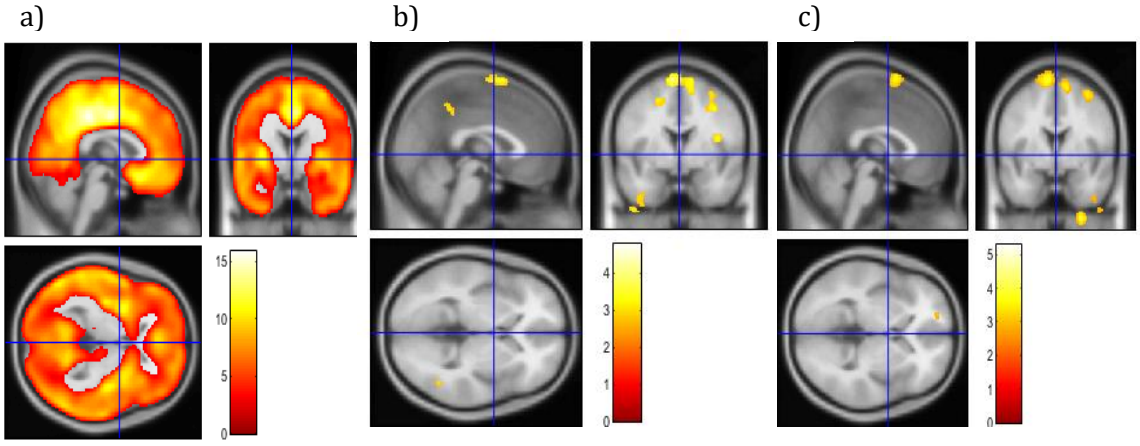

Figure 12 - Comparison between AD and HC groups of SUVr PiB PET images of group 4070 (a)) and BP (b)) and DVR (c)) PK PET images of group 4060 using CER as reference region. These comparisons were performed in SPM12 for a p-value < 0.001 and 100 voxels as extent threshold.

According with the Figures 7 to 11, is possible to verify that, when CER is used as reference region, higher differences at the voxel level between AD and HC groups of PK PET images, comparing with SVCA4, are observed.

Across the Tables 4 to 8 in bold are represented the three brain regions most recurrently found, i.e., the brain regions with the most differences at the voxel level between groups of PK PET images: dorsal posterior cingulate (BA31), orbitofrontal cortex (BA11) and premotor cortex (BA6). From the characteristic brain regions of PiB positive PET images: PC; OC; MTC; PI; PS; ACing; C; PCing; P; Pmen; and B; the PCing (posterior cingulate) have a correspondence in Tables 4-8 with the dorsal posterior cingulate (BA31) and PC (prefrontal cortex) with both orbitofrontal cortex

(BA11) and premotor cortex (BA6). However, PK PET images overall did not present differences between AD and HC groups at the voxel level for the different characteristic brain regions of PiB positive PET images.

According with the results of Tables 4 to 8 and with the work developed by Bradburn et al., "new" brain regions were chosen to be extracted from PK PET images: frontal lobe (FL); temporal lobe (TL); frontal-temporal space (FTS); superior frontal gyrus (SFG); middle frontal gyrus (MFG); precentral gyrus (PG); inferior frontal gyrus (IFG); superior temporal gyrus (STG); middle temporal gyrus (MTG); inferior temporal gyrus (ITG); amygdala (A); hippocampus (H); inferior parietal lobule (IPL); and superior parietal lobule (SPL) [79].

It was also observed relevant differences at voxel level between AD and HC groups of SUVr PiB PET images of group 4070 (Figure 12a)). Whereas the two considered quantified PK PET images (Figure 12b) and c)) do not show substantial differences.

Correlation at voxel level between PK PET images of group 4060 and SUVr PiB PET images of group 4070

The correlation at voxel level between PK PET images of group 4060 and SUVr PiB PET images of group 4070 was computed in the toolbox BPM, using regression analysis and a positive T-contrast. The visualization of the Figures 13-16 was performed in SPM5.

The identification of the brain regions more correlated at the voxel level between BP and DVR PK and SUVr PiB PET images was based on the coordinates of the clusters with the most correlation found (Tables 9 to 12).

SUVr PiB PET images using CER as reference region (Ref) & BP PK PET images

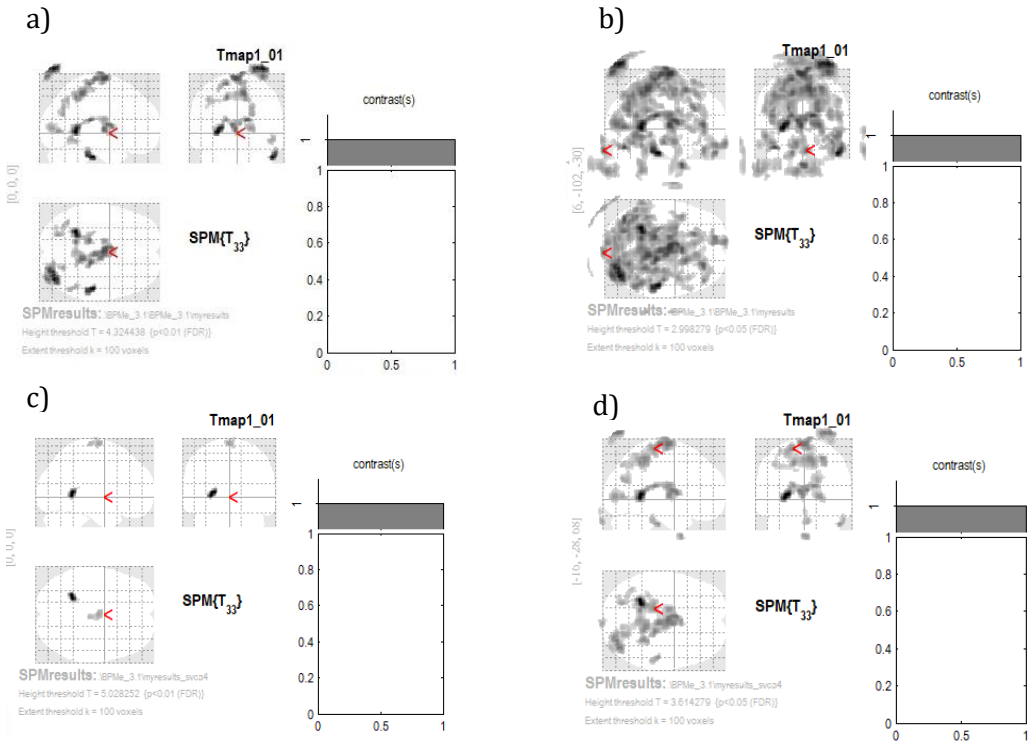

Figure 13 - Correlation at voxel level between BP PK and SUVr PiB PET images. To visualize in SPM5 it was defined in a) and c) a p-value < 0.01 and in b) and d) p-value < 0.05 and 100 voxels as extent threshold. In a) and b) BP PK was normalized using CER and in c) and d) using SVCA4. For both cases SUVr PiB was normalized using CER.

Table 9 - Correspondence between the coordinates of the found clusters in BP PK PET images normalized by CER and SVCA4, and the brain regions [77, 78].

BP PK reference region	Cluster's coordinates	Brain Region
CER	(-28; -48; 2)	Outside defined Brodmann's Areas (BAs)
	(52; 24; -34)	
	(38; -80; 88)	
	(-2; -8; 76)	
	(14; -26; 18)	
	(-24; -74; 4)	
	(2; 10; -50)	
	(22; 40; 6)	
	(6; -102; -30)	
	(-40; -72; -24)	Left-BA19 (Associative Visual C)
	(20; -82; 6)	Right-PrimVisual (17)
	(-16; -28; 68)	Left-PrimMotor (4)
SVCA4	(-24; -46; 6)	Outside defined Brodmann's Areas (BAs)
	(0; -8; 74)	
	(28; -82; 90)	
	(52; -24; -34)	
	(22; -84; 4)	
	(2; 10; -50)	
	(6; -102; -30)	
	(-16; -28; 68)	Left-PrimMotor (4)
	(18; -70; 26)	Right-BA19 (Associative Visual C)

According with the Figure 13 and Table 9, when SUVr PiB PET images are normalized by CER, it is possible to verify that, for CER as reference region of BP PK images, there is correlation at voxel level in visual cortex (Left-BA19 - Associative Visual C), primary visual cortex (Right-PrimVisual (17)) and primary motor cortex (Left-PrimMotor (4)) between BP PK and SUVr PiB of group 4070 PET images. For SVCA4 as reference region, there is correlation at voxel level in primary motor cortex (Left-PrimMotor (4)) and visual cortex (Left-BA19 - Associative Visual C).

SUVr PiB PET images using CER as Ref & DVR PK PET images

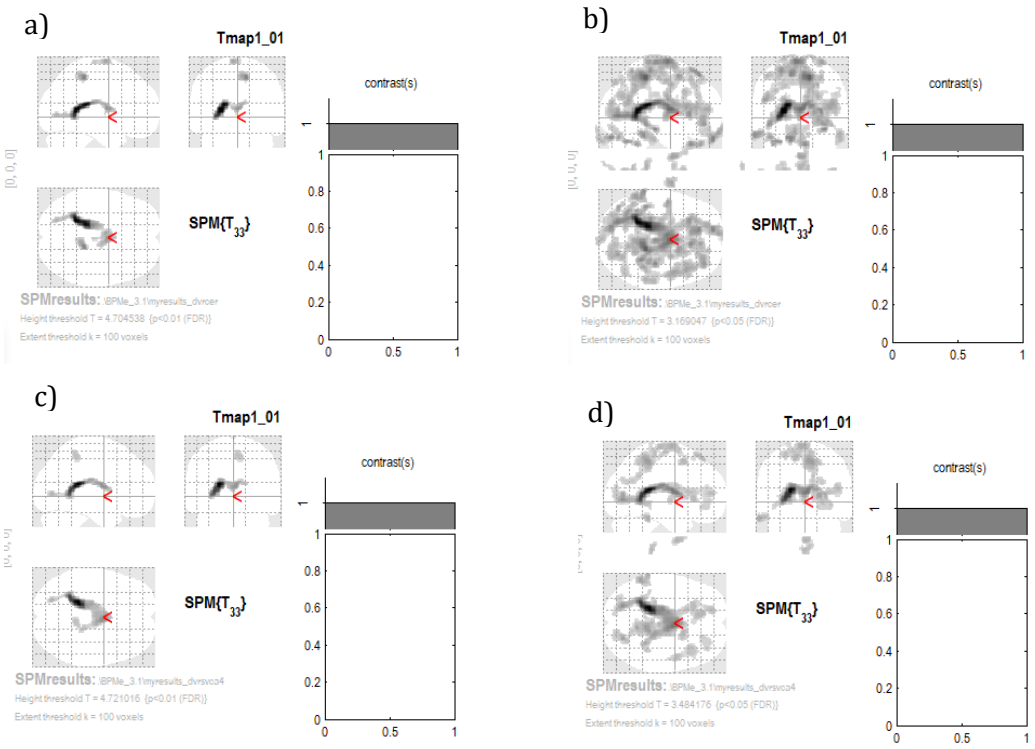

Figure 14 - Correlation at voxel level between DVR PK and SUVr PiB PET images. To visualize in SPM5 it was defined in a) and c) a p-value < 0.01 and in b) and d) p-value < 0.05 and 100 voxels as extent threshold. In a) and b) DVR PK was normalized using CER and in c) and d) using SVCA4. For both cases SUVr PiB was normalized using CER.

Table 10 - Correspondence between the coordinates of the found clusters in DVR PK PET images normalized by CER and SVCA4, and the brain regions [77, 78].

DVR PK reference region	Cluster's coordinates	Brain Region
CER	(-24; -46; 10)	Outside defined Brodmann's Areas (BAs)
	(12; -36; 54)	
	(-12; 60; -28)	
	(-18; -84; -28)	
	(-6; -4; 76)	Left-BA6 (Premotor Cortex)
	(-64; -38; -24)	Left-BA21 (Middle Temporal Gyrus)
	(8; 28; -36)	Right-BA11 (Orbitofrontal Cortex)
	(-26; -28; 64)	Left -PrimMotor (4)
SVCA4	(-20; -38; 16)	Outside defined Brodmann's Areas (BAs)
	(-58; -48; -76)	
	(8; -52; -74)	
	(-4; -6; 76)	
	(2; 4; -52)	
	(6; -40; 56)	Right-SensoryAssoc (5)
	(20; -72; 8)	Right-PrimVisual (17)
	(-64; -38; -22)	Left-BA21 (Middle Temporal Gyrus)
	(14; 12; 56)	Right-BA6 (Premotor Cortex)

According with the Figure 14 and Table 10, when SUVr PiB PET images are normalized by CER, for CER as reference region of DVR PK images, there is correlation at voxel level in premotor cortex (Left-BA6), middle temporal gyrus (Left-BA21), orbitofrontal cortex (Right-BA11) and primary motor cortex (Left-PrimMotor (4)) between DVR PK and SUVr PiB of group 4070 PET images. For SVCA4 as reference region, there is correlation at voxel level in primary somatosensory cortex (Right-SensoryAssoc (5)), primary visual cortex (Right-PrimVisual (17)), middle temporal gyrus (Left-BA21) and premotor cortex (Right-BA6).

SUVr PiB PET images using WM as Ref & BP PK PET images

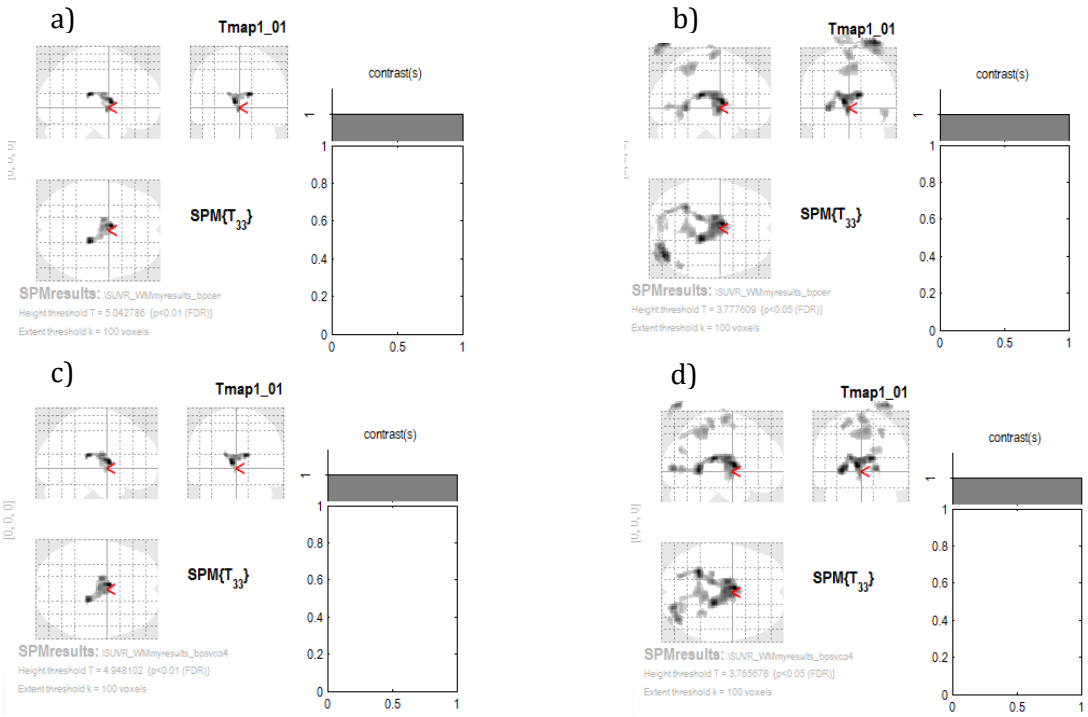

Figure 15 - Correlation at voxel level between BP PK and SUVr PiB PET images. To visualize in SPM5 it was defined in a) and c) a p-value < 0.01 and in b) and d) p-value < 0.05 and 100 voxels as extent threshold. In a) and b) BP PK was normalized using CER and in c) and d) using SVCA4. For both cases SUVr PiB was normalized using WM.

Table 11 - Correspondence between the coordinates of the found clusters in BP PK PET images normalized by CER and SVCA4, and the brain regions [77, 78].

BP PK reference region	Cluster's coordinates	Brain Region
CER	(-6; 4; 8)	Outside defined Brodmann's Areas (BAs)
	(36; -78; 90)	
	(0; -10; 72)	
	(8; -40; 56)	RightSensoryAssoc (5)
	(52; -56; -8)	Right-Fusiform (37)
SVCA4	(-6; 4; 8)	Outside defined Brodmann's Areas (BAs)
	(22; -84; 4)	
	(36; -78; 90)	
	(0; -10; 72)	
	(8; -40; 56)	RightSensoryAssoc (5)
	(-24; -28; 62)	Left-PrimMotor (4)
	(28; -46; 56)	RightSensoryAssoc (5)

According with the Figure 15 and Table 11, when SUVr PiB PET images are normalized by WM, for CER as reference region of BP PK images, there is correlation at voxel level in primary somatosensory cortex (Right-SensoryAssoc (5)) and fusiform gyrus (Right-Fusiform (37)) between BP PK and SUVr PiB of group 4070 PET images. For SVCA4 as reference region, there is correlation at voxel level in primary somatosensory cortex (Right-SensoryAssoc (5)) and primary motor cortex (Left-PrimMotor (4)).

SUVr PiB PET images using WM as Ref & DVR PK PET images

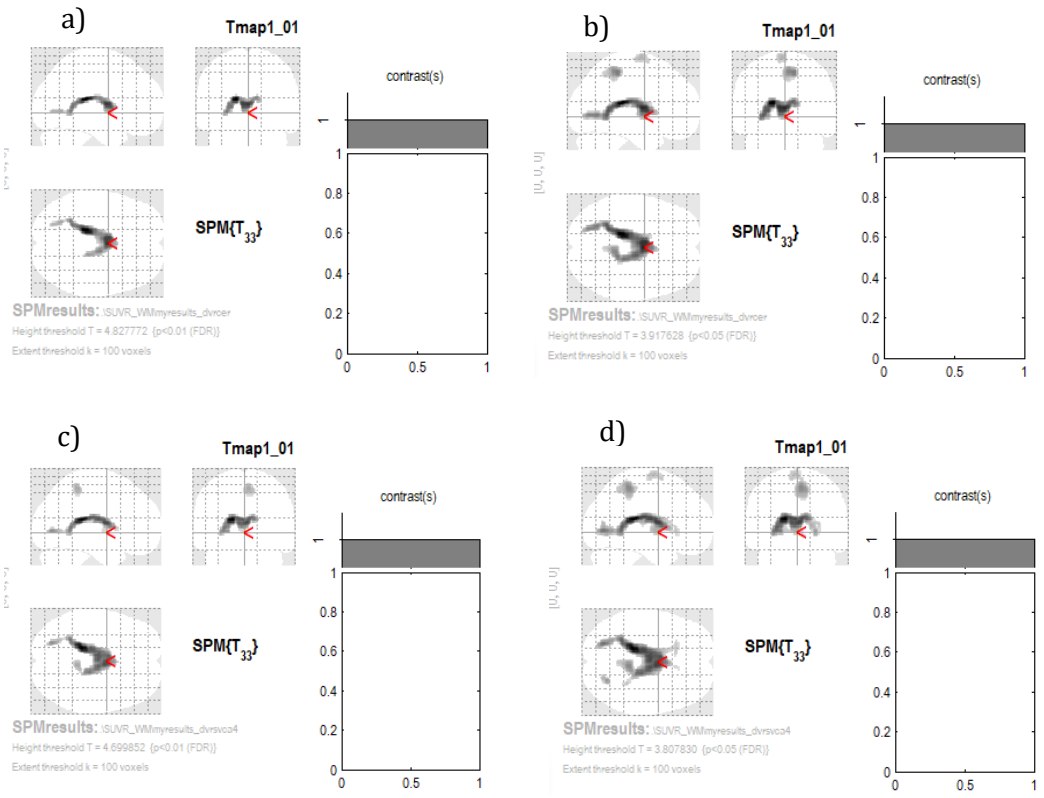

Figure 16 - Correlation at voxel level between DVR PK and SUVr PiB PET images. To visualize in SPM5 it was defined in a) and c) a p-value < 0.01 and in b) and d) p-value < 0.05 and 100 voxels as extent threshold. In a) and b) DVR PK was normalized using CER and in c) and d) using SVCA4. For both cases PiB SUVr was normalized using WM.

Table 12 - Correspondence between the coordinates of the found clusters in DVR PK PET images normalized by CER and SVCA4, and the brain regions [77, 78].

DVR PK reference region	Cluster's coordinates	Brain Region
CER	(-16; -30; 16)	Outside defined Brodmann's Areas (BAs)
	(12; -34; 56)	
	(-4; -4; 74)	Left-BA6 (Premotor Cortex)
SVCA4	(-16; -30; 16)	Outside defined Brodmann's Areas (BAs)
	(-2; -6; 74)	
	(6; -40; 56)	RightSensoryAssoc (5)
	(24; -68; 0)	Right-BA19 (Associative Visual C)

According with the Figure 16 and Table 12, when SUVr PiB PET images are normalized by WM, for CER as reference region of DVR PK images, there is correlation at voxel level in premotor cortex (Left-BA6) between DVR PK and SUVr PiB of group 4070 PET images. For SVCA4 as reference region, there is correlation at voxel level in

primary somatosensory cortex (Right-SensoryAssoc (5)) and visual cortex (Left-BA19 - Associative Visual C).

3.3.2 - Region of Interest (ROI) based analysis

Unlike voxel based analysis, after images alignment and smoothing, it was required to define the brain regions which were more relevant to solve the proposed problem and, consequently, to proceed the images analysis. Thus, comparing with what happen at voxel level, ROI based analysis is more dependent of some pre-defined hypotheses [80].

Feature extraction

PiB PET images feature extraction

Due to physiological differences such as weight and height, the injected radioactivity concentration varies between individuals. Thus, to make the individuals of the group TOT comparable, the sum of all PiB PET images of the group TOT was represented in terms of SUVr. SUVr is a dimensionless ratio used to distinguish between "normal" and "abnormal" levels of uptake. This ratio normalises the uptake values of a ROI to the mean uptake value within a region containing non-specific binding, the reference region [81-83]. In line with this, for group TOT, the features, i.e., the mean intensity values of several brain regions (PC, OC, MTC, PI, PS, ACing, C, PCing, P, Pmen and B) of SUVr PiB PET images, were extracted according with Equation 1). Where both brain region mean value uptake and reference region (CER, GM, WM) mean value uptake where extracted using masks defined on the T1 MRI template ICBM152 in Mango software. On the other hand, for group 4070 the features were extracted just using masks defined on the T1 MRI template ICBM152 using two different reference regions: CER and WM.

These brain regions were chosen according with the criteria used by the nuclear physicians to label a PET image as PiB positive. For the subjects with more than one scan, i.e., more than one dynamic PET acquisition, the SUVr considered resulted from the mean of the SUVr of each scan.

1) $SUVr = \frac{Brain\ region\ mean\ value\ uptake}{Reference\ region\ mean\ value\ uptake}$;

PK PET images feature extraction

PK PET images were quantified in six different ways: 1) $SUVr_{4060\text{-}CER}$; 2) $SUVr_{4060\text{-}SVCA4}$; 3) $BP_{4060\text{-}CER}$; 4) $BP_{4060\text{-}SVCA4}$; 5) $DVR_{4060\text{-}CER}$ and 6) $DVR_{4060\text{-}SVCA4}$. From 1) to 4) the mean intensity values of the same brain regions used in PiB PET images (PC, OC, MTC, PI, PS, ACing, C, PCing, P, Pmen and B) were extracted using brain masks, defined on the T1 MRI template ICBM152 for 2mm resolution in Mango software. More regions were extracted in 3) to 6) PK PET images: FL; TL; FTS; SFG; MFG; PG; IFG; STG; MTG; ITG; A; H; IPL; and SPL. These "new" brain regions were chosen according with the information gathered by the group Bradburn et al. and based on the voxel based analysis results obtained from the comparison between AD and HC groups of different quantified PK PET images [79].

FEATURE SELECTION

Feature selection is one of the core concepts in machine learning. It allows a faster training of the algorithm, reduces the complexity of the model and makes it easier to interpret, improves the accuracy of the model, when the right subset of features is selected to train the machine learning model, and avoids overfitting [84, 85]

There are three main different approaches to do the feature selection: 1) filter-based feature selection; 2) wrapper-based feature selection; and 3) embedded-based feature selection [85].

In the present study, two filter-based feature selection approaches were applied: independent two sample T-test and principal component analysis (PCA) technique. The independent two sample T-test is a univariate approach since it involves the analysis of a single variable at a time. On the other hand, PCA technique is a multivariate approach considering it examines two or more variables at once [86].

The independent two sample T-test was applied to all quantified PET images and PCA technique just in the cases where 5 or more features resulted from the independent two sample T-test, and in a dataset of several features extracted from SUVr PiB PET images of group 4070 and BP and DVR PK PET images of group 4060.

In order to avoid overfitting the rule of thumb of using just one feature for each five subjects was adopted. In line with this, a subset of 7 features for group TOT and 8 features for the rest of the cases was stipulated to be obtained by each one of these approaches (two sample T-test and PCA) [85].

Fisher's F-test and two sample T-test

In this univariate test, the means of each variable (features –mean intensity values of the brain region considered) of the two groups (AD and HC) are compared under the assumption that both samples are random, independent and came from normally distributed population, with unknow but equal variances [87]. In line with this, before proceeding with the two sample T-test, it was verified if the variances of each variable were equal, i.e., if they were homogeneous. To do that, Fisher's F-test was performed. If the p-value obtained in this test was greater than 0.05 the two variances were considered homogeneous (equal variances), otherwise they were non-homogeneous. Two sample T-test was implemented according with this information [87].

As results of the two sample T-test, it was obtained the p-value and the mean of each feature for each group, AD and HC. If the p-value of the two sample T-test was lower than 0.05 the null hypothesis - the means of the measurement variable for each sample are equal - was rejected and the feature was selected. In accordance with the rule of thumb of using just one feature for each five subjects, the 7 (group TOT) and 8 (rest of the cases) features with the lowest p-values that had passed the two sample T-test, i.e., that had a p-value lower than 0.05, were the chosen ones to build the binary classifier [87, 88].

The results of the Fisher's F-test and two sample T- test, the percentage difference of sample means and the global percentage difference are presented in the Appendix A (Table(A) 1 to Table(A) 11). The global percentage difference was

calculated by the mean of the percentage difference of sample means, for the features with two sample T-test p-value lower than 0.05.

Graphics 1 to 6 were constructed according with the two sample T-test p-value present in Table(A) 1 to Table(A) 5 and Table(A) 8 of Appendix A.

SUVr PiB of group TOT (Ref -CER)

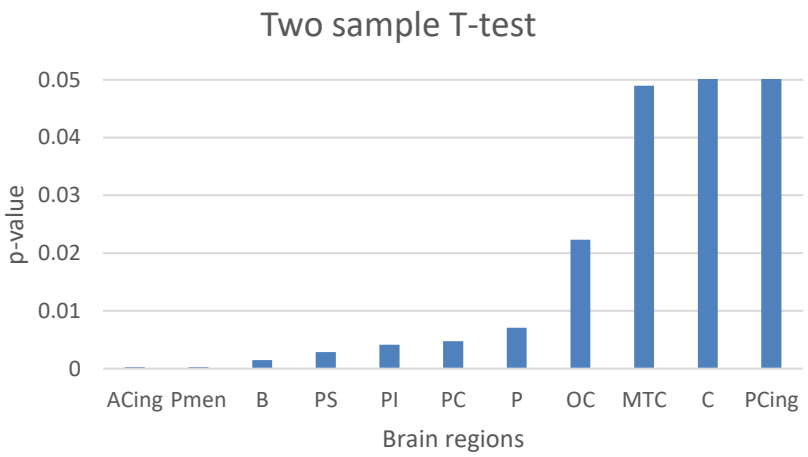

Graphic 1 - Brain regions (x-axis) in increasing order of two sample T-test p-value (y-axis) for SUVr PiB of group TOT using CER as reference region.

The features that failed the two sample T-test, C and PCing, were automatically excluded. In the horizontal axis (x-axis) of Graphic 1 is present the brain regions in increasing order of two sample T-test p-value. According with that, the 7 features selected to build the classifier were the Acing, Pmen, B, PS, PI, PC and P. A classifier only based on features extracted from SUVr PiB PET images of the group TOT when the CER is used as reference region.

SUVr PiB of group TOT (Ref -GM)

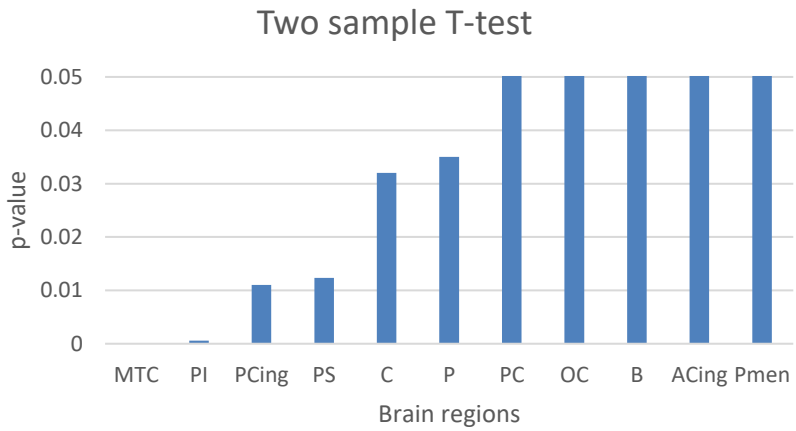

Graphic 2- Brain regions (x-axis) in increasing order of two sample T-test p-value (*y*-axis) for SUVr PiB of group TOT using GM as reference region.

For this specific case just 6 features, MTC, PI, PCing, PS, C, and P passed the two sample T-test; and so, these were the ones selected to build the classifier. A classifier only based on features extracted from SUVr PiB PET images of the group TOT, when the GM is used as reference region. It is important to mentioned that it was stated a length of 7 features to construct the binary classifier to avoid under and overfitting. Another important aspect is the negative percentage difference of sample means of the features MTC, PCing and C (Appendix A Table(A) 2). Since they have a negative percentage difference of sample means, *a priori* these features do not have clinical meaning. Thus, it is logical to postulate that GM probably do not represent the best reference region to do the normalization of PiB PET images.

To test if these conditions have a negative influence in the performance of the classifier, an additional classifier using 7 features and avoiding MTC, PCing and C was constructed.

SUVr PiB of group TOT (Ref -WM)

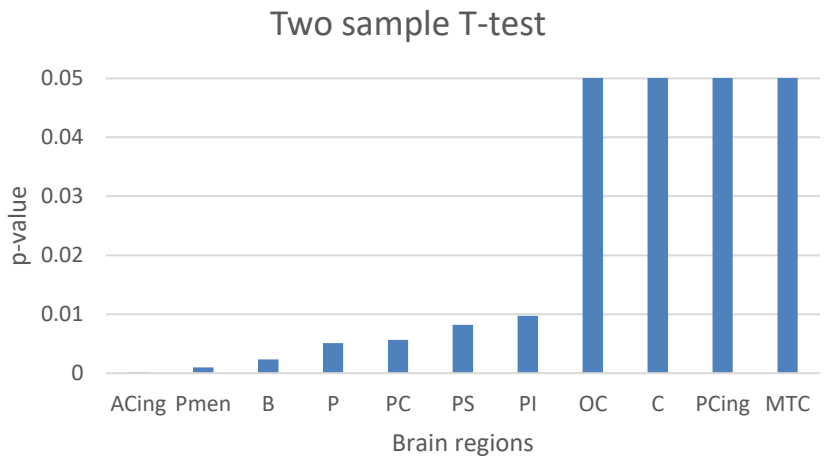

Graphic 3 - Brain regions (x-axis) in increasing order of two sample T-test p-value (y-axis) for SUVr PiB of group TOT using WM as reference region.

The features that failed the two sample T-test, OC, C, PCing and MTC, were automatically excluded. In the horizontal axis (x-axis) of Graphic 3 is present the brain regions in increasing order of two sample T-test p-value. According with that, the 7 features selected to build the classifier were Acing, Pmen, B, P, PC, PS and PI. A classifier only based on features extracted from SUVr PiB PET images of the group TOT, when the WM is used as reference region.

The global percentage difference (%) obtained for PiB PET images of group TOT were 30.811%, 0.650% and 22.371%, for CER, GM and WM as reference region, respectively (Appendix A - Table(A) 1 to Table(A) 3). Due to the low global percentage difference (%) obtained when the GM was used as reference region (0.650%), this reference region was not used in PiB PET images of group 4070.

SUVr PiB of group 4070 (Ref -CER)

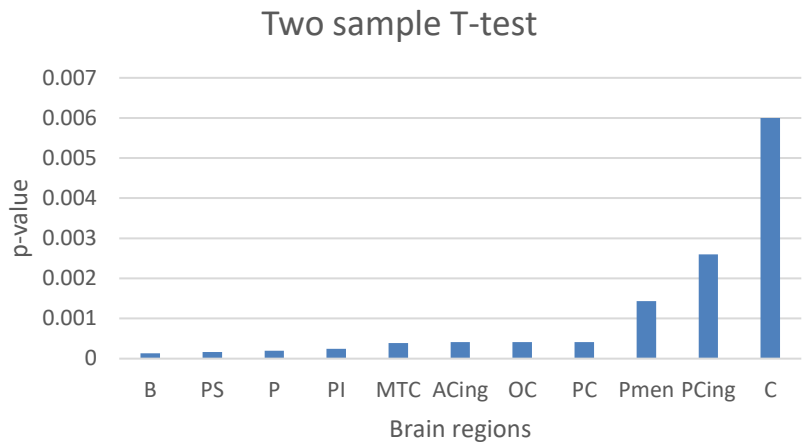

Graphic 4 - Brain regions (x-axis) in increasing order of two sample T-test p-value (y-axis) for SUVr PiB of group 4070 using CER as reference region.

For this specific case all the features passed the two sample T-test; and so, none of these features were automatically excluded. In the horizontal axis (x-axis) of Graphic 4 is present the brain regions in increasing order of two sample T-test p-value. According with that, the 8 features selected to build the classifier were the B, PS, P, PI, MTC, Acing, OC and PC. A classifier only based on features extracted from SUVr PiB PET images of the group 4070 when the CER was used as reference region

SUVr PiB of group 4070 (Ref -WM)

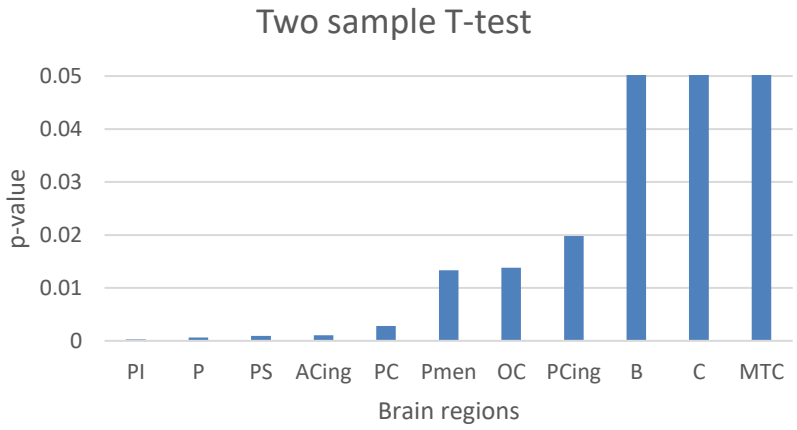

Graphic 5 - Brain regions (x-axis) in increasing order of two sample T-test p-value (y-axis) for SUVr PiB of group 4070 using WM as reference region.

The features that failed the two sample T-test, B, C and MTC, were automatically excluded. In the horizontal axis (x-axis) of Graphic 5 is present the brain regions in increasing order of two sample T-test p-value. According with that, the 8 features selected to build the classifier were PI, P, PS, Acing, PC, Pmen, OC and PCing. A classifier only based on features extracted from SUVr PiB PET images of the group 4070 when the WM is used as reference region.

The global percentage difference (%) obtained for PiB PET images of group 4070 were 40.245% and 19.975%, for CER and WM as reference region, respectively (Appendix A- Table(A) 4 and Table(A) 5).

SUVr PK of group 4060

From the results of Table(A) 6 and Table(A) 7 present in Appendix A, it is possible to verify that all the features extracted from SUVr PK PET images for both reference regions (CER and SVCA4) failed the two sample T-test. Due to these results, none of these features were selected; and so, no classifier only based on features extracted from SUVr PK PET images was constructed. For the same reasons, the global percentage difference (%) was not to calculated.

BP PK of group 4060 (Ref -CER)

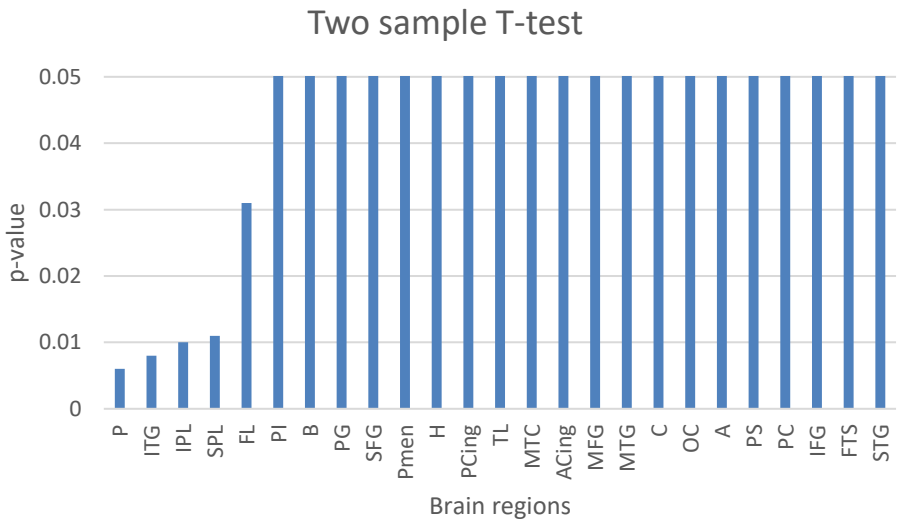

Graphic 6 - Brain regions (x-axis) in increasing order of two sample T-test p-value (y-axis) for BP PK of group 4060 using CER as reference region.

For this specific case just 5 features, P, ITG, IPL, SPL, FL passed the two sample T-test. It was established a length of 8 features to construct the binary classifier to avoid under and overfitting. Since a classifier constructed just using these 5 features would be probably underfitting, no classifier only based on features extracted from PK BP PET images using CER as reference region, was constructed.

BP PK of group 4060 (Ref-SVCA4)

For this specific case, just IPL, SPL and P passed the two sample T-test (Appendix A – Table(A) 9). Due to these results, no classifier only based on features extracted from BP PK 4060 images, when the SVCA4 is used as reference region was constructed.

According with these results, it is logical to postulate that PK biodistribution among groups is not related to any, besides P, characteristic brain region of PiB positive PET images; and so, these brain regions were not tested for DVR PK PET images.

The global percentage difference (%) obtained for BP PK PET images of group 4060 were 2.320% and 4.100%, for CER and SVCA4 as reference region, respectively (Appendix A- Table(A) 8 and Table(A) 9).

DVR PK of group 4060

Besides SFG and P and SFG, all features extracted from DVR PK PET images for CER and SVCA4 as reference region, respectively, failed the two sample T-test (Appendix A- Table(A) 10 and Table(A) 11). Due to these results, no classifier only based on features extracted from DVR PK PET images was constructed.

The global percentage difference (%) obtained for DVR PK PET images of group 4060 were 3.100% for both CER and SVCA4 as reference region (Appendix A- Table(A) 10 and Table(A) 11).

A summary of the most relevant results obtained in this section – feature selection, two sample T-test, are presented in the Table 13.

Table 13 - Part of the results obtained in this section- feature selection, two sample T-test.

PET images	Reference region	Nº of features w/ p-value < 0.05	Global percentage difference (%)
SUVr PiB of group TOT	CER	9/11	30.811
	GM	6/11	0.650
	WM	7/11	22.371
SUVr PiB of group 4070	CER	All (11/11)	40.245
	WM	8/11	19.975
BP PK of group 4060	CER	5/25	2.320
	SVCA4	3/25	4.100
DVR PK of group 4060	CER	2/15	3.100
	SVCA4	1/15	3.100

In comparison with PK PET images, PiB PET images present higher values for the ratio between the features that passed the two sample T-test and the total considered features and for the global percentage difference (Table 13).

PCA technique

PCA was the second approach used to select the features to construct the binary classifier. PCA is a valuable linear transformation technique normally used in datasets with many features. This technique identifies the existing correlation between the features - if a strong correlation between features exists, the attempt to reduce the dimensionality is required. In line with this, PCA take the dataset with many variables, and simplify it turning the original variables into a smaller number of new variables, the "Principal Components". This linear transformation fits the dataset to a new coordinate system. The most variance is found on the first coordinate, and each subsequent coordinate is orthogonal to the last and explain a lesser variance [89, 90]. The features with the highest contribution to the “Principal Component” with the most variance, the first “Principal Component”, are probably the most relevant ones to construct the classifier. Thus, this was the criterion used to select the features by PCA technique. It is important to notice that the higher the variance of the first “Principal Component” better will be the approximation assumed by this criterion.

Before performing the PCA technique, it was necessary to guarantee standardization, i.e., the different variables were mapped to the same scale. This task

was done according with the Equation 2), where standardized variables (x_i') were the result of the subtraction of the variable mean (μ) to each observed value of the variable (x_i) divided by the variable standard deviation (σ) [91].

2) $x_i' = \frac{x_i - \mu}{\sigma}$;

After standardization, PCA technique was performed on different sets of features extracted from different quantified PET images: three sets composed by the features extracted from SUVr PiB PET images of group TOT for CER, GM and WM as reference region; other two sets composed by the features extracted from SUVr PiB PET images of group 4070 for CER and WM as reference region; the sixth set composed by the features extracted from BP PK PET images of group 4060 for CER as reference region; and the last one by a mixture of features with the lowest two sample T-test p-value, and thus probably the most relevant ones to construct the classifier. The last set of features, extracted from SUVr PiB 4070, BP and DVR PK 4060 PET images of 39 subjects (18 AD and 21 HC), was composed by:

- PC, PI, PS, ACing and P of SUVr PiB 4070 PET images (CER and WM as Ref);
- B of SUVr PiB 4070 PET images (CER as Ref);
- IPL, P and SPL of BP PK 4060 PET images (CER and SVCA4 as Ref);
- SFG of DVR PK 4060 PET images (CER and SVCA4 as Ref);
- P of DVR PK 4060 PET images (CER as Ref).

SUVr PiB of group TOT (Ref-CER)

In Figure(B) 1 of Appendix B is presented the percentage of variance of each "Principal Component" for this case, SUVr PiB of group TOT using CER as reference region. The first "Principal Component", Dim.1, explains 66.464% of the total variance, which means that nearly all the information (84.170%) in the dataset (11 variables) can be encapsulated just by the first two "Principal Components", Dim.1(66.464%) and Dim2 (17.706%).

The Graphic 7, brain regions (x-axis) in decreasing order of the percentage of contribution to the first "Principal Component" (y-axis), was constructed according with the information present in Figure(B) 2 of Appendix B.

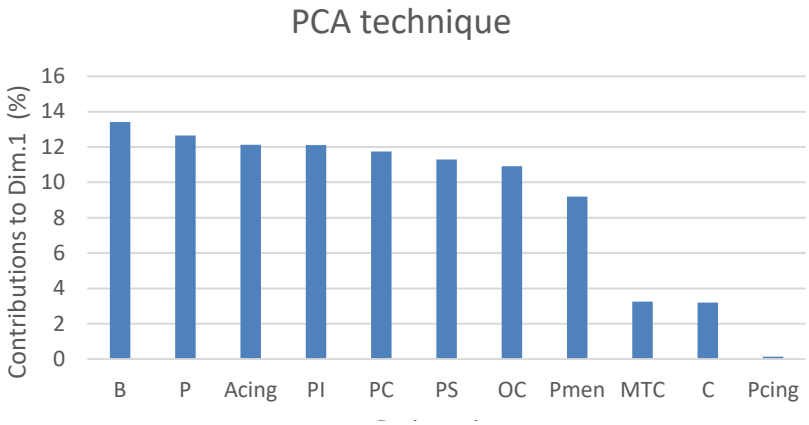

Graphic 7 - Brain regions (x-axis) in decreasing order of the percentage of contribution to the first "Principal Component" (y-axis), Dim.1, for SUVr PiB of group TOT using CER as reference region.

According with the contributions of each variable to the first "Principal Component" presented in Graphic 7, B, P, Acing, PI, PC, PS and OC were the 7 selected features to construct the classifier. A classifier only based on SUVr PiB PET images of group TOT for CER as reference region.

SUVr PiB of group TOT (Ref-GM)

In Figure(B) 3 of Appendix B is presented the percentage of variance of each "Principal Component" for this case, SUVr PiB of group TOT using GM as reference region. Dim.1, Dim.2 and Dim.3 explains 48.127%, 19.407% and 10.455%, respectively, of the total variance, which means that nearly all the information (77,989%) in the dataset (11 variables) can be encapsulated by these three principal components.

The Graphics 8, brain regions (x-axis) in decreasing order of the percentage of contribution to the first "Principal Component" (y-axis), was constructed according with the information present in Figure(B) 4 of Appendix B.

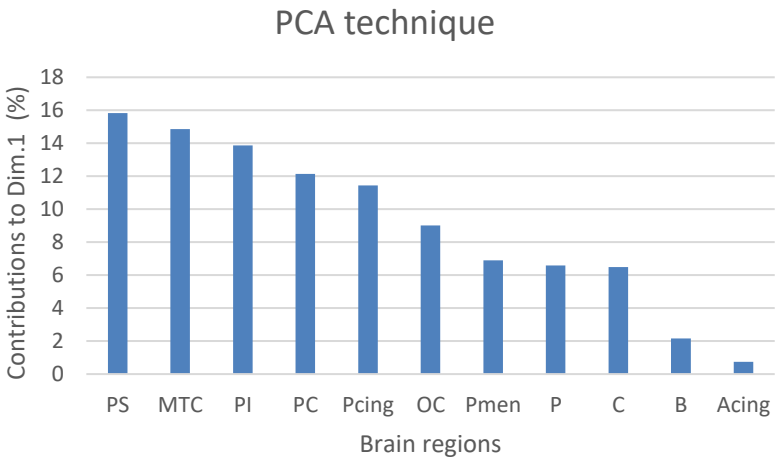

Graphic 8 - Brain regions (x-axis) in decreasing order of the percentage of contribution to the first "Principal Component" (y-axis), Dim.1, for SUVr PiB of group TOT using GM as reference region.

According with the contributions of each variable to the first "Principal Component" present in Graphic 8, PS, MTC, PI, PC, PCing, OC and Pmen were the 7 selected features to construct the classifier. A classifier only based on SUVr PiB PET images of group TOT for GM as reference region.

In the section "two sample T-test" it was mentioned the construction of an additional classifier only based on SUVr PiB PET images of group TOT for GM as reference region. A classifier using 7 features and avoiding the brain regions MTC, PCing and C was constructed according with the information present in Graphic 8. So, the selected features to construct the additional classifier were PS, PI, PC, OC, Pmen, P and B.

SUVr PiB TOT (Ref-WM)

In Figure(B) 5 of Appendix B is presented the percentage of variance of each "Principal Component" for this case, SUVr PiB of group TOT using WM as reference region. The first two "Principal Components", Dim.1 and Dim.2, explains 53.679% and 20.415%, respectively, of the total variance, which means that nearly all the information (74.094%) in the dataset (11 variables) can be encapsulated by these two principal components.

The Graphics 9, brain regions (x-axis) in decreasing order of the percentage of contribution to the first "Principal Component" (y-axis), was constructed according with the information present in Figure(B) 6 of Appendix B.

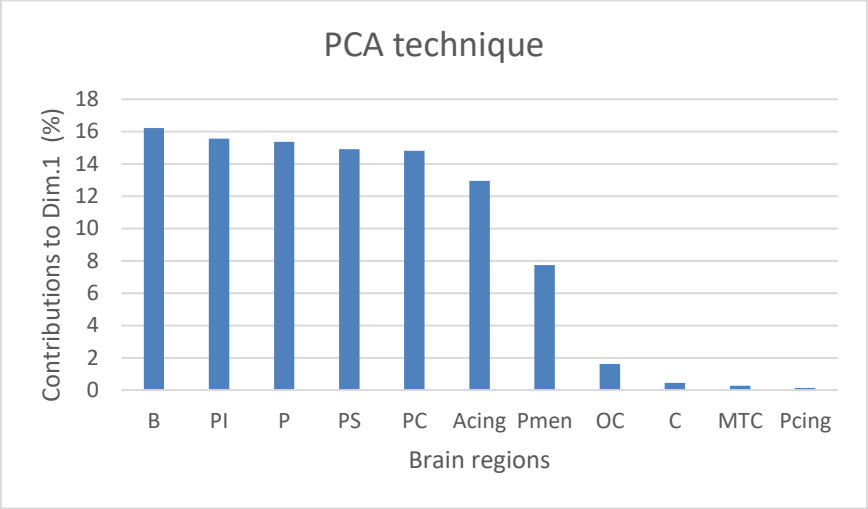

Graphic 9 - Brain regions (x-axis) in decreasing order of the percentage of contribution to the first "Principal Component" (y-axis), Dim.1, for SUVr PiB of group TOT using WM as reference region.

According with the contributions of each variable to the first "Principal Component" present in Graphic 9, B, PI, P, PS, PC, Acing and Pmen were the 7 selected features to construct the classifier. A classier only based on SUVr PiB PET images of group TOT for WM as reference region.

SUVr PiB of group 4070 (Ref-CER)

In Figure(B) 7 of Appendix B is presented the percentage of variance of each "Principal Component" for this case, SUVr PiB of group 4070 using CER as reference region. The first "Principal Component", Dim.1, explains 82,165% of the total variance, which means that nearly all the information in the dataset (11 variables) can be encapsulated just by that one "Principal Component".

The Graphics 10, brain regions (x-axis) in decreasing order of the percentage of contribution to the first "Principal Component" (y-axis), was constructed according with the information present in Figure(B) 8 of Appendix B.

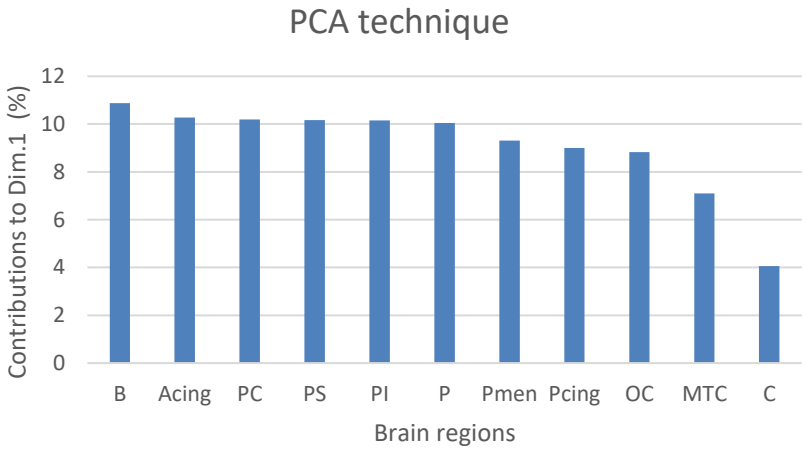

Graphic 10 - Brain regions (x-axis) in decreasing order of the percentage of contribution to the first "Principal Component" (y-axis), Dim.1, for SUVr PiB of group 4070 using CER as reference region.

According with the contributions of each variable to the first "Principal Component" present in Graphic 10, B, Acing, PC, PS, PI, P, Pmen and PCing were the 8 features selected to construct the classifier. A classifier only based on SUVr PiB PET images of group 4070 for CER as reference region.

SUVr PiB PET images of group 4070 (Ref-WM)

In Figure(B) 9 of Appendix B is presented the percentage of variance of each "Principal Component" for this case, SUVr PiB of group 4070 using WM as reference region. Dim.1 explains 61.498% of the total variance, which means that nearly all the information (78.992%) in the dataset (11 variables) can be encapsulated by Dim.1(61.498%) and Dim2 (17.494%).

The Graphics 11, brain regions (x-axis) in decreasing order of the percentage of contribution to the first "Principal Component" (y-axis), was constructed according with the information present in Figure(B) 10 of Appendix B.

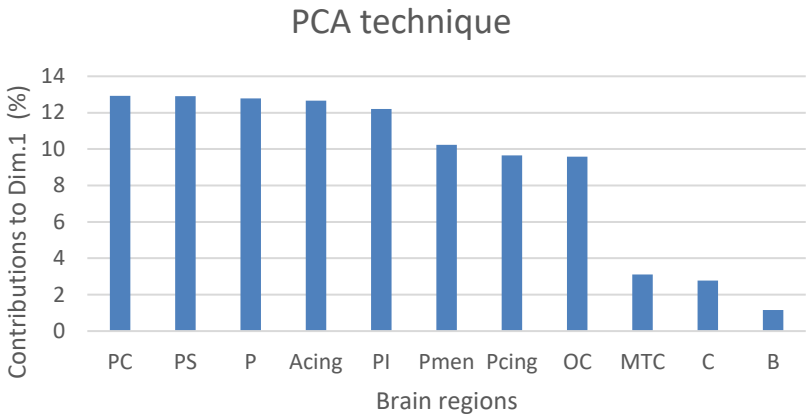

Graphic 11 - Brain regions (x-axis) in decreasing order of the percentage of contribution to the first "Principal Component" (y-axis), Dim.1, for SUVr PiB of group 4070 using WM as reference region.

According with the contributions of each variable to the first "Principal Component" present in Graphic 11, PC, PS, P, Acing, PI, Pmen, PCing and OC were the selected features to construct the classifier. A classifier only based on SUVr PiB PET images of group 4070 for WM as reference region.

BP PK of group 4060 (Ref-CER)

In Figure(B) 11 of Appendix B is presented the percentage of variance of each "Principal Component" for this case, BP PK of group 4060 using CER as reference region. Dim.1 explains 49.442% of the total variance, which means that nearly all the information (70.206%) in the dataset can be encapsulated by Dim.1(49.442%) and Dim2 (20.764%).

The Graphics 12, brain regions (x-axis) in decreasing order of the percentage of contribution to the first "Principal Component" (y-axis), was constructed according with the information present in Figure(B) 12 of Appendix B.

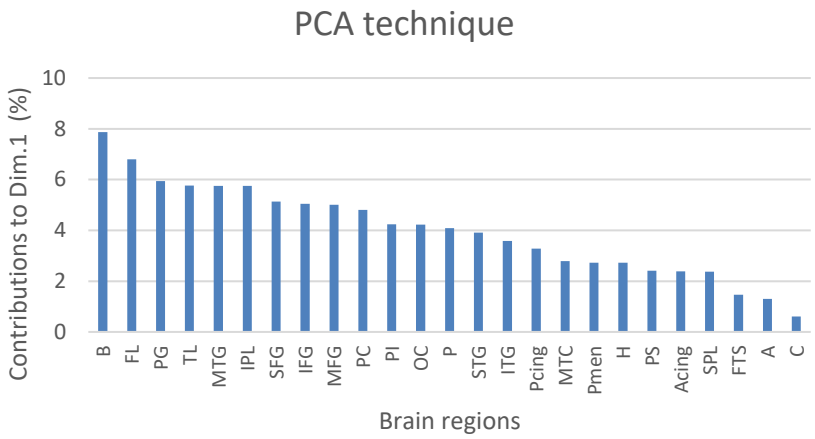

Graphic 12 - Brain regions (x-axis) in decreasing order of the percentage of contribution to the first "Principal Component" (y-axis), Dim.1, for BP PK of group 4060 using CER as reference region.

According with the contributions of each variable to the first "Principal Component" present in Graphic 12, B, FL, PG, TL, MTG, IPL, SFG and IFG were the 8 selected features to construct the classifier. A classifier only based on BP PK PET images of group 4060 for CER as reference region.

Mixture of features extracted from SUVr PiB 4070, BP and DVR PK 4060 PET images

In Figure(B) 13 of Appendix B is presented the percentage of variance of each "Principal Component" for this case, mixture of features extracted from PET images of groups 4070 and 4060. Dim.1 explains 61.262% of the total variance, which means that nearly all the information (80.200%) in the dataset can be encapsulated by Dim.1(61.262%) and Dim2 (18.938%).

The Graphics 13, brain regions (x-axis) in decreasing order of the percentage of contribution to the first "Principal Component" (y-axis), was constructed according with the information present in Figure(B) 14 of Appendix B.

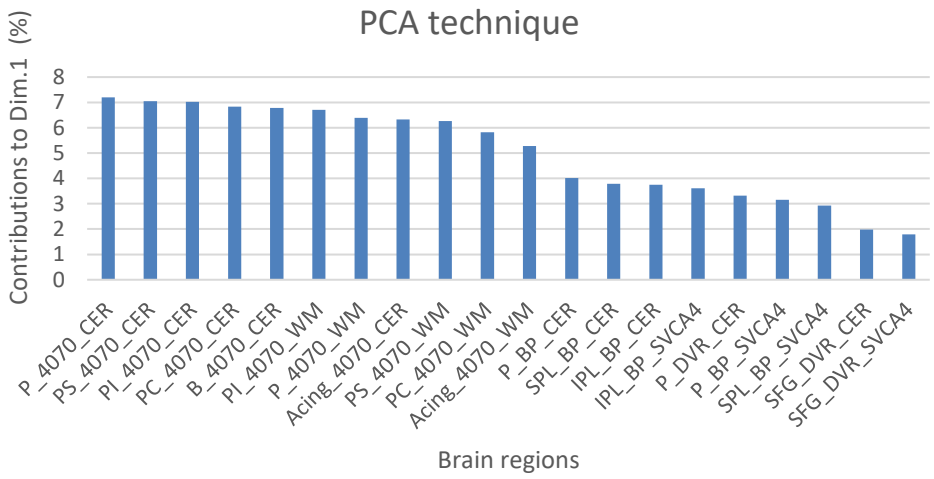

Graphic 13 - Brain regions (x-axis) in decreasing order of the percentage of contribution to the first "Principal Component" (y-axis), Dim.1, for a mixture of features extracted from SUVr PiB of group 4070 and BP and DVR PK of group 4060.

According with the contributions of each variable to the first "Principal Component" present in Graphic 13, five different datasets of features were chosen to construct the binary classifier: 1) the first dataset chosen was composed by P, PS, PI, PC, B and Acing from $SUVr_{4070\text{-}CER}$, and PI and P from $SUVr_{4070\text{-}WM}$; 2) the second was composed by P, PS, PI, PC and B from $SUVr_{4070\text{-}CER}$, and P, SPL and IPL from $BP_{4060\text{-}CER}$; 3) the third was composed by P, PS, PI, PC, B and Acing from $SUVr_{4070\text{-}CER}$, and P from both BP and DVR PK 4060 for CER as reference region; 4) the fourth was composed by P, PS, PI, PC and B from $SUVr_{4070\text{-}CER}$, PI and P from $SUVr_{4070\text{-}WM}$, and P from $BP_{4060\text{-}CER}$; 5) the last dataset was composed by P, PS, PI, PC, B and Acing from $SUVr_{4070\text{-}CER}$, PI from $SUVr_{4070\text{-}WM}$, and P from $BP_{4060\text{-}CER}$.

The datasets obtained by the two feature selection approaches (two sample T-test and PCA technique) are presented in Table 14. The features in bold represent the disagreements of the two features selection approaches.

Table 14 - Different datasets of features obtained by the two feature selection approaches (two sample T-test and PCA technique) used to construct the binary classifiers. Where GM* represents the dataset of features selected to construct the classifier only based on features extracted from SUVr PiB PET images of group TOT using GM as reference region and avoiding features which *a priori* do not have clinical meaning.

		Two sample T-test	**PCA**
SUVr PiB of group TOT	CER	PS, B, PI, PC, P, **Pmen** and Acing	PS, B, PI, PC, P, **OC** and Acing
	GM	PS, MTC, PI, **C**, Pcing and **P**	PS, **PC**, MTC, PI, **OC**, Pcing and **Pmen**
	GM*	-	PS, PI, PC, OC, Pmen, P and B
	WM	PS, PC, Acing, PI, B, Pmen and P	
SUVr PiB of group 4070	CER	P, PI, B, PS, **OC**, Acing, PC and **MTC**	P, PI, B, PS, **PCing**, Acing, PC and **Pmen**
	WM	PS, PC, PI, OC, Acing, Pcing, Pmen and P	
BP PK of group 4060	CER	-	IPL, B, FL, TL, SFG, MTG, IFG and PG
Mixture of features extracted from group 4070 and 4060	1st attempt	-	PI, PS, P, PC, B and Acing from SUVr PiB 4070 (CER as ref.) and PI and P from SUVr PiB 4070 (WM as ref.)
	2nd attempt	-	PI, PS, P, PC, B from SUVr PiB 4070 (CER as ref.) and P, SP and IPL from BP PK 4060 (CER as ref.)
	3rd attempt	-	PI, PS, P, PC, B and Acing from SUVr PiB 4070 (CER as ref.) and P from both BP and DVR PK 4060 (CER as ref.)
	4th attempt	-	PI, PS, P, PC and B from SUVr PiB 4070 (CER as ref.), PI and P from SUVr PiB 4070 (WM as ref.) and P from BP PK 4060 (CER as ref.)
	5th attempt	-	PI, PS, P, PC, B and Acing from SUVr PiB 4070 (CER as ref.), PI from SUVr PiB 4070 (WM as ref.) and P from BP PK 4060 (CER as ref.)

The resulting datasets given by two sample T-test and PCA technique disagreed in three cases: 1) in the selection of one of the features extracted from $SUVr_{TOT\text{-}CER}$, where two sample T-test selected Pmen and PCA OC; 2) in $SUVr_{TOT\text{-}GM}$, where two sample T-test selected C and P and PCA OC, PC and Pmen; 3) and in the selection of two of the features extracted from $SUVr_{4070\text{-}CER}$, where two sample T-test selected OC and MTC and PCA PCing and Pmen (Table 14).

Even though two sample T-test is univariate and PCA technique is multivariate, these two approaches presented similar results in the selection of features extracted from the different quantified PiB PET images.

Classification (CONSTRUCTION OF THE CLASSIFIER IN MATLAB)

To construct the classifier the dataset of features was split in two, training and test sets. The training set was used to build the mathematical model for classification, and in the test set the model was validated.

The ML algorithm chosen to build the mathematical model, in the training set, was the SVM, since it represents a powerful binary classifier appropriate to high dimensional problems. SVM was computed in MATLAB using three different kernels: linear, polynomial (poly) and radial basis function (rbf) [33].

Due to the relatively small subject's dataset size, the model technique used to validate the ML algorithm was the Leave One Out Cross Validation (LOOCV). The LOOCV technique is a cross validation technique that uses a single observation from the subject's dataset to validate the dataset in the test set, while the remaining observations are used to train the classifier. This procedure is repeated until all observations of the dataset have been classified once in the test set [92].

Diagnostic tests determine the presence (test positive) or absence (test negative) of diseases in a subject. The main goal is to achieve a test with the lowest error possible. Test validation is the evaluation method performed to determine how good the diagnostic test is at identifying subjects with and without a disease or condition. To do that, a comparison between the test results and the gold standard, that establishes the true status of the subject, was performed [93, 94].

Table 15 shows the results of a diagnostic test where columns summarise the gold standard results and rows summarise the test results. Subjects with the disease testing positive and negative are denoted by true positive (TP) and false negative (FN), and healthy subjects HC testing positive and negative are denoted by false positive (FP) and true negative (TN). The total number of subjects is given by the sum of TP, FN, FP and TN [94].

Table 15 – Subjects denotation according with the diagnostic tests results (rows) obtained and the results of Gold Standard Test (columns) [94].

Results of diagnostic tests	**Results of Gold Standard Test**	
	Disease present	**Disease absent**
Test positive	True positive (TP)	False positive (FP)
Test negative	False negative (FN)	True negative (TN)

In the present work, to validate the results of the diagnostic tests given by the binary classifiers, three objective measures of test performance were calculated: accuracy, sensitivity and specificity.

The accuracy of the classifier expresses its power to identify correctly subjects with and without the disease. In line with this, the most desire test would have 100% accuracy. The accuracy of a test is calculated by the ratio of true positives (TP) and true negatives (TN), and all evaluated cases. Mathematically, it can be expressed by Equation 3) [93, 94].

3) Accuracy $=\frac{TN+TP}{Total}$;

The sensitivity of the classifier represents its ability to correctly identify subjects with the disease condition. It represents the proportion of subjects with the disease (TP and FN) that are correctly identified by the test (TP). Mathematically, it can be expressed by Equation 4) [93, 94].

4) Sensitivity $=\frac{TP}{TP+FN}$;

Lastly, specificity is the ability of the classifier to correctly identify HC. It is the proportion of healthy subjects (TN and FP) that are correctly identified by the test (TN). Mathematically, it can be expressed by Equation 5) [93, 94].

5) Specificity $=\frac{TN}{TN+FP}$;

Group TOT

Sixteen different classifiers using features extracted from SUVr PiB PET images of the group TOT as input were built. One for each reference region (CER, GM and WM), for each different kernel (linear, rbf and poly) and, for CER and GM, for each feature selection approach. It was also constructed an additional classifier using GM as reference region avoiding the features MTC, PCing and C, which *a priori* do not have clinical meaning.

The results of the three objective measures of test performance, accuracy, sensitivity and specificity, for the classifiers only based on features extracted from SUVr PiB PET images of the group TOT are presented in Tables 16 to 21.

Results of the classifier only based on features extracted from SUVr PiB PET images of group TOT (Ref-CER): feature selection (two sample T-test)

Features dataset length: 7 (B, P, Acing, PI, PC, PS and Pmen)
Subjects dataset length: 35

Table 16 - Confusion matrix results of the classifier only based on features extracted from SUVr PiB PET images of group TOT for CER as reference region. The features used to construct this classifier were selected by the two sample T-test.

Kernel	TN	FN	FP	TP	Accuracy	Sensitivity	Specificity
Linear	18	1	3	13	0.886	0.929	0.857
rbf	18	1	3	13	0.886	0.929	0.857
poly	19	3	2	11	0.857	0.786	0.905

Results of the classifier only based on features extracted from SUVr PiB PET images of group TOT (Ref-CER): feature selection (PCA)

Features dataset length: 7 (B, P, Acing, PI, PC, PS and OC)
Subjects dataset length: 35

Table 17 - Confusion matrix results of the classifier only based on features extracted from SUVr PiB PET images of group TOT for CER as reference region. The features used to construct this classifier were selected by the PCA technique.

Kernel	TN	FN	FP	TP	Accuracy	Sensitivity	Specificity
Linear	18	3	3	11	0.829	0.786	0.857
rbf	17	1	4	13	0.857	0.929	0.810
poly	17	4	4	10	0.771	0.714	0.810

Results of the classifier only based on features extracted from SUVr PiB PET images of group TOT (Ref-GM): feature selection (two sample T-test)

Features dataset length: 6 (MTC, PI, PS, C, Pcing, P)
Subjects dataset length: 35

Table 18 - Confusion matrix results of the classifier only based on features extracted from SUVr PiB PET images of group TOT for GM as reference region. The features used to construct this classifier were selected by the two sample T-test.

Kernel	TN	FN	FP	TP	Accuracy	Sensitivity	Specificity
Linear	17	5	4	9	0.743	0.643	0.810
rbf	16	2	5	12	0.800	0.857	0.762
poly	15	2	6	12	0.771	0.857	0.714

Results of the classifier only based on features extracted from SUVr PiB PET images of group TOT (Ref-GM): feature selection (PCA)

Features dataset length: 7 (PC, MTC, PI, PS, OC, Pcing, Pmen)
Subjects dataset length: 35

Table 19 - Confusion matrix results of the classifier only based on features extracted from SUVr PiB PET images of group TOT for GM as reference region. The features used to construct this classifier were selected by the PCA technique.

Kernel	TN	FN	FP	TP	Accuracy	Sensitivity	Specificity
Linear	18	3	3	11	0.829	0.786	0.857
rbf	16	3	5	11	0.771	0.786	0.762
poly	20	6	1	8	0.800	0.571	0.952

Results of the additional classifier only based on features extracted from SUVr PiB PET images of group TOT (Ref-GM): feature selection (avoiding features which a priori do not have clinical meaning)

Features dataset length: 7 (PS, PI, PC, OC, Pmen, P and B)
Subjects dataset length: 35

Table 20 - Confusion matrix results of the classifier only based on features extracted from SUVr PiB PET images of group TOT for GM as reference region. A classifier constructed avoiding features which *a priori* do not have clinical meaning.

Kernel	TN	FN	FP	TP	Accuracy	Sensitivity	Specificity
Linear	17	3	4	11	0.800	0.786	0.810
rbf	16	6	5	8	0.686	0.571	0.762
poly	15	5	6	9	0.686	0.643	0.714

Results of the classifier only based on features extracted from SUVr PiB PET images of group TOT (Ref-WM): feature reduction (two sample T-test and PCA)

Features dataset length: 7 (B, P, PS, PC, PI, Acing, Pmen)
Subjects dataset length: 35

Table 21 - Confusion matrix results of the classifier only based on features extracted from SUVr PiB PET images of group TOT for WM as reference region.

Kernel	TN	FN	FP	TP	Accuracy	Sensitivity	Specificity
Linear	18	2	3	12	0.857	0.857	0.857
rbf	17	3	4	11	0.800	0.786	0.810
poly	18	5	3	9	0.771	0.643	0.857

The results of accuracy, sensitivity and specificity obtained for the first group studied – group TOT – for the three different reference regions considered, using three distinct kernels and, for CER and GM as reference region, using different features selection approaches, are summarized in Table 22.

Table 22 - Accuracy, sensitivity and specificity of the classifiers build for the group TOT using three different reference region, three distinct kernels and, for CER and GM as reference region, using different features selection approaches. Where * represents the feature selection approach used to construct an additional classifier avoiding features which *a priori* do not have clinical meaning.

		Cerebellum			Grey Matter			White Matter		
		Linear	rbf	poly	Linear	rbf	poly	Linear	rbf	poly
Accuracy	Two sample T-test	0.886	0.886	0.857	0.743	0.800	0.771	0.857	0.800	0.771
	PCA	0.829	0.857	0.771	0.829	0.771	0.800			
	*	-	-	-	0.800	0.686	0.686	-	-	-
Sensitivity	Two sample T-test	0.929	0.929	0.786	0.643	0.857	0.857	0.857	0.786	0.643
	PCA	0.786	0.929	0.714	0.786	0.786	0.571			
	*	-	-	-	0.786	0.571	0.643	-	-	-
Specificity	Two sample T-test	0.857	0.857	0.905	0.810	0.762	0.714	0.857	0.810	0.857
	PCA	0.857	0.810	0.810	0.857	0.762	0.952			
	*	-	-	-	0.810	0.762	0.714	-	-	-

For the classifier only based on SUVr PiB PET images of group TOT, the best set of accuracy (0.886), sensitivity (0.929) and specificity (0.857) was obtained using

both linear and rbf kernel, for CER as reference region and two sample T-test as feature selection approach.

Group 4070

Nine different classifiers, using features extracted from SUVr PiB PET images of the group 4070 as input were built. One classifier for each reference region considered (CER and WM), for each different kernel and, for CER as reference region, one for two sample T-test and another one for PCA technique. The results of the three objective measures of test performance, accuracy, sensitivity and specificity, for the classifiers only based on features extracted from SUVr PiB PET images of the group 4070 are presented in Tables 23 to 25.

Results of the classifier only based on features extracted from SUVr PiB PET images of group 4070 (Ref-CER) feature selection (two sample T-test)

Features dataset length: 8 (PC, PI, PS, Acing, P, B, OC, MTC)
Subjects dataset length: 40

Table 23 - Confusion matrix results of the classifier only based on features extracted from SUVr PiB PET images of group 4070 when the CER is used as reference region and two sample T-test as feature selection approach.

Kernel	TN	FN	FP	TP	Accuracy	Sensitivity	Specificity
Linear	18	2	3	17	0.875	0.895	0.857
rbf	17	0	4	19	0.900	1.000	0.810
poly	18	2	3	17	0.875	0.895	0.857

Results of the classifier only based on features extracted from SUVr PiB PET images of group 4070 (Ref-CER) feature selection (PCA)

Features dataset length: 8 (PC, PI, PS, Acing, P, B, PCing, Pmen)
Subjects dataset length: 40

Table 24 - Confusion matrix results of the classifier only based on features extracted from SUVr PiB PET images of group 4070 when the CER is used as reference region and PCA as feature selection approach.

Kernel	TN	FN	FP	TP	Accuracy	Sensitivity	Specificity
Linear	18	2	3	17	0.875	0.895	0.857
rbf	18	0	3	19	0.925	1.000	0.857
poly	18	4	3	15	0.825	0.790	0.857

Results of the classifier only based on features extracted from SUVr PiB PET images of group 4070 (Ref-WM) feature selection (two sample T-test and PCA)

Features dataset length: 8 (PS, PC, PI, OC, Acing, PCing, Pmen, P)
Subjects dataset length: 40

Table 25 - Confusion matrix results of the classifier only based on features extracted from SUVr PiB PET images of group 4070 when the WM is the reference region.

Kernel	TN	FN	FP	TP	Accuracy	Sensitivity	Specificity
Linear	16	3	5	16	0.800	0.842	0.762
rbf	16	1	5	18	0.850	0.947	0.762
poly	19	2	2	17	0.900	0.895	0.905

The results of accuracy, sensitivity and specificity obtained for the second group studied – group 4070 – for the two different reference regions considered, using three distinct kernels, and, for CER as reference region, using the two features selection approaches, are summarized in Table 26.

Table 26 - Accuracy, sensitivity and specificity of the classifiers build for the group 4070 using two different reference region, three distinct kernels and, for CER as reference region, using two features selection approaches.

		Cerebellum			White Matter		
		Linear	rbf	poly	Linear	rbf	poly
Accuracy	Two sample T-test	0.875	0.900	0.875	0.800	0.850	0.900
	PCA	0.875	0.925	0.825			
Sensitivity	Two sample T-test	0.895	1.000	0.895	0.842	0.947	0.895
	PCA	0.895	1.000	0.790			
Specificity	Two sample T-test	0.857	0.810	0.857	0.762	0.762	0.905
	PCA	0.857	0.857	0.857			

The best results obtained for group 4070 were the ones regarding the features selected by PCA technique with the CER as reference region and the rbf as kernel; accuracy of 0.925, sensitivity of 1.000 and specificity of 0.857.

Group 4060

Three different classifiers using features extracted from BP PK PET images of the group 4060 as input were built. One classifier for each different kernel using CER as reference region and PCA technique as feature selection approach.

The results of the three objective measures of test performance, accuracy, sensitivity and specificity, for the classifiers only based on features extracted from BP PK PET images of the group 4060 are presented in Table 27.

Results of the classifier only based on features extracted from BP PK PET images of group 4060 (Ref-CER) feature selection (PCA)

Features dataset length: 8 (B, FL, TL, SFG, IFG, MTG, PG, IPL)
Subjects dataset length: 40

Table 27 - Confusion matrix results of the classifier only based on features extracted from BP PK PET images of group 4060 when the CER is used as reference region and PCA as feature selection approach.

Kernel	**TN**	**FN**	**FP**	**TP**	**Accuracy**	**Sensitivity**	**Specificity**
Linear	15	8	6	11	0.650	0.579	0.714
rbf	14	16	7	3	0.425	0.158	0.667
poly	11	11	10	8	0.475	0.421	0.524

The best results obtained for the group 4060 were the ones using a linear kernel; accuracy of 0.675, sensitivity of 0.579 and specificity of 0.714.

The binary classifier constructed just using features extracted from BP PK PET images of the group 4060 shows, for all used kernels, a weak performance (Table 27), compared with the performance of the classifier obtained when the features were extracted from the first two groups (TOT - Table 22, and 4070 – Table 26).

Mixture of features extracted from images of groups 4070 and 4060

Fifteen different classifiers based on different combinations of features were constructed. According with PCA technique, these features are the most relevant ones for the construction of the classifier. One classifier for each one of the 5 different features datasets selected by PCA technique and one for each kernel. The results of

the three objective measures of test performance, accuracy, sensitivity and specificity, for these classifiers are presented in Tables 28 to 32.

Results of the classifiers based on different mixture of features (the most relevant ones according with PCA technique to construct the classifier)

1st attempt

Features dataset length: 8
→ From SUVr PiB 4070 (Ref- CER): PI, PS, P, PC, B, Acing
→ From SUVr PiB 4070 (Ref-WM): PI, P
Subjects dataset length: 39

Table 28- Confusion matrix results of the classifier based on different mixture of features extracted from SUVr PiB PET images of group 4070 for CER and WM as reference region.

Kernel	TN	FN	FP	TP	Accuracy	Sensitivity	Specificity
Linear	18	1	3	17	0.897	0.944	0.857
Rbf	18	0	3	18	0.923	1.000	0.857
Poly	17	4	4	14	0.795	0.778	0.810

2nd attempt

Features dataset length: 8
→ From SUVr PiB 4070 (Ref- CER): PI, PS, P, PC, B
→ From BP PK 4060 (Ref- CER): P, SPL, IPL
Subjects dataset length: 39

Table 29 - Confusion matrix results of the classifier based on different mixture of features extracted from SUVr PiB PET images of group 4070 and BP PK PET images of group 4060 for CER as reference region.

Kernel	TN	FN	FP	TP	Accuracy	Sensitivity	Specificity
Linear	16	3	5	15	0.795	0.833	0.762
Rbf	17	2	4	16	0.846	0.889	0.810
Poly	15	5	6	13	0.718	0.722	0.714

3rd attempt

Features dataset length: 8
→ From SUVr PiB 4070 (Ref- CER): PI, PS, P, PC, B, Acing
→ From BP PK 4060 (Ref- CER): P
→ From DVR PK 4060(Ref- CER): P
Subjects dataset length: 39

Table 30 - Confusion matrix results of the classifier based on different mixture of features extracted from SUVr PiB PET images of group 4070, BP and DVR PK PET images of group 4060 for CER as reference region.

Kernel	TN	FN	FP	TP	Accuracy	Sensitivity	Specificity
Linear	18	2	3	16	0.872	0.889	0.857
Rbf	16	3	5	15	0.795	0.833	0.762
Poly	18	3	3	15	0.846	0.833	0.857

4th attempt

Features dataset length: 8

→ From SUVr PiB 4070 (Ref- CER): PI, PS, P, PC, B

→ From SUVr PiB 4070 (Ref- WM): PI, P

→ From BP PK 4060 (Ref- CER): P

Subjects dataset length: 39

Table 31 - Confusion matrix results of the classifier based on different mixture of features extracted from SUVr PiB PET images of group 4070 for CER and WM as reference region and BP PK PET images of group 4060 for CER as reference region.

Kernel	TN	FN	FP	TP	Accuracy	Sensitivity	Specificity
Linear	18	2	3	16	0.872	0.889	0.857
rbf	18	2	3	16	0.872	0.872	0.872
poly	19	3	2	15	0.872	0.833	0.905

5th attempt

Features dataset length: 8

→ From SUVr PiB 4070 (Ref- CER): PI, PS, P, PC, B, Acing

→ From SUVr PiB 4070 (Ref- WM): PI

→ From BP PK 4060 (Ref- CER): P

Subjects dataset length: 39

Table 32 - Confusion matrix results of the classifier based on different mixture of features extracted from SUVr PiB PET images of group 4070 for CER and WM as reference region and BP PK PET images of group 4060 for CER as reference region.

Kernel	TN	FN	FP	TP	Accuracy	Sensitivity	Specificity
Linear	18	2	3	16	0.872	0.889	0.857
rbf	18	0	3	18	0.923	1.000	0.857
poly	19	1	2	17	0.923	0.944	0.905

In Table 33 is presented the most relevant results obtained in this section, ROI based analysis – classification.

Table 33 - Part of the results obtained in this section, ROI based analysis - classification.

Classifier input	Accuracy	Sensitivity	Specificity	Feature selection approach	Kernel
$SUVr_{TOT-CER}$	0.886	0.929	0.857	Two sample T-test	Linear and rbf
$SUVr_{TOT-GM}$	0.829	0.786	0.857	PCA	Linear
$SUVr_{TOT-WM}$	0.857	0.857	0.857	Both	linear
$SUVr_{4070-CER}$	**0.925**	**1.000**	**0.857**	PCA	rbf
$SUVr_{4070-WM}$	0.900	0.895	0.905	Both	poly
$BP_{4060-CER}$	0.675	0.632	0.714	Two sample T-test	linear
First attempt ($SUVr_{4070-CER}$ and $SUVr_{4070-WM}$)	0.923	1.000	0.857	PCA	rbf
Fifth attempt ($SUVr_{4070-CER}$, $SUVr_{4070-WM}$ and $BP_{4060-CER}$)	0.923	0.944	0.905	PCA	poly

Both for CER and for WM the binary classifier with the best results were the ones using the second group (group 4070) as input classifier. Within the group 4070 the classifier using CER as reference region was the one presenting the best performance (bold in Table 33).

In Table 33 it is possible to verify that the fifth attempt presents a slightly lower value for accuracy (0.923) and sensitivity (0.944), when compared to the overall binary classifier with the best performance obtained - accuracy of 0.925 and sensitivity of 1 (bold in the Table 33). However, it was the one that presented the best specificity performance (0.905).

CORRELATION AT REGIONAL LEVEL BETWEEN BP PK PET IMAGES OF GROUP 4060 AND SUVR PIB PET IMAGES OF GROUP 4070

There are three main methods to perform correlation analysis, Pearson correlation, Kendall rank correlation and Spearman [95].

Pearson correlation, also known as parametric correlation test, is represented by the Pearson correlation coefficient and expresses the strength of the linear association between two variables. Since this method can only be performed when the two variables present a normal distribution, Shapiro-Wilk test was used to check the normality of the variables. If the two p-values of the variables under correlation were greater than the significance level, 0.05, the distribution of the data were not significantly different from normal distribution and the normality was assumed. The p-value obtained in the Shapiro-Wilk test are presented in Table 34 [95, 96].

On the other hand, the Kendall rank correlation and Spearman are non-parametric rank-based measures of association. Both methods can be used in data randomly distributed, i.e., in data that did not pass the Shapiro-Wilk test [95, 96].

Correlation coefficients (r) take a range of values between -1 to +1. A value of 0 indicates that there is no correlation between the two variables and values greater and less than 0 indicates a positive and negative association, respectively. Stronger correlations of the two variables is associated to *r* values closer to either +1 or -1 depending on whether the relationship is positive or negative, respectively [95].

Table 34 - p-value obtained in the Shapiro-Wilk test for the different considered features.

	Shapiro-Wilk test (p-value)			
	$SUVr_{4070\text{-}CER}$	**$BP_{4060\text{-}CER}$**	**$SUVr_{4070\text{-}WM}$**	**$BP_{4060\text{-}SVCA4}$**
PC	0.003	0.619	0.003	0.011
OC	5.076E-03	3.435E-04	0.006	0.007
MTC	0.044	0.145	0.919	0.605
PI	0.006	0.033	0.002	0.214
PS	0.012	0.048	0.005	0.011
Acing	0.010	0.042	0.016	0.879
C	0.163	0.438	0.043	0.616
P	0.002	0.431	6.286E-04	0.172
PCing	0.054	0.260	0.238	0.059
Pmen	0.001	0.226	0.036	0.560
B	0.012	0.128	1.261E-05	0.473

As it was mentioned, to apply Pearson correlation, the two p-values obtained in the Shapiro-Wilk test of the variables under correlation need to be greater than the significance level 0.05. Table 35 shows the variables were the Pearson correlation can be (✓) or not (✗) be applied.

Table 35 - Pair of variables were the Pearson correlation can be or not be applied.

		Shapiro-Wilk test (result)	
		$SUVr_{4070\text{-}CER}$	**$SUVr_{4070\text{-}WM}$**
PC	**$BP_{4060\text{-}CER}$**	✗	✗
	$BP_{4060\text{-}SVCA4}$	✗	✗
OC	**$BP_{4060\text{-}CER}$**	✗	✗
	$BP_{4060\text{-}SVCA4}$	✗	✗
MTC	**$BP_{4060\text{-}CER}$**	✗	✓
	$BP_{4060\text{-}SVCA4}$	✗	✓
PI	**$BP_{4060\text{-}CER}$**	✗	✗
	$BP_{4060\text{-}SVCA4}$	✗	✗
PS	**$BP_{4060\text{-}CER}$**	✗	✗
	$BP_{4060\text{-}SVCA4}$	✗	✗
Acing	**$BP_{4060\text{-}CER}$**	✗	✗
	$BP_{4060\text{-}SVCA4}$	✗	✗
C	**$BP_{4060\text{-}CER}$**	✓	✗
	$BP_{4060\text{-}SVCA4}$	✓	✗
P	**$BP_{4060\text{-}CER}$**	✗	✗
	$BP_{4060\text{-}SVCA4}$	✗	✗
PCing	**$BP_{4060\text{-}CER}$**	✓	✓
	$BP_{4060\text{-}SVCA4}$	✓	✓
Pmen	**$BP_{4060\text{-}CER}$**	✗	✗
	$BP_{4060\text{-}SVCA4}$	✗	✗
Brain	**$BP_{4060\text{-}CER}$**	✗	✗
	$BP_{4060\text{-}SVCA4}$	✗	✗

In consonance with the results of Table 35, Pearson correlation was applied in eight pairs of variables (test result - ✓). Since Spearman can be used in data that do not come from a bivariate normal distribution, all data was applied using this method of correlation analysis.

In Table 36 is presented the results of the p-values and the coefficients of correlation, r, given by Pearson and Spearman correlation.

Table 36 - P-values and the coefficients of correlation, r, given by Pearson and Spearman correlation.

		$SUVr_{4070\text{-}CER}$				$SUVr_{4070\text{-}WM}$			
		Pearson		**Spearman**		**Pearson**		**Spearman**	
		p-value	**r**	**p-value**	**r**	**p-value**	**r**	**p-value**	**r**
$BP_{4060\text{-}CER}$	PC	-	-	0.415	0.134	-	-	0.899	0.021
	OC	-	-	**0.029**	**0.351**	-	-	0.140	0.240
	MTC	-	-	0.065	0.299	0.594	0.088	0.522	0.105
	PI	-	-	**0.009**	**0.416**	-	-	0.051	0.316
	PS	-	-	0.082	0.282	-	-	0.202	0.209
	ACing	-	-	0.801	-0.042	-	-	0.966	0.007
	C	0.054	0.311	**0.021**	**0.370**	-	-	**0.003**	**0.471**
	P	-	-	**0.002**	**0.489**	-	-	**0.014**	**0.392**
	PCing	0.639	0.077	0.199	0.210	0.813	0.039	0.683	0.067
	Pmen	-	-	0.460	0.122	-	-	0.381	0.144
	B	-	-	0.085	0.280	-	-	0.384	0.143
$BP_{4060\text{-}SVCA4}$	PC	-	-	0.937	-0.013	-	-	0.542	-0.100
	OC	-	-	0.154	0.232	-	-	0.358	0.151
	MTC	-	-	0.478	0.117	0.649	0.075	0.774	0.047
	PI	-	-	**0.012**	**0.399**	-	-	**0.040**	**0.331**
	PS	-	-	0.248	0.189	-	-	0.452	0.124
	ACing	-	-	0.246	-0.190	-	-	0.365	-0.149
	C	0.230	0.197	0.238	0.193	-	-	**0.022**	**0.368**
	P	-	-	**0.002**	**0.475**	-	-	**0.006**	**0.437**
	PCing	0.600	-0.087	0.982	0.004	0.674	-0.070	0.588	-0.089
	Pmen	-	-	0.472	0.119	-	-	0.322	0.162
	B	-	-	0.781	0.046	-	-	0.608	-0.084

Values of Table 36 in bold represent p-values lower than the significance level 0.05. Consequently, the two variables associated to these p-values are significantly correlated.

In the Pearson correlation all pair of features tested presented a p-value higher than the significance level alpha, 0.05. Thus, using this method of analysis no correlation between BP PK and SUVr PiB PET images was found at regional level [95].

In the Spearman eleven pairs of variables presented a p-value less than the significance level alpha. $BP_{4060\text{-}CER}$ and $SUVr_{4070\text{-}CER}$ are correlated positively in OC, PI, C and P, with a correlation coefficient of 0.351, 0.416, 0.370 and 0.489, respectively; $BP_{4060\text{-}CER}$ and $SUVr_{4070\text{-}WM}$ are correlated positively in C and P, with a correlation coefficient of 0.471 and 0.392, respectively; $BP_{4060\text{-}SVCA4}$ and $SUVr_{4070\text{-}CER}$ are correlated positively in PI and P, with a correlation coefficient of 0.399 and 0.475, respectively; and $BP_{4060\text{-}SVCA4}$ and $SUVr_{4070\text{-}WM}$ are correlated positively in PI, C and P, with a correlation coefficient of 0.331, 0.368 and 0.437, respectively [95].

Overall, when using the CER as reference region of PiB PET images, stronger correlation with BP PK PET images were found compared to normalization based on WM. What is possible to see in: P where the correlation coefficient between $BP_{4060\text{-}CER}$ and SUVr PiB PET images normalized by CER is 0.489, greater than 0.392 using WM; and in PI and P where the correlation coefficient between $BP_{4060\text{-}SVCA4}$ and SUVr PiB PET images normalized by CER is 0.399 and 0.475, greater than 0.331 and 0.437, respectively, using WM.

In the Figures bellow, Figures 17 to 20, are presented the scatter plots showing the existing correlation in several brain regions between BP PK of group 4060 and SUVr PiB of group 4070. The *abline()* function was performed in RStudio to add the corresponding regression line, blue line of the Figures 17 to 20 [97].

Positive correlation in different brain regions between $BP_{4060\text{-}CER}$ and $SUVr_{4070\text{-}CER}$

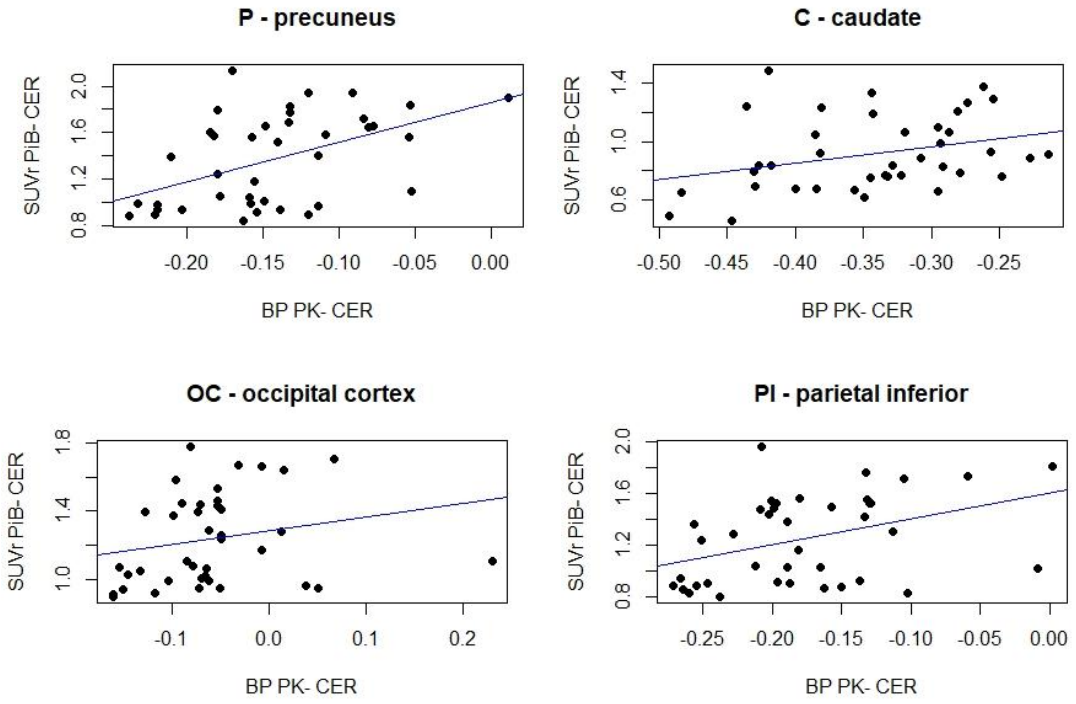

Figure 17 - Scatter plots showing the positive correlation in P, C, OC and PI between $BP_{4060\text{-}CER}$ and $SUVr_{4070\text{-}CER}$.

Positive correlation in different brain regions between $BP_{4060\text{-}CER}$ and $SUVr_{4070\text{-}WM}$

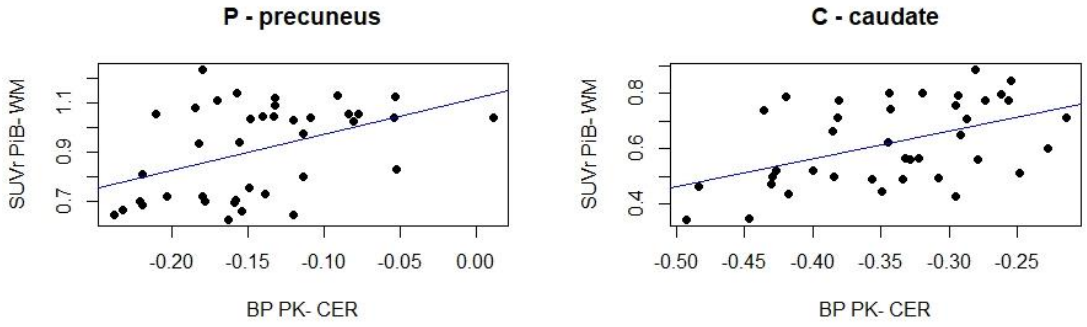

Figure 18 - Scatter plots showing the positive correlation in P and C between $BP_{4060\text{-}CER}$ and $SUVr_{4070\text{-}WM}$.

Positive correlation in different brain regions between $BP_{4060\text{-}SVCA4}$ and $SUVr_{4070\text{-}CER}$

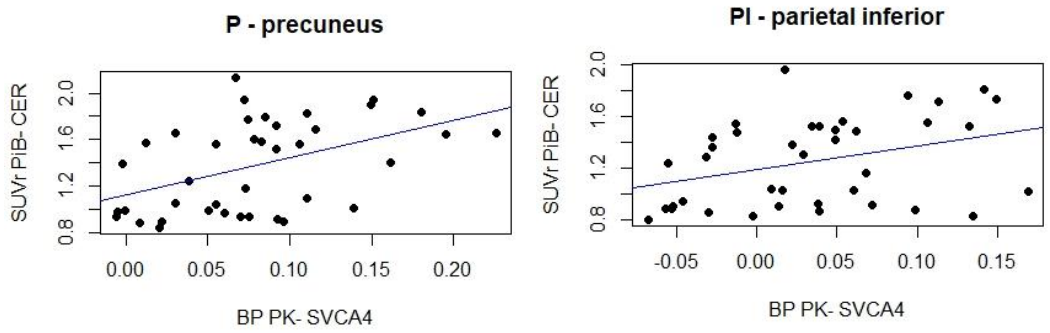

Figure 19 - Scatter plots showing the positive correlation in P and PI between $BP_{4060\text{-}SVCA4}$ and $SUVr_{4070\text{-}CER}$.

Positive correlation in different brain regions between $BP_{4060\text{-}SVCA4}$ and $SUVr_{4070\text{-}WM}$

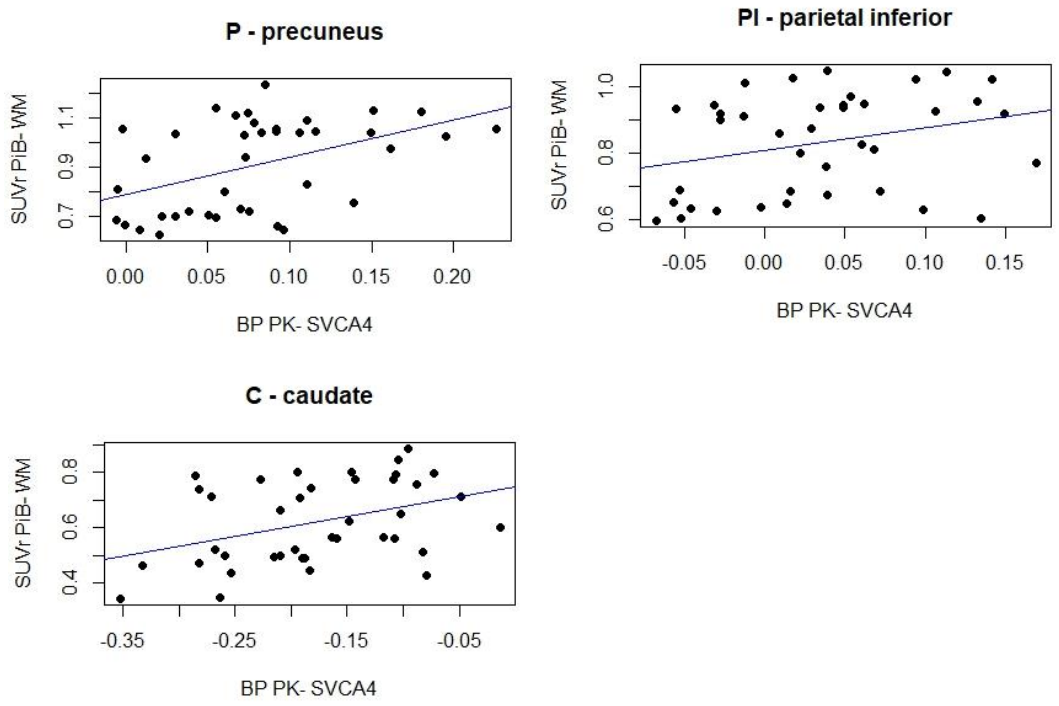

Figure 20 - Scatter plots showing the positive correlation in P, PI and C between $BP_{4060\text{-}SVCA4}$ and $SUVr_{4070\text{-}WM}$.

Through the scatter plots (Figures 17 to 20) it is possible to see a positive correlation in several brain regions between BP PK of group 4060 and SUVr PiB of group 4070. It is also possible to verify that when the CER is used as reference region, the values of BP are mainly negative. Which suggests that CER may not represent the best reference region to be used in the normalization of PK PET images. On the other hand, when the SVCA4 is the approach used to obtain the reference region, the values of BP are mainly positive.

CHAPTER 3 (DISCUSSION)

Voxel Based Analysis – Conclusions

PK PET images comparison between groups – Conclusions

According with the results exposed in Table 4-8 and with Figures 7-11, it was found that, when CER was used as reference region, higher differences at the voxel level between AD and HC groups of PK PET images (SUVr, BP and DVR), comparing with SVCA4, were observed. Even though the main hypothesis is that PET images bear differences between AD and HC groups, these differences can be biased. To our knowledge, SVCA4 gives the reference region with the less specific binding to PK. Thus, the differences at the voxel level using CER may be a result of their specific binding to PK. So, although CER is associated to higher differences between groups at the voxel level, **SVCA4 is likely the approach that gives the more accurate quantification of PK PET. This implies that there are just small differences at voxel level between AD and HC group of PK PET images. The reason why is probably related to the fact that activated microglia is associated to neuroinflammation and this process is characteristic of each subject, i.e., is random distributed and degreed in the brain of the AD patients. This reduces the likelihood of finding a substantial effect.**

Also, in Figures 7 to 11, are presented three different quantification outputs of PK PET images, SUVr, BP and DVR. Through the comparison of these Figures and just looking for the b) part of the figures, when SVCA4 is used as reference region, it is possible to conclude that the quantification output associated to the most differences between AD and HC groups is the DVR. However, since all the quantification methods are robust and the differences between BP and DVR are small, **the quantification outputs, BP or DVR, are relatively similar and none can be declared as the best one to quantify PK PET images.**

PiB and PK images comparison between groups – Conclusions

In addition, results from the voxel-based analysis present in Figure 12 - SUVr PiB of group 4070 presents a relevant difference at voxel level between AD and HC groups. Conversely, the two considered quantified PK PET images did not show big differences –suggests that **PK biodistribution in the brain does not indeed differentiate groups.** Moreover, this also indicates that when the disease is present, **if they exist, there are probably just a few features extracted from PK PET images that can be used to improve the performance of the classifiers only based on PiB PET images.**

Voxel wise correlation in different brain regions between PK of group 4060 and SUVr PiB of group 4070 – conclusion

There were five brain regions where the correlation at voxel level between PK and SUVr PiB PET images agreed the most for all reference regions considered, primary motor cortex, primary visual cortex, somatosensory association cortex, associative visual cortex and premotor cortex. It is interesting to noticed that all these brain regions are related to motor function and visual spatial orientation.

ROI Based Analysis – Conclusions

Feature selection – conclusion

Results from Table 13 - in comparison with PK PET images, PiB PET images present much higher values for the ratio between the features that passed the two sample T-test and the total considered features, and for the global percentage difference - are directly linked to the conclusions mentioned above, **PK biodistribution in the brain does not differentiate groups reliably in any brain region.** Within PK PET images, BP PK PET images using CER as reference region presented the higher values for the ratio between the features that passed the two

sample T-test and the total considered features. This agrees with the result obtained in the voxel-based analysis, **in PK PET images, CER as reference region** allow the most differences between AD and HC groups. **However, as it was mentioned, these differences are probably biased by the specific binding of CER to PK.** This agrees with the slightly lower values of the global percentage differences obtained using CER as reference region, 2.320 and 3.100, comparing with the ones obtained using SVCA4, 4.100 and 3.100, for BP and DVR, respectively.

The resulting datasets given by two sample T-test and PCA technique disagreed in three cases. Since the T-test is univariate and PCA technique is multivariate the existence of disagreements is not unexpected. According with the number of disagreements present in Table 14, it is logical to postulate that **the feature selection can be done by either two sample T-test or PCA technique, when the features are extracted from quantified PiB PET images.** However, even though the similarity of the classifiers performance given by these two approaches, overall **PCA technique was the one with the best results** (Table 33). For PK PET images, no classifier was constructed only using features selected by two sample T-test (Table 14). The difficulty in the selection of features extracted from PK PET images by two sample T-test is probably because the **Two sample T-test is a univariate approach and due to the low percentage differences of sample means obtain for BP PK PET images. So, it is logical to postulate, for PK PET images, two sample T-test is not the obvious approach to choose to do the feature selection.**

Classification – conclusion

According to the results obtained in Table 22, it is possible to conclude that somehow **the algorithm can extract important information to build the binary classifier from features which *a priori* do not had overt clinical meaning.**

The binary classifier only based on features extracted from BP PK PET images (Table 27), shows a weak performance, when compared with the first two groups (TOT and 4070). What is in agreement with the above mentioned conclusions, **if they exist, there are probably just few features extracted from PK PET images able to be use to improve the classifier performance.**

According to the results of Table 33 - the overall binary classifier with the best performance; accuracy of 0.925, sensitivity of 1.000 and specificity of 0.857; was obtained for the group 4070, using CER as reference region, rbf as kernel and PCA technique as feature selection approach. The group 4070 is composed by PET images acquired during the **characteristic accumulation time** of PiB, between minute 40 and 70, after administration. So, it is possible to state that **the most important information extracted from the features are presented in this time interval.** It can be also concluded, that **CER represents the best reference region.** What also means that **CER represents the brain region where amyloid accumulation bears the least differences between HC and AD patients.** Results from Table 33 show also that the use of one feature extracted from PK PET images (5th attempt), although it does not improve neither the accuracy nor the sensitivity of the classifier, can be used to improve their specificity. However, since specificity represents the capacity of classifying correctly the HC, for this specificity case it is better to have a higher value for the sensitivity than for the specificity.

ROI based correlation in different brain regions between BP PK of group 4060 and SUVr PiB of group 4070 PET images – conclusion

BP PK PET images correlated positively in some brain regions with PiB-PET images normalized by both the CER and WM. $BP_{4060\text{-}CER}$ and $SUVr_{4070\text{-}CER}$ are correlated positively in OC, PI, C and P, $BP_{4060\text{-}CER}$ and $SUVr_{4070\text{-}WM}$ in C and P, $BP_{4060\text{-}SVCA4}$ and $SUVr_{4070\text{-}CER}$ in PI and P, and $BP_{4060\text{-}SVCA4}$ and $SUVr_{4070\text{-}WM}$ in PI, C and P. Since, both P and PI have important roles in visuospatial processing, ROI based correlation results are directly linked with the obtained in voxel wise correlation [98, 99].

Results from Table 36 - when using the CER as reference region of PiB PET images, stronger correlation with BP PK PET images were found compared to normalization based on WM –agrees with the aforementioned conclusion, for PiB PET images of group 4070 **CER represents the best reference region.** To our knowledge, if the reference region considered has specific binding to PK, the binding potential will be underestimated [43]. In the Figures 17 to 20 it is possible to see that when CER is used as reference region, the values of BP are mainly negative. On the other hand,

when the SVCA4 is the approach used to obtain the reference region, the values of BP are mainly positive. **CER as certainly specific binding to PK; thus, it not represents the best reference region to be used in the quantification of PK PET images.** This conclusion proves the assumptions considered in voxel based analysis conclusions - **SVCA4 is certainly the approach that gives the more accurate quantification of PK PET.**

Final remarks

After confrontation of the results obtained - features extracted at regional level from PK PET images did not improve, neither the accuracy nor the sensitivity of the classifier only based on features extracted from PiB PET images - different alternatives to build a new classifier using features extracted from PK PET images were considered. Since all the features were extracted at regional level, the alternative considered was the extraction of features from PK PET images using voxel-based methods texture analysis. However, this alternative was not carried forward since:

→ For this problem, texture do not have clinical meaning in PET images;

→ PK PET images, even at voxel level, presented only small differences between AD and HC groups;

→ The classifier only based on features extracted from PiB PET images have already a great performance;

→ The inclusion of features extracted from PK PET images implies the production and administration of another radiopharmaceutical and the acquisition of more PET images, which is invasive, very expensive and time-consuming.

Future work

The characterization of PiB retention (positive or negative) in MCI patients is tricky. There are evidences of at least three separate binding sites for PiB on the Aβ polymer fibrils, each with its own specific affinity. If one of these sites had an higher association with the development of AD and/or MCI subjects a possible refinement of amyloid imaging could be done to improve AD and/or MCI diagnosis [34].

According with scientists, activated microglia may be present years before the clinical and behavioural signs of the disease start to appear. In line with this, features extracted from PK PET images, although they did not represent a core key in the resolution of the problem proposed - binary classification in AD - they may represent in a different problem –classification of MCI subjects.

Overall, according with the present study, the classifier only based on features extracted from PiB PET images of group 4070, using CER as reference region, was the classifier who solved more accurately the problem proposed, binary classification in AD. Additionally it was also found a positive correlation between PK and PiB in brain region responsible for motor function and visual processing.

BIBLIOGRAPHY

[1]-https://faculty.washington.edu/chudler/cells.html (15/01/19)

[2]-https://biology.tutorvista.com/cell/nerve-cell.html (27/01/2019)

[3]-https://www.neuronup.com/en/neurorehabilitation/disease (25/11/2018)

[4]-Minh, N. Van, Vien, V., & Kim, S. J. (2008). Intermediate phases in synthesis of AlPO4-5 molecular sieve: A study of XRD and Raman spectroscopy. *2008 8th IEEE Conference on Nanotechnology, IEEE-NANO*, 800–803. https://doi.org/10.1109/NANO.2008.239

[5]-https://www.alz.org/media/Documents/alzheimers-facts-and-figures-2019-r.pdf (08/07/2019)

[6]-Blennow, K., Leon, M. J. De, & Zetterberg, H. (2006). *Alzheimer ' s disease*. *368*, 387–403.

[7]-Klöppel, S., Stonnington, C. M., Chu, C., Draganski, B., Scahill, R. I., Rohrer, J. D., … Frackowiak, R. S. J. (2008). Automatic classification of MR scans in Alzheimer's disease. *Brain*, *131*(3), 681–689. https://doi.org/10.1093/brain/awm319

[8]-https://www.alz.org/alzheimers-dementia/what-is-alzheimers (26/11/2018)

[9]-https://www.alz.org/alzheimers-dementia/what-is-alzheimers/risk-factors (25/11/2018)

[10]-Santana, I., Farinha, F., Freitas, S., Rodrigues, V., & Carvalho, Á. (2015). Estimativa da prevalência da demência e da doença de Alzheimer em Portugal. *Acta Médica Portuguesa*, *7*, 182–188. https://doi.org/0870-399X

[11]-https://www.alz.org/alzheimers-dementia/what-is-dementia/related_conditions/mild-cognitive-impairment (25/11/2018)

[12]-Schuitemaker, A., Kropholler, M. A., Boellaard, R., van der Flier, W. M., Kloet, R. W., van der Doef, T. F., … van Berckel, B. N. M. (2013). Microglial activation in Alzheimer's disease: An (R)-[11C]PK11195 positron emission tomography study. *Neurobiology of Aging*, *34*(1), 128–136. https://doi.org/10.1016/j.neurobiolaging.2012.04.021

[13]-Vemuri, P., & Jack, C. R. (2010). Role of structural MRI in Alzheimer's disease. *Alzheimer's Research and Therapy*, *2*(4). https://doi.org/10.1186/alzrt47

[14]-Blennow, K., Zetterberg, H., & Fagan, A. M. (2012). Fluid biomarkers in Alzheimer disease. *Cold Spring Harbor Perspectives in Medicine*, *2*(9). https://doi.org/10.1101/cshperspect.a006221

[15]-McKhann, G. M., Knopman, D. S., Chertkow, H., Bradley, H. T., Clifford, J. J. R., Kawas, C. H., … Phelps, C. H. (2011). NIH Public Access. *Alzheimers Dement*, *7*(3), 263–269. https://doi.org/10.1016/j.jalz.2011.03.005.

[16]-https://www.news-medical.net/health/What-is-a-Biomarker.aspx (15/01/19)

[17]-https://www.sciencedirect.com/topics/neuroscience/biomarkers (15/01/19)

[18]-Lashley, T., Schott, J. M., Weston, P., Murray, C. E., Wellington, H., Keshavan, A., … Zetterberg, H. (2018). Molecular biomarkers of Alzheimer's disease: progress and prospects. *Disease Models & Mechanisms*, *11*(5), dmm031781. https://doi.org/10.1242/dmm.031781

[19]-Kulic, L., & Unschuld, P. G. (2016). Recent advances in cerebrospinal fluid biomarkers for the detection of preclinical Alzheimer's disease. *Current Opinion in Neurology*, *29*(6), 749–755. https://doi.org/10.1097/WCO.0000000000000399

[20]-https://www.webmd.com/brain/cerebrospinal-fluid-facts#1 (09/11/2018)

[21]-https://www.nibib.nih.gov/science-education/science-topics/magnetic-resonance-imaging-mri (26/11/2018)

[22]-https://www.nhs.uk/conditions/mri-scan/ (26/11/2018)

[23]-Symms, M., Jäger, H. R., Schmierer, K., & Yousry, T. A. (2004). A review of structural magnetic resonance neuroimaging. *Journal of Neurology, Neurosurgery and Psychiatry*, *75*(9), 1235–1244. https://doi.org/10.1136/jnnp.2003.032714

[24]-Xiao, Z., Ding, Y., Lan, T., Zhang, C., Luo, C., & Qin, Z. (2017). Brain MR Image Classification for Alzheimer's Disease Diagnosis Based on Multifeature Fusion. *Computational and Mathematical Methods in Medicine*, *2017*, 1–13. https://doi.org/10.1155/2017/1952373

[25]-https://www.iaea.org/topics/radiotracers (14/01/2018)

[26]-Radiotracers, P. E. T. (n.d.). PET Radiotracers. *Clinical PET and PET/CT*, *167*, 45–67. https://doi.org/10.1007/1-84628-100-8_2

[27]-http://www.iop.org/education/teacher/resources/teaching-medical-physics/positron/page_56317.html (26/11/2018)

[28]-https://www.britannica.com/science/annihilation (26/11/2018)

[29]-https://www.radiologyinfo.org/en/info.cfm?pg=pet (26/11/2018)

[30]-Cohen, A. D., & Klunk, W. E. (2014). Early detection of Alzheimer's disease using

PiB and FDG PET. *Neurobiology of Disease*, *72*(Part A), 117–122. https://doi.org/10.1016/j.nbd.2014.05.001

[31]-Wiley, C. A., Lopresti, B. J., Venneti, S., Price, J., Klunk, W. E., DeKosky, S. T., & Mathis, C. A. (2009). Carbon 11–Labeled Pittsburgh Compound B and Carbon 11–Labeled (. *Archives of Neurology*, *66*(1), 60–67.

[32]-https://www-pub.iaea.org/MTCD/publications/PDF/trs465_web.pdf (27/01/2019)

[33]-Oliveira, F., Leuzy, A., Castelhano, J., Chiotis, K., Hasselbalch, S. G., Rinne, J., … Castelo-Branco, M. (2018). Data driven diagnostic classification in Alzheimer's disease based on different reference regions for normalization of PiB-PET images and correlation with CSF concentrations of Aβ species. *NeuroImage: Clinical*, *20*(July), 603–610. https://doi.org/10.1016/j.nicl.2018.08.023

[34]-Johnson, K. A. (2006). Amyloid imaging of Alzheimer's disease using Pittsburgh compound B. *Current Neurology and Neuroscience Reports*, *6*(6), 496–503. https://doi.org/10.1007/s11910-006-0052-5

[35]-Yeo, J. M., Waddell, B., Khan, Z., & Pal, S. (2015). A systematic review and meta-analysis of 18F-labeled amyloid imaging in Alzheimer's disease. *Alzheimer's and Dementia: Diagnosis, Assessment and Disease Monitoring*, *1*(1), 5–13. https://doi.org/10.1016/j.dadm.2014.11.004

[36]-http://www.turkupetcentre.net/petanalysis/input_function.html#reference (30/06/2019)

[37]-https://www.thefreedictionary.com/perfusion (04/07/2019)

[38]–Turkheimer, F. E., Edison, P., Pavese, N., Roncaroli, F., Anderson, A. N., Hammers, A., … Brooks, D. J. (2007). Reference and target region modeling of C-11 -(R)-PK11195 brain studies. *Journal of Nuclear Medicine*, *48*(1), 158–167. https://doi.org/48/1/158 [pii]

[39]-Carson, R. E. (2003). 6 Tracer Kinetic Modeling in PET *. *Positron Emission Tomography: Basic Science and Clinical Practice*, (July 2006), 147–179. https://doi.org/10.1016/j.cpet.2007.08.003

[40]-Ichise, M, Meyer, J. H., & Yonekura, Y. (2001). An introduction to PET and SPECT neuroreceptor quantification models. *Journal of Nuclear Medicine : Official Publication, Society of Nuclear Medicine*, *42*(5), 755–763. Retrieved from http://www.ncbi.nlm.nih.gov/pubmed/11337572

[41]-http://www.turkupetcentre.net/petanalysis/input_function.html (08/06/2019)

[42]-Yaqub, M., Van Berckel, B. N. M., Schuitemaker, A., Hinz, R., Turkheimer, F. E., Tomasi, G., … Boellaard, R. (2012). Optimization of supervised cluster analysis for extracting reference tissue input curves in (R)-[11C]PK11195 brain PET studies. *Journal of Cerebral Blood Flow and Metabolism*, *32*(8), 1600–1608. https://doi.org/10.1038/jcbfm.2012.59

[43]-http://www.turkupetcentre.net/petanalysis/model_reference_tissue.html (08/06/2019)

[44]-Müller, A. C., & Guido, S. (2015). Introduction to Machine Learning with Python and Scikit-Learn. In Kukuruku Hub. Retrieved from http://kukuruku.co/hub/python/introduction-to-machine-learning-with-python-andscikit-learn

[45]-Mohri, M. (2012). Fundations of Machine Learning. In *Machine Learning*.

[46]-R. Gad, A. (2016). Automatic Machine Learning Classification of Alzheimer's Disease Based on Selected Slices from 3D Magnetic Resonance Imagining. *International Journal of Biomedical Science and Engineering*, *4*(6), 50. https://doi.org/10.11648/j.ijbse.20160406.11

[47]-https://www.geeksforgeeks.org/cross-validation-machine-learning/ (16/01/19)

[48]-https://machinelearningmastery.com/k-fold-cross-validation/ (16/01/19)

[49]-https://www.sciencedirect.com/topics/computer-science/bayes-classifier (08/07/19)

[50]-http://www.statsoft.com/textbook/naive-bayes-classifier (23/01/2019)

[51]-https://brilliant.org/wiki/bayes-theorem/ (23/01/2019)

[52]-https://towardsdatascience.com/the-kernel-trick-c98cdbcaeb3f (01/07/2019)

[53]-https://blog.usejournal.com/machine-learning-algorithms-use-cases-72646df1245f (01/07/2019)

[54]-Lee, J. S., Kim, C., Shin, J. H., Cho, H., Shin, D. S., Kim, N., … Seong, J. K. (2018). Machine Learning-based Individual Assessment of Cortical Atrophy Pattern in Alzheimer's Disease Spectrum: Development of the Classifier and Longitudinal Evaluation. *Scientific Reports*, *8*(1), 1–10. https://doi.org/10.1038/s41598-018-22277-x

[55]-Pagani, M., Nobili, F., Morbelli, S., Arnaldi, D., Giuliani, A., Öberg, J., … De Carli, F. (2017). Early identification of MCI converting to AD: a FDG PET study. *European Journal of Nuclear Medicine and Molecular Imaging*, *44*(12), 2042–2052. https://doi.org/10.1007/s00259-017-3761-x

[56]-Manley, G. (2013). *Public Access NIH Public Access*. 117–122. https://doi.org/10.1038/mp.2011.182.doi

[57]-https://www.synonym.com/synonyms/striatum (19/01/2018)

[58]–Parbo, P., Ismail, R., Hansen, K. V., Amidi, A., Mårup, F. H., Gottrup, H., … Brooks, D. J. (2017). Brain inflammation accompanies amyloid in the majority of mild cognitive impairment cases due to Alzheimer's disease. *Brain*, *140*(7), 2002–2011. https://doi.org/10.1093/brain/awx120

[59]-Kulic, L., & Unschuld, P. G. (2016). Recent advances in cerebrospinal fluid biomarkers for the detection of preclinical Alzheimer's disease. *Current Opinion in Neurology*, *29*(6), 749–755. https://doi.org/10.1097/WCO.0000000000000399

[60]-http://ric.uthscsa.edu/mango/ (05/03/2019)

[61]-https://www.sciencedirect.com/topics/neuroscience/statistical-parametric-mapping (17/11/2018)

[62]-https://www.fil.ion.ucl.ac.uk/spm/ (17/11/2018)

[63]–Dimitrova, N., Zamudio, J. R., Jong, R. M., Soukup, D., Resnick, R., Sarma, K., … Jacks, T. (2017). Public Access NIH Public Access. *PLoS ONE*, *32*(7), 736–740. https://doi.org/10.1371/journal.pone.0178059

[64]-https://www.rstudio.com/products/rstudio/ (08/04/2019)

[65]-https://www.r-project.org/ (08/04/2019)

[66]-https://www.codementor.io/innat_2k14/preferable-tools-for-machine-learning-python-matlab-r-jfozzpphz (05/06/2019)

[67]-https://www.mathworks.com/products/matlab.html (05/06/2019)

[68]-https://www.dicomstandard.org/ (25/01/2019)

[69]-Logan, J. (2000). Graphical analysis of PET data applied to reversible and irreversible tracers. *Nuclear Medicine and Biology*, *27*(7), 661–670. https://doi.org/10.1016/S0969-8051(00)00137-2

[70]-Ichise, M., Liow, J. S., Lu, J. Q., Takano, A., Model, K., Toyama, H., … Carson, R. E. (2003). Linearized reference tissue parametric imaging methods: Application to

[11C]DASB positron emission tomography studies of the serotonin transporter in human brain. *Journal of Cerebral Blood Flow and Metabolism*, *23*(9), 1096–1112. https://doi.org/10.1097/01.WCB.0000085441.37552.CA

[71]-Shiroishi, M. S., Lerner, A., Boyko, O. B., Booker, M. T., Hwang, D. H., Go, J. L., … Kim, P. E. (2014). Image Coregistration: Quantitative Processing Framework for the Assessment of Brain Lesions. *Journal of Digital Imaging*, *27*(3), 369–379. https://doi.org/10.1007/s10278-013-9655-y

[72]-https://www.stars-project.org/en/knowledgeportal/magazine/image-analysis/automated-image-processing-workflow/image-co-registration/ (09/04/2019)

[73]-http://brainmap.org/training/BrettTransform.html (05/03/2019)

[74]–https://www.lead-dbs.org/about-the-mni-spaces/ (05/06/2019)

[75]-https://support.brainvoyager.com/brainvoyager/functional-analysis-preparation/29-pre-processing/86-spatial-smoothing (08/07/2019)

[76]-http://www.unicog.org/docs/glm_anova (01/07/2019)

[77]-sprout022.sprout.yale.edu/mni2tal/mni2tal.html (28/04/2019)

[78]-http://www.fmriconsulting.com/brodmannconn/index.php?q=BA_18 (28/04/2019)

[79]-Bradburn, S., Murgatroyd, C., & Ray, N. (2019). Neuroinflammation in mild cognitive impairment and Alzheimer's disease: A meta-analysis. *Ageing Research Reviews*, *50*(November 2018), 1–8. https://doi.org/10.1016/j.arr.2019.01.002

[80]-https://link.springer.com/article/10.1007/s13721-013-0035-9

[81]-https://github.com/villeneuvelab/vlpp/wiki/PET-Tutorial (11/02/2019)

[82]-https://www.sciencedirect.com/topics/medicine-and-dentistry/standardized-uptake-value (21/03/2019)

[83]–Villemagne, V., Keefe, G. O., & Rowe, C. (2007). *PIB-PET segmentation for automatic SUVR normalisation without MR information Department of Electrical*. (June 2014). https://doi.org/10.1109/ISBI.2007.356860

[84]-https://towardsdatascience.com/feature-selection-techniques-in-machine-learning-with-python-f24e7da3f36e (08/05/2019)

[85]-https://www.analyticsvidhya.com/blog/2016/12/introduction-to-feature-selection-methods-with-an-example-or-how-to-select-the-right-variables/ (08/05/2019)

[86]-http://valmikiacademy.com/module-two-t-test/ (13/06/2019)
[87]-https://www.r-bloggers.com/two-sample-students-t-test-1/ (24/03/2019)
[88]-http://rcompanion.org/handbook/I_03.html (25/03/2019)
[89]-https://www.datacamp.com/community/tutorials/pca-analysis-r (14/04/2019)
[90]-https://plot.ly/ipython-notebooks/principal-component-analysis/ (15/04/2019)
[91]-https://statisticsbyjim.com/glossary/standardization/?fbclid=IwAR13FbAwFaYb3Lx-5_VfaEy6B7G8Fy62FBiZ52Zs3IIeh4LLLsb41m66J5Y (09/05/2019)
[92]-https://haifengl.github.io/smile/api/java/smile/validation/LOOCV.html (05/04/2019)
[93]-Baratloo, A., Hosseini, M., Negida, A., & El Ashal, G. (2015). Part 1: Simple Definition and Calculation of Accuracy, Sensitivity and Specificity. *Emergency (Tehran, Iran)*, *3*(2), 48–49.
[94]-Wong, H. B., & Lim, G. H. (2011). Measures of diagnostic accuracy: Sensitivity, specificity, PPV and NPV. *Proceedings of Singapore Healthcare*, *20*(4), 316–318. https://doi.org/10.1177/201010581102000411
[95]-http://www.sthda.com/english/wiki/correlation-test-between-two-variables-in-r (15/06/2019)
[96]-https://statistics.laerd.com/statistical-guides/pearson-correlation-coefficient-statistical-guide.php (15/06/2019)
[97]-http://sphweb.bumc.bu.edu/otlt/MPH-Modules/BS/R/R5_Correlation-Regression/R5_Correlation-Regression_print.html (02/07/2019)
[98]-https://reliawire.com/precuneus/ (20/06/2019)
[99]-https://www.sciencedirect.com/topics/neuroscience/inferior-parietal-lobule (20/06/2019)

The two excutables, *2DslicesTimeFramesTo3D* and *BP_KINETICMODEL,* provided by the ICNAS, were made by Francisco PM Oliveira.

APPENDICES

A - FISHER'S F-TEST AND TWO SAMPLE T-TEST

PiB SUVr group TOT (Ref-CER)

Table(A) 1 - Brain regions considered, p-value of the Fisher's F-test, homogeneity of variances, p-value of the two sample T-test and test result, mean of the brain region for AD and HC groups, percentage difference of sample means (%) and global percentage difference.

Brain regions	**Fisher's F-test** (p-value)	**Fisher's F-test result**	**Two sample T-test** (p-value)	**Two sample T-test result**	**Mean brain region AD**	**Mean brain region HC**	**Percentage difference of sample means (%)**
PC	0.340	✓	0.005	✓	1.356	0.996	36.000
OC	0.065	✓	0.022	✓	1.448	1.135	31.300
MTC	0.051	✓	0.049	✓	1.004	0.928	7.600
PI	0.591	✓	0.004	✓	1.469	1.083	38.600
PS	0.262	✓	0.003	✓	1.380	0.948	43.200
ACing	0.004	✗	2.650E-04	✓	1.368	1.088	28.000
C	0.155	✓	0.171	✗	0.951	0.878	-
PCing	0.022	✗	0.509	✗	1.157	1.107	-
P	0.542	✓	0.007	✓	1.608	1.171	43.700
Pmen	0.001	✗	2.740E-04	✓	1.424	1.186	23.800
B	0.244	✓	0.001	✓	1.304	1.053	25.100
Global percentage difference (%)							**30.811**

PiB SUVr group TOT (Ref-GM)

Table(A) 2 - Brain regions considered, p-value of the Fisher's F-test, homogeneity of variances, p-value of the two sample T-test and test result, mean of the brain region for AD and HC groups, percentage difference of sample means (%) and global percentage difference.

Brain regions	Fisher's F-test (p-value)	Fisher's F-test result	Two sample T-test (p-value)	Two sample T-test result	Mean brain region AD	Mean brain region HC	Percentage difference of sample means (%)
PC	0.359	✓	0.066	✗	1.051	0.938	-
OC	0.002	✗	0.190	✗	1.123	1.073	-
MTC	0.451	✓	1.040E-04	✓	0.784	0.908	-12.400
PI	0.122	✓	5.560E-04	✓	1.141	1.020	12.100
PS	0.105	✓	0.012	✓	1.071	0.893	17.800
ACing	0.042	✗	0.404	✗	1.058	1.034	-
C	0.159	✓	0.032	✓	0.743	0.839	-9.600
PCing	0.067	✓	0.011	✓	0.913	1.063	-15.00
P	0.027	✗	0.035	✓	1.246	1.136	11.0000
Pmen	0.005	✗	0.495	✗	1.111	1.137	-
B	9.620E-04	✗	0.323	✗	1.012	1.000	-
Global percentage difference (%)							**0.650**

PiB SUVr group TOT (Ref-WM)

Table(A) 3 - Brain regions considered, p-value of the Fisher's F-test, homogeneity of variances, p-value of the two sample T-test and test result, mean of the brain region for AD and HC groups, percentage difference of sample means (%) and global percentage difference.

Brain regions	Fisher's F-test (p-value)	Fisher's F-test result	Two sample T-test (p-value)	Two sample T-test result	Mean brain region AD	Mean brain Region HC	Percentage difference of sample means (%)
PC	0.979	✓	0.006	✓	1.075	0.833	24.200
OC	0.004	✗	0.278	✗	1.152	1.038	-
MTC	0.617	✓	0.981	✗	0.798	0.799	-
PI	0.188	✓	0.010	✓	1.169	0.904	26.500
PS	0.087	✓	0.008	✓	1.098	0.792	30.600
ACing	0.010	✗	1.840E-04	✓	1.083	0.912	17.100
C	0.373	✓	0.690	✗	0.756	0.740	-
PCing	0.024	✗	0.907	✗	0.928	0.935	-
P	0.628	✓	0.005	✓	1.276	0.979	29.700
Pmen	0.005	✗	9.520E-04	✓	1.134	1.001	13.300
B	0.654	✓	0.002	✓	1.035	0.883	15.200
Global percentage difference (%)							**22.371**

PiB SUVr group 4070 (Ref-CER)

Table(A) 4 - Brain regions considered, p-value of the Fisher's F-test, homogeneity of variances, p-value of the two sample T-test and test result, mean of the brain region for AD and HC groups, percentage difference of sample means (%) and global percentage difference.

Brain regions	**Fisher's F-test** (p-value)	**Fisher's F-test**	**Two sample T-test** (p-value)	**Two sample T-test result**	**Mean brain region AD**	**Mean Brain region HC**	**Percentage difference of sample means (%)**
PC	0.615	✓	4.200E-04	✓	1.352	0.939	41.300
OC	0.266	✓	4.120E-04	✓	1.449	1.053	39.600
MTC	0.026	✗	3.850E-04	✓	1.067	0.906	16.100
PI	0.816	✓	2.440E-04	✓	1.529	1.002	52.700
PS	0.977	✓	1.670E-04	✓	1.301	0.866	43.500
Acing	0.804	✓	4.100E-04	✓	1.645	1.144	50.100
C	0.159	✓	0.006	✓	1.024	0.811	21.300
PCing	0.059	✓	0.003	✓	1.528	1.131	39.700
P	0.477	✓	1.980E-04	✓	1.698	1.084	61.400
Pmen	0.020	✗	0.001	✓	1.491	1.083	40.800
B	0.828	✓	1.330E-04	✓	1.370	1.008	36.200
Global percentage difference (%)							**40.245**

PiB SUVr group 4070 (Ref-WM)

Table(A) 5 - Brain regions considered, p-value of the Fisher's F-test, homogeneity of variances, p-value of the two sample T-test and test result, mean of the brain region for AD and HC groups, percentage difference of sample means (%) and global percentage difference.

Brain regions	**Fisher's F-test** (p-value)	**Fisher's F-test results**	**Two sample T-test** (p-value)	**Two sample T-test result**	**Mean brain region AD**	**Mean Brain region HC**	**Percentage difference of sample means (%)**
PC	0.456	✓	0.003	✓	0.854	0.676	17.8
OC	0.139	✓	0.014	✓	0.915	0.759	15.6
MTC	0.025	✗	0.444	✗	0.678	0.660	-
PI	0.024	✗	2.600E-04	✓	0.962	0.720	24.2
PS	0.392	✓	9.220E-04	✓	0.821	0.625	19.6
ACing	0.230	✓	0.001	✓	1.036	0.823	21.3
C	0.422	✓	0.190	✗	0.651	0.589	-
PCing	0.115	✓	0.020	✓	0.969	0.820	14.9
P	0.274	✓	6.520E-04	✓	1.072	0.778	29.4
Pmen	0.047	✗	0.013	✓	0.957	0.787	17
B	< 1.124E-011	✗	0.171	✗	253.9	0.728	-
Global percentage difference (%)							**19.975**

PK SUVr group 4060 (Ref-CER)

Table(A) 6 - Brain regions considered, p-value of the Fisher's F-test, homogeneity of variances, p-value of the two sample T-test and test result, mean of the brain region for AD and HC groups, percentage difference of sample means (%) and global percentage difference.

Brain regions	**Fisher's F-test** (p-value)	**Fisher's F-test result**	**Two sample T-test** (p-value)	**Two sample T-test result**	**Mean brain region AD**	**Mean Brain region HC**	**Percentage difference of sample means (%)**
PC	0.147	✓	0.462	✗	0.827	0.811	-
OC	0.019	✗	0.442	✗	0.938	0.920	-
MTC	0.150	✓	0.791	✗	0.901	0.906	-
PI	0.923	✓	0.081	✗	0.838	0.796	-
PS	0.035	✗	0.343	✗	0.834	0.802	-
Acing	0.483	✓	0.878	✗	0.814	0.817	-
C	0.763	✓	0.229	✗	0.628	0.656	-
PCing	0.441	✓	0.478	✗	0.869	0.860	-
P	0.647	✓	0.059	✗	0.869	0.832	-
Pmen	0.713	✓	0.691	✗	0.869	0.860	-
B	0.760	✓	0.393	✗	0.856	0.842	-

PK SUVr group 4060 (Ref-SVCA4)

Table(A) 7 - Brain regions considered, p-value of the Fisher's F-test, homogeneity of variances, p-value of the two sample T-test and test result, mean of the brain region for AD and HC groups, percentage difference of sample means (%) and global percentage difference.

Brain regions	**Fisher's F-test** (p-value)	**Fisher's F-test result**	**Two sample T-test** (p-value)	**Two sample T-test result**	**Mean brain region AD**	**Mean Brain region HC**	**Percentage difference of sample means (%)**
PC	0.361	✓	0.685	✗	1.048	1.040	-
OC	0.011	✗	0.756	✗	1.188	1.180	-
MTC	0.454	✓	0.231	✗	1.141	1.164	-
PI	0.892	✓	0.084	✗	1.060	1.022	-
PS	0.078	✓	0.466	✗	1.057	1.028	-
Acing	0.593	✓	0.324	✗	1.031	1.049	-
C	0.692	✓	0.071	✗	0.794	0.841	-
PCing	0.455	✓	0.754	✗	1.080	1.074	-
P	0.349	✓	0.093	✗	1.101	1.069	-
Pmen	0.181	✓	0.830	✗	1.099	1.104	-
B	0.926	✓	0.772	✗	1.084	1.081	-

PK BP group 4060 (Ref-CER)

Table(A) 8 - Brain regions considered, p-value of the Fisher's F-test, homogeneity of variances, p-value of the two sample T-test and test result, mean of the brain region for AD and HC groups, percentage difference of sample means (%) and global percentage difference.

Brain regions	**Fisher's F-test** (p-value)	**Fisher's F-test result**	**Two sample T-test** (p-value)	**Two sample T-test result**	**Mean brain region AD**	**Mean Brain region HC**	**Percentage difference of sample means (%)**
PC	0.062	✓	0.408	✗	-0.155	-0.171	-
OC	0.018	✗	0.374	✗	-0.051	-0.071	-
MTC	0.072	✓	0.234	✗	-0.076	-0.095	-
PI	0.975	✓	0.053	✗	-0.157	-0.198	-
PS	0.064	✓	0.405	✗	-0.154	-0.185	-
ACing	0.079	✓	0.317	✗	-0.138	-0.155	-
C	0.882	✓	0.356	✗	-0.354	-0.333	-
PCing	0.139	✓	0.158	✗	-0.136	-0.161	-
P	0.422	✓	0.006	✓	-0.120	-0.167	-4.700
Pmen	0.842	✓	0.114	✗	-0.091	-0.120	-
B	0.826	✓	0.060	✗	-0.121	-0.145	-
FL	0.797	✓	0.031	✓	-0.118	-0.147	2.400
TL	0.253	✓	0.216	✗	-0.098	-0.115	-
FTS	0.937	✓	0.590	✗	-0.148	-0.135	-
SFG	0.230	✓	0.066	✗	-0.136	-0.165	-
MFG	0.078	✓	0.323	✗	-0.121	-0.139	-
PG	0.847	✓	0.065	✗	-0.141	-0.165	-
IFG	0.416	✓	0.557	✗	-0.106	-0.114	-
STG	0.736	✓	0.760	✗	-0.155	-0.150	-
MTG	0.939	✓	0.324	✗	-0.080	-0.095	-
ITG	0.031	✗	0.008	✓	-0.009	-0.053	4.400
A	0.597	✓	0.401	✗	0.054	0.034	--
H	0.069	✓	0.115	✗	0.001	-0.034	-
IPL	0.663	✓	0.010	✓	-0.134	-0.175	4.100
SPL	0.338	✓	0.011	✓	-0.144	-0.198	5.400
Global percentage difference (%)							**2.320**

PK BP group 4060 (Ref-SVCA4)

Table(A) 9 - Brain regions considered, p-value of the Fisher's F-test, homogeneity of variances, p-value of the two sample T-test and test result, mean of the brain region for AD and HC groups, percentage difference of sample means (%) and global percentage difference.

Brain regions	**Fisher's F-test** (p-value)	**Fisher's F-test results**	**Two sample T-test** (p-value)	**Two sample T-test result**	**Mean brain region AD**	**Mean brain region HC**	**Percentage difference of sample means (%)**
PC	0.166	✓	0.937	✗	0.051	0.049	-
OC	0.0568	✓	0.850	✗	0.181	0.176	-
MTC	0.719	✓	0.919	✗	0.144	0.143	-
PI	0.988	✓	0.141	✗	0.048	0.016	-
PS	0.031	✗	0.857	✗	0.041	0.033	-
ACing	0.935	✓	0.940	✗	0.070	0.068	-
C	0.810	✓	0.119	✗	-0.201	-0.161	-
PCing	0.363	✓	0.444	✗	0.078	0.064	-
P	0.206	✓	0.019	✓	0.098	0.056	4.200
Pmen	0.160	✓	0.413	✗	0.130	0.113	-
B	0.594	✓	0.352	✗	0.091	0.081	-
FL	0.924	✓	0.169	✗	0.094	0.079	-
TL	0.445	✓	0.957	✗	0.119	0.118	-
FTS	0.287	✓	0.261	✗	0.063	0.096	-
SFG	0.653	✓	0.239	✗	0.075	0.056	-
MFG	0.117	✓	0.895	✗	0.093	0.090	-
PG	0.681	✓	0.297	✗	0.069	0.0574	-
IFG	0.618	✓	0.487	✗	0.113	0.122	-
STG	0.763	✓	0.155	✗	0.054	0.076	-
MTG	0.944	✓	0.952	✗	0.145	0.146	-
ITG	0.129	✓	0.074	✗	0.230	0.196	-
A	0.812	✓	0.912	✗	0.309	0.306	-
H	0.617	✓	0.408	✗	0.239	0.217	-
IPL	0.448	✓	0.024	✓	0.076	0.044	3.200
SPL	0.302	✓	0.041	✓	0.067	0.018	4.900
Global percentage difference (%)							**4.100**

PK DVR group 4060 (Ref-CER)

Table(A) 10 - Brain regions considered, p-value of the Fisher's F-test, homogeneity of variances, p-value of the two sample T-test and test result, mean of the brain region for AD and HC groups, percentage difference of sample means (%) and global percentage difference.

Brain regions	**Fisher's F-test** (p-value)	**Fisher's F-test result**	**Two sample T-test** (p-value)	**Two sample T-test Result**	**Mean brain region AD**	**Mean brain region HC**	**Percentage difference of sample means (%)**
FL	0.670	✓	0.081	✗	0.727	0.704	-
TL	0.775	✓	0.892	✗	0.740	0.738	-
FTS	0.192	✓	0.843	✗	0.737	0.734	-
SFG	0.995	✓	0.023	✓	0.746	0.713	3.300
MFG	0.450	✓	0.163	✗	0.743	0.721	-
PG	0.657	✓	0.077	✗	0.739	0.716	-
IFG	0.396	✓	0.423	✗	0.750	0.739	-
STG	0.888	✓	0.501	✗	0.727	0.737	-
MTG	0.740	✓	0.761	✗	0.774	0.770	-
ITG	0.871	✓	0.123	✗	0.795	0.773	-
A	0.968	✓	0.660	✗	0.863	0.855	-
H	0.483	✓	0.180	✗	0.808	0.782	-
IPL	0.874	✓	0.122	✗	0.739	0.719	-
SPL	0.369	✓	0.067	✗	0.753	0.724	-
P	0.809	✓	0.034	✓	0.777	0.748	2.900
Global percentage difference (%)							**3.100**

PK DVR group 4060 (REF-SVCA4)

Table(A) 11 - Brain regions considered, p-value of the Fisher's F-test, homogeneity of variances, p-value of the two sample T-test and test result, mean of the brain region for AD and HC groups, percentage difference of sample means (%) and global percentage difference.

Brain regions	**Fisher's F-test** (p-value)	**Fisher's F-test result**	**Two sample T-test** (p-value)	**Two sample T-test result**	**Mean brain region AD**	**Mean brain region HC**	**Percentage difference of sample means (%)**
FL	0.765	✓	0.127	✗	0.914	0.895	-
TL	0.806	✓	0.765	✗	0.933	0.938	-
FTS	0.332	✓	0.762	✗	0.924	0.930	-
SFG	0.408	✓	0.027	✓	0.935	0.904	3.100
MFG	0.982	✓	0.251	✗	0.932	0.915	-
PG	0.680	✓	0.173	✗	0.927	0.91	-
IFG	0.280	✓	0.720	✗	0.944	0.938	-
STG	0.929	✓	0.149	✗	0.914	0.935	-
MTG	0.929	✓	0.994	✗	0.977	0.977	-
ITG	0.497	✓	0.155	✗	1.005	0.981	-
A	0.720	✓	0.899	✗	1.084	1.087	-
H	0.963	✓	0.326	✗	1.017	0.995	-
IPL	0.708	✓	0.360	✗	0.924	0.912	-
SPL	0.530	✓	0.249	✗	0.942	0.92	-
P	0.886	✓	0.172	✗	0.969	0.948	-
Global percentage difference (%)							**3.100**

B - PCA TECHNIQUE

PiB SUVr group TOT (Ref-CER)

	eigenvalue	variance.percent	cumulative.variance.percent
Dim.1	7.311091390	66.4644672	66.46447
Dim.2	1.947643990	17.7058545	84.17032
Dim.3	0.685715064	6.2337733	90.40409
Dim.4	0.517113142	4.7010286	95.10512
Dim.5	0.225912025	2.0537457	97.15887
Dim.6	0.133473982	1.2133998	98.37227
Dim.7	0.089539604	0.8139964	99.18627
Dim.8	0.039613243	0.3601204	99.54639
Dim.9	0.028918345	0.2628940	99.80928
Dim.10	0.016211649	0.1473786	99.95666
Dim.11	0.004767565	0.0433415	100.00000

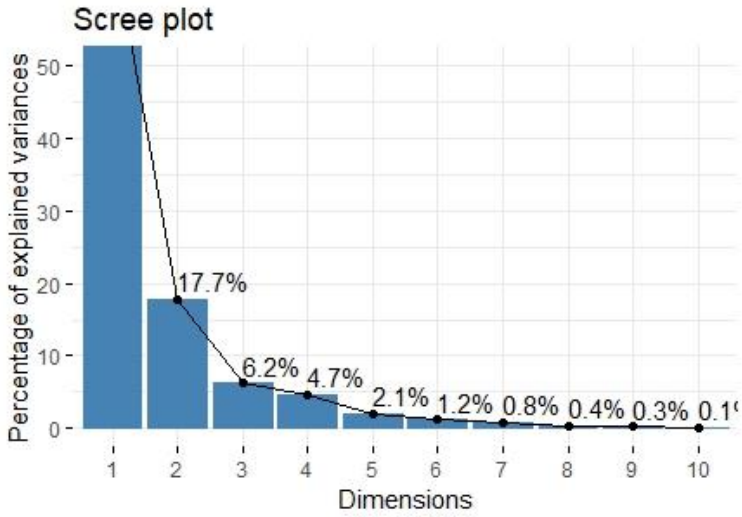

Figure(B) 1 - Eigenvalues (top) and scree plot (down) for the dataset of features extracted from PiB SUVr PET images of the group TOT using CER as reference region.

$contrib

	Dim.1	Dim.2	Dim.3	Dim.4	Dim.5	Dim.6	Dim.7	Dim.8
PC	11.7544648	2.7989832	2.9802125	0.595025287	2.1700349	21.34155060	26.083249	8.01551093
OC	10.9104271	5.0050720	0.7443246	0.003069357	1.9251737	65.55707285	6.737664	2.06122858
MTC	3.2444725	18.1231309	26.1665701	40.353713742	8.8493982	0.17114963	1.260855	0.05353696
PI	12.1121420	3.0636893	1.7337196	0.376166154	6.3094385	1.66607799	14.681299	5.91309296
PS	11.2964485	5.7732883	2.7813522	0.027481019	4.1061002	8.05046263	6.835480	1.24119969
Acing	12.1200525	2.3229749	0.0987194	0.287407400	15.3155813	0.23798517	9.442089	55.31307717
C	3.1903087	19.7856822	12.6414128	55.037319862	1.6017897	1.41411528	4.627931	0.87943287
Pcing	0.1292565	32.3575003	46.8406709	0.058765065	15.2917528	0.21838686	4.255840	0.06252999
P	12.6478127	1.1125747	1.8783949	1.501367575	0.6136285	1.16170114	17.507157	1.14964091
Pmen	9.1877572	9.5349310	3.3153088	1.749217683	43.4618586	0.16386627	1.862705	24.17443956
B	13.4068576	0.1221732	0.8193144	0.010466855	0.3552438	0.01763157	6.705731	1.13631038

	Dim.9	Dim.10	Dim.11
PC	6.25965672	0.06247561	17.93883680
OC	2.45230285	0.86524576	3.73841900
MTC	1.05803528	0.05587574	0.66326201
PI	1.87324830	52.14578113	0.12534519
PS	48.06904178	11.80625348	0.01289193
Acing	3.90943711	0.23054086	0.72213503
C	0.01805795	0.59260453	0.21134505
Pcing	0.40207747	0.31663044	0.06658991
P	32.37850139	27.34718906	2.70203268
Pmen	0.71095450	5.73889215	0.10006943
B	2.86868664	0.83851123	73.71907295

Figure(B) 2 - Contributions to the principal components of each variable (brain region).

PiB SUVr group TOT (Ref-GM)

	eigenvalue	variance.percent	cumulative.variance.percent
Dim.1	5.29400652	48.1273320	48.12733
Dim.2	2.13482050	19.4074591	67.53479
Dim.3	1.15007933	10.4552666	77.99006
Dim.4	0.87809558	7.9826871	85.97274
Dim.5	0.48622021	4.4201837	90.39293
Dim.6	0.38646766	3.5133424	93.90627
Dim.7	0.30256401	2.7505819	96.65685
Dim.8	0.14209342	1.2917584	97.94861
Dim.9	0.11881210	1.0801100	99.02872
Dim.10	0.07672973	0.6975430	99.72626
Dim.11	0.03011093	0.2737358	100.00000

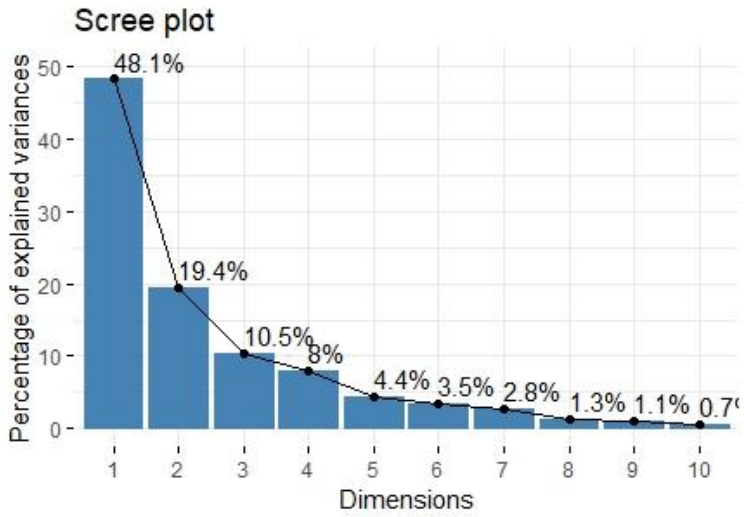

Figure(B) 3 - Eigenvalues (top) and scree plot (down) for the dataset of features extracted from PiB SUVr PET images of the group TOT using GM as reference region.

$contrib

	Dim.1	Dim.2	Dim.3	Dim.4	Dim.5	Dim.6	Dim.7	Dim.8
PC	12.1393584	0.8234830	12.276192	13.92765243	3.48906733	0.2014833	5.5509746	11.73717558
OC	9.0092725	1.7762692	1.009818	34.37917917	22.20305867	9.6018799	6.7097804	0.65530759
MTC	14.8591560	0.3756242	2.342769	4.79166908	0.13339489	14.8111919	14.5428411	16.02467411
PI	13.8737712	4.4298843	1.274962	0.77892481	16.09471075	0.1990323	1.3380455	19.00863696
PS	15.8298822	0.8179094	2.000638	0.01734743	12.96286724	0.8899822	1.0932012	0.05343494
Acing	0.7349194	27.5381934	2.319576	26.61127239	9.16806102	8.7911908	0.8920057	17.65935612
C	6.4849918	14.4593790	13.560340	0.32418996	3.35588233	8.1197374	42.2694547	5.27965271
Pcing	11.4387225	1.6696905	3.566639	10.95038619	30.93986894	7.8485190	0.6650610	0.04480331
P	6.5823343	5.2304437	29.047550	0.85129531	1.45684094	45.6302715	0.9156288	0.62007586
Pmen	6.8920118	17.4276595	13.286684	0.13535095	0.18127414	3.3658960	11.4084133	28.49800543
B	2.1555799	25.4514638	19.314833	7.23273228	0.01497374	0.5408157	14.6145936	0.41887739

	Dim.9	Dim.10	Dim.11
PC	12.4489562	4.3297008	23.0759564
OC	0.9458953	0.1807184	13.5288210
MTC	0.4239311	3.4525476	28.2422011
PI	18.2599235	21.9231620	2.8189466
PS	1.7141165	64.3458796	0.2747416
Acing	4.4385652	1.4576618	0.3891983
C	3.7230616	2.0517365	0.3715737
Pcing	32.3172556	0.4406619	0.1183926
P	9.2432718	0.2889936	0.1332942
Pmen	15.6602322	1.3667672	1.7777059
B	0.8247911	0.1621707	29.2691685

Figure(B) 4 - Contributions to the principal components of each variable (brain region).

PiB SUVr group TOT (Ref-WM)

	eigenvalue	variance.percent	cumulative.variance.percent
Dim.1	5.90468514	53.67895583	53.67896
Dim.2	2.24569770	20.41543360	74.09439
Dim.3	0.88805450	8.07322270	82.16761
Dim.4	0.78848707	7.16806423	89.33568
Dim.5	0.56058795	5.09625411	94.43193
Dim.6	0.36660789	3.33279897	97.76473
Dim.7	0.10237508	0.93068253	98.69541
Dim.8	0.07036391	0.63967194	99.33508
Dim.9	0.03749332	0.34084834	99.67593
Dim.10	0.02509858	0.22816891	99.90410
Dim.11	0.01054887	0.09589884	100.00000

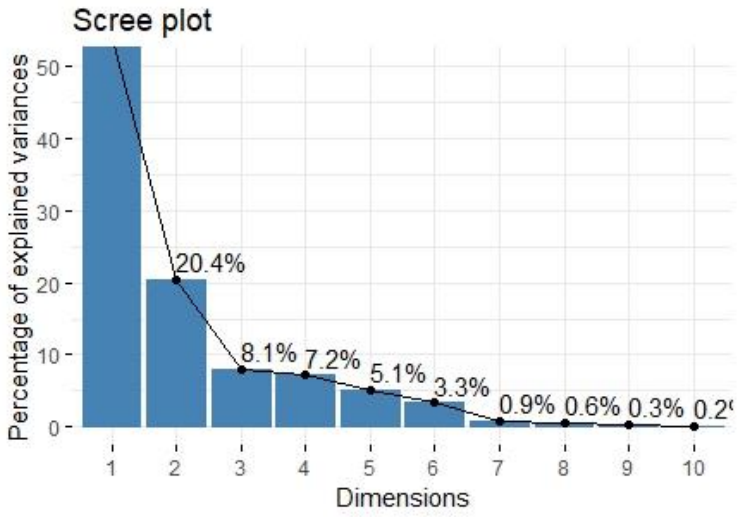

Figure(B) 5 - Eigenvalues (top) and scree plot (down) for the dataset of features extracted from PiB SUVr PET images of the group TOT using WM as reference region.

$contrib

	Dim.1	Dim.2	Dim.3	Dim.4	Dim.5	Dim.6	Dim.7	Dim.8
PC	14.8200292	0.58909916	2.00171208	2.8287507	3.01220908	5.2432575	11.9002602	23.2382012
OC	1.6141467	5.36066774	72.22700004	15.2985576	3.57922642	0.2203954	1.0178395	0.4203413
MTC	0.2576349	27.01523495	0.89321031	0.2550187	64.37040408	0.7465030	2.2133477	2.6369260
PI	15.5590915	0.59441401	0.98124394	0.9765501	0.32142648	6.9689970	5.6017015	4.6814201
PS	14.9125473	2.09503898	0.57219403	2.0616124	0.08764687	6.6378474	2.2129033	0.1950057
Acing	12.9390352	4.50759133	0.06196094	1.3907230	0.36075266	17.7336965	42.4751838	15.4165434
C	0.4506095	20.09843633	2.46897092	48.7289837	18.05256116	1.9106265	7.1717914	0.1499915
Pcing	0.1212474	25.40996652	15.57497351	17.7346522	7.23355604	26.5020412	5.4398121	0.2917865
P	15.3615272	0.46744850	0.09822648	4.1678667	0.05409081	1.6396080	10.9960875	23.9335015
Pmen	7.7401224	13.83963444	4.78673971	6.0972476	0.81124305	29.5340180	10.2581952	25.4781795
B	16.2240087	0.02246803	0.33376803	0.4600374	2.11688334	2.8630096	0.7128779	3.5581033

	Dim.9	Dim.10	Dim.11
PC	10.231697161	2.600138e+00	23.534645720
OC	0.092629430	3.065255e-06	0.169192797
MTC	0.991879082	1.091080e-01	0.510733301
PI	1.477949537	5.470656e+01	8.130643450
PS	48.456871226	2.252330e+01	0.245034769
Acing	4.872683879	1.946979e-01	0.047131414
C	0.005163487	9.560393e-01	0.006826156
Pcing	1.250103685	4.216009e-01	0.020259854
P	28.097443235	1.490700e+01	0.277203959
Pmen	0.301168117	7.098416e-01	0.443610313
B	4.222411162	2.871714e+00	66.614718267

Figure(B) 6 - Contributions to the principal components of each variable (brain region).

PiB SUVr group 4070 (Ref-CER)

	eigenvalue	variance.percent	cumulative.variance.percent
Dim.1	9.038142641	82.16493310	82.16493
Dim.2	1.140242612	10.36584193	92.53078
Dim.3	0.336508990	3.05917264	95.58995
Dim.4	0.164018284	1.49107531	97.08102
Dim.5	0.143431945	1.30392677	98.38495
Dim.6	0.062313282	0.56648438	98.95143
Dim.7	0.055974902	0.50886275	99.46030
Dim.8	0.022501258	0.20455689	99.66485
Dim.9	0.021519422	0.19563111	99.86048
Dim.10	0.013310268	0.12100244	99.98149
Dim.11	0.002036394	0.01851267	100.00000

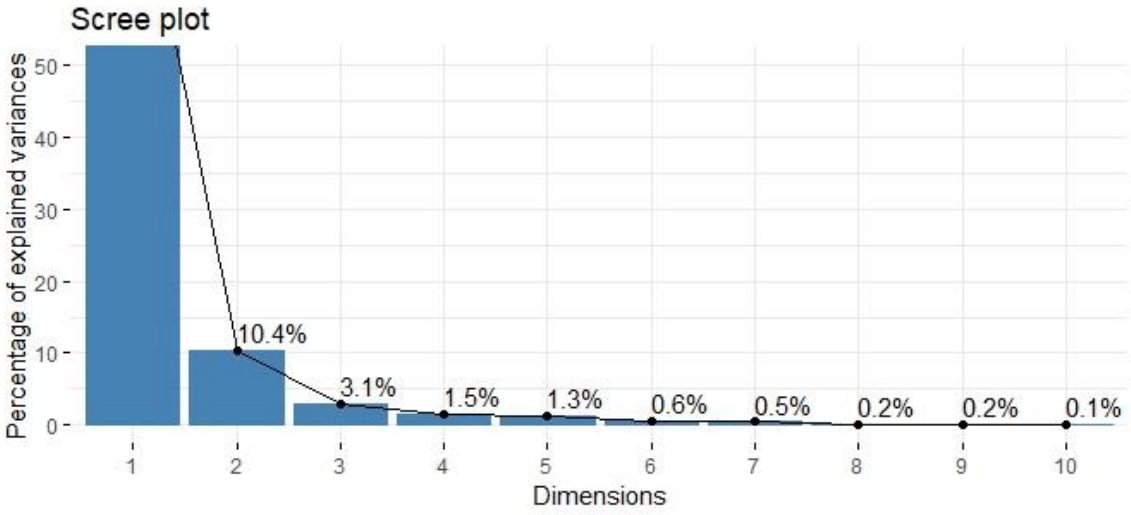

Figure(B) 7 - Eigenvalues (top) and scree plot (down) for the dataset of features extracted from PiB SUVr PET images of the group 4070 using cerebellum as reference region.

$contrib

	Dim.1	Dim.2	Dim.3	Dim.4	Dim.5	Dim.6
PC	10.200606	2.13469504	4.295098e+00	13.0354384	1.40567760	1.6275439
OC	8.825365	11.27118317	2.199492e-01	0.1983949	34.17282285	35.1840417
MTC	7.100912	19.57981651	2.151897e+01	12.7432639	23.71655106	11.2554411
PI	10.146814	5.04449849	9.540871e-01	0.9070930	0.01120568	2.2980341
PS	10.161454	3.94329853	5.146440e-02	6.6560879	0.44014469	14.9219756
Acing	10.279052	0.06354351	3.774332e+00	13.5068017	15.19386971	0.7935543
C	4.053976	40.79652435	4.653455e+01	4.7807034	2.16460989	0.3912546
Pcing	8.995206	5.34519802	1.346412e+01	34.8032303	3.79430232	0.1314651
P	10.051494	5.23161125	2.491066e-05	7.7069740	1.40968847	2.4252481
Pmen	9.310271	5.87130434	8.804609e+00	3.0929751	17.01206348	30.8742532
B	10.874850	0.71832678	3.827952e-01	2.5690375	0.67906426	0.0971882

	Dim.7	Dim.8	Dim.9	Dim.10	Dim.11
PC	7.477436	8.45309001	30.145204527	1.634666e+01	4.878546976
OC	2.238664	0.35948704	0.801220960	1.632234e+00	5.096637177
MTC	0.136395	0.13835069	1.829527458	5.787768e-01	1.401997006
PI	4.345544	71.03645315	2.598820909	1.956703e+00	0.700746741
PS	12.925990	10.31647129	8.024029532	3.249721e+01	0.061876644
Acing	9.758178	1.01754738	21.663497322	2.002372e+01	3.925902114
C	1.082138	0.09612220	0.001101478	3.668838e-02	0.062329138
Pcing	31.731086	0.23399567	1.497565107	7.856842e-07	0.003830472
P	6.298282	8.19929981	31.346758669	2.689285e+01	0.437764958
Pmen	22.802379	0.13483015	2.043382712	1.525442e-02	0.038677690
B	1.203907	0.01435261	0.048891327	1.989606e-02	83.391691085

Figure(B) 8 - Contributions to the principal components of each variable (brain region).

PiB SUVr group 4070 (Ref-WM)

	eigenvalue	variance.percent	cumulative.variance.percent
Dim.1	6.76481426	61.4983115	61.49831
Dim.2	1.92437429	17.4943117	78.99262
Dim.3	0.90055342	8.1868493	87.17947
Dim.4	0.52390991	4.7628173	91.94229
Dim.5	0.35918601	3.2653274	95.20762
Dim.6	0.23010602	2.0918729	97.29949
Dim.7	0.11932919	1.0848108	98.38430
Dim.8	0.08925140	0.8113763	99.19568
Dim.9	0.03609662	0.3281511	99.52383
Dim.10	0.02764507	0.2513188	99.77515
Dim.11	0.02473381	0.2248528	100.00000

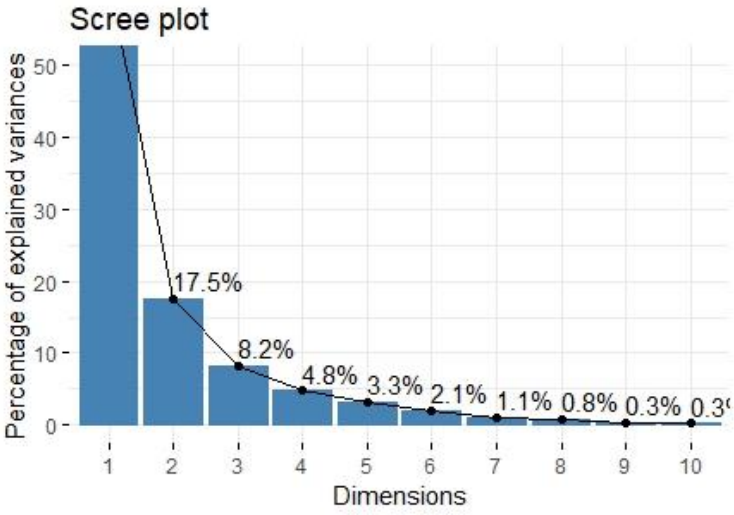

Figure(B) 9 - Eigenvalues (top) and scree plot (down) for the dataset of features extracted from PiB SUVr PET images of the group 4070 using WM as reference region.

$contrib

	Dim.1	Dim.2	Dim.3	Dim.4	Dim.5	Dim.6
PC	12.917199	1.70348392	1.5731567	0.0636592	2.8116361	16.7964929
OC	9.586955	8.41601543	0.8941947	16.5742765	11.6888179	4.5965224
MTC	3.101504	24.08597956	7.2411789	44.8022608	1.0219283	5.2805107
PI	12.200600	6.38668439	0.7087632	1.4248916	1.3299193	0.3672178
PS	12.906550	3.28380098	2.2880327	0.2007010	1.4341653	0.8673131
Acing	12.667910	0.09576292	2.5536239	8.8089151	2.1008059	14.3763523
C	2.776408	23.51237491	13.1478546	24.7466685	24.3885228	9.7535400
PCing	9.661917	7.49650588	2.6599699	1.5321627	16.0606275	35.7901893
P	12.782620	4.29297909	1.3383425	0.1964624	0.7374284	2.3979395
Pmen	10.239941	6.64293368	0.6032983	1.4814919	29.7127077	4.3206937
B	1.158397	14.08347923	66.9915846	0.1685103	8.7134409	5.4532283

	Dim.7	Dim.8	Dim.9	Dim.10	Dim.11
PC	1.321947e+01	0.99993065	1.217652376	34.1211822	1.457614e+01
OC	2.936424e+00	42.27031147	0.137703916	2.0150400	8.837387e-01
MTC	1.193822e-07	11.25095179	0.002507211	3.1519218	6.125657e-02
PI	1.783970e-01	9.54733759	56.660376265	11.0926052	1.032081e-01
PS	3.672605e+00	16.68318091	5.206826099	18.0625791	3.539425e+01
Acing	1.521745e+01	1.26483978	7.683675706	22.2317730	1.299889e+01
C	1.235034e+00	0.02036016	0.165304091	0.1145173	1.394163e-01
PCing	2.413715e+01	0.83722075	0.588741040	1.2345778	9.358491e-04
P	4.498472e+00	7.38993323	25.429663272	5.1606149	3.577554e+01
Pmen	3.485950e+01	7.13588309	2.863143736	2.1297831	1.061913e-02
B	4.548997e-02	2.60005058	0.044406289	0.6854055	5.600739e-02

Figure(B) 10- Contributions to the principal components of each variable (brain region).

PK BP group 4060 (Ref-CER)

	eigenvalue	variance.percent	cumulative.variance.percent
Dim.1	12.360397663	49.441590652	49.44159
Dim.2	5.191113682	20.764454728	70.20605
Dim.3	2.117135818	8.468543272	78.67459
Dim.4	1.423471216	5.693884866	84.36847
Dim.5	0.944844708	3.779378834	88.14785
Dim.6	0.605110344	2.420441376	90.56829
Dim.7	0.526678002	2.106712007	92.67501
Dim.8	0.336971097	1.347884389	94.02289
Dim.9	0.318280880	1.273123520	95.29601
Dim.10	0.237948459	0.951793837	96.24781
Dim.11	0.177120911	0.708483643	96.95629
Dim.12	0.163630839	0.654523355	97.61081
Dim.13	0.153004262	0.612017048	98.22283
Dim.14	0.118944642	0.475778569	98.69861
Dim.15	0.090470351	0.361881403	99.06049
Dim.16	0.069515231	0.278060926	99.33855
Dim.17	0.054873365	0.219493461	99.55805
Dim.18	0.032582842	0.130331369	99.68838
Dim.19	0.027465223	0.109860893	99.79824
Dim.20	0.018428990	0.073715962	99.87195
Dim.21	0.012192051	0.048768203	99.92072
Dim.22	0.008377269	0.033509078	99.95423
Dim.23	0.007263309	0.029053238	99.98328
Dim.24	0.003140978	0.012563914	99.99585
Dim.25	0.001037865	0.004151458	100.00000

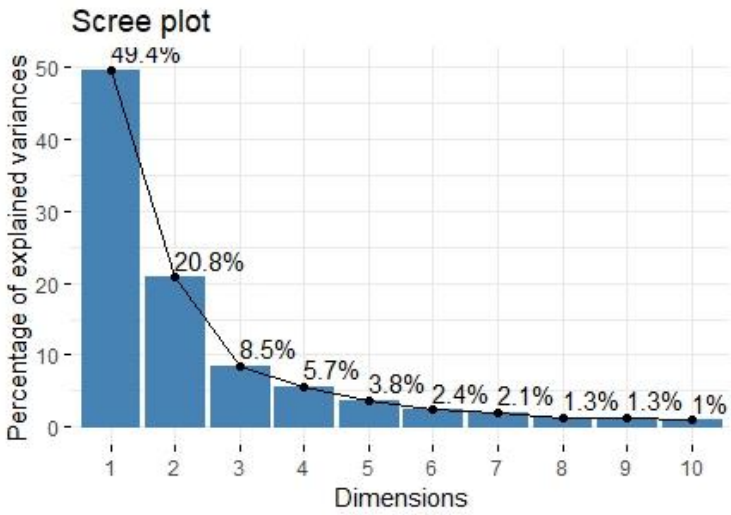

Figure(B) 11 - Eigenvalues (top) and scree plot (down) for the dataset of features extracted from PK BP PET images of the group 4060 using CER as reference region.

$contrib

	Dim.1	Dim.2	Dim.3	Dim.4	Dim.5	Dim.6
Frontal Lobe	6.7969255	1.002629e-01	0.320593076	5.0590784	6.02280552	0.072219994
Temporal Lobe	5.7586511	4.114488e+00	0.537954322	0.7802665	3.03285625	0.699262088
Frontal-Temporal Space	1.4688509	6.773216e-01	25.051892626	0.2099237	0.85691543	28.924265367
Superior frontal gyrus	5.1396995	1.782150e+00	0.178175501	7.1920036	9.16360895	0.069295896
Middle frontal gyrus	5.0120886	2.374736e+00	2.841246518	3.0555879	11.39396911	1.753617564
Precentral gyrus	5.9473187	1.566517e+00	1.238008321	1.0040478	0.45334200	2.052286102
Inferior frontal gyrus	5.0414885	2.253908e-01	11.759253209	0.1056940	0.07018254	0.075876142
Superior temporal gyrus	3.9120574	1.225364e+00	13.489724520	0.2386046	10.04426482	0.037958029
Middle temporal gyrus	5.7545878	3.010154e-01	2.584315847	6.6035807	5.85195847	3.466451737
Inferior temporal gyrus	3.5880780	5.344209e+00	0.145374255	7.5236829	0.02427944	0.115111251
Amygdala	1.2950613	6.557096e+00	0.189900612	7.5959531	6.07612398	25.480022206
Hippocampus	2.7213272	7.196972e+00	4.258615196	2.2699782	2.73706555	0.009384234
Inferior parietal lobule	5.7515676	1.343834e+00	3.951077958	1.3099234	1.97536073	0.085410375
Superior parietal lobule	2.3667781	6.719978e+00	9.933903071	0.5438178	0.42856015	10.900663694
PC	4.8104549	3.565047e+00	3.892449413	2.7332457	6.28980711	1.616314078
OC	4.2257024	3.284204e+00	0.465103587	6.7714823	0.69376724	6.853032660
MTC	2.7878074	1.015953e+01	0.776062486	1.0102705	0.64385017	0.000540922
PI	4.2383879	6.745140e+00	2.289994657	0.8362539	2.37628524	0.284969044
PS	2.4085509	1.061391e+01	0.007095414	2.8027996	1.60307912	0.081569559
Acing	2.3887552	7.439251e+00	0.082513993	0.4438287	3.25711883	0.237172705
C	0.6118444	6.054178e+00	0.022133371	25.2212846	14.16651228	0.014166626
Pcing	3.2792735	5.640111e-01	5.377865081	16.1531222	12.21592980	1.715074438
P	4.0910682	3.953018e+00	8.312251982	0.1009351	0.37520034	10.429622160
Pmen	2.7307133	8.091579e+00	2.185273493	0.1880691	0.22649869	4.649290405
B	7.8729617	8.001056e-04	0.109221494	0.2465658	0.02065823	0.376422723

Figure(B) 12 - Contributions to the first six principal components of each variable (brain region).

Mixture of features extracted from SUVr PiB group 4070, BP and DVR PK group 4060 PET images

	eigenvalue	variance.percent	cumulative.variance.percent
Dim.1	1.225240e+01	6.126199e+01	61.26199
Dim.2	3.787593e+00	1.893796e+01	80.19996
Dim.3	1.335024e+00	6.675120e+00	86.87508
Dim.4	7.716983e-01	3.858492e+00	90.73357
Dim.5	6.173892e-01	3.086946e+00	93.82052
Dim.6	4.557530e-01	2.278765e+00	96.09928
Dim.7	3.051537e-01	1.525768e+00	97.62505
Dim.8	1.785637e-01	8.928187e-01	98.51787
Dim.9	9.412500e-02	4.706250e-01	98.98849
Dim.10	8.640052e-02	4.320026e-01	99.42050
Dim.11	5.582563e-02	2.791281e-01	99.69962
Dim.12	3.224812e-02	1.612406e-01	99.86086
Dim.13	1.560040e-02	7.800202e-02	99.93887
Dim.14	6.884369e-03	3.442185e-02	99.97329
Dim.15	4.154191e-03	2.077096e-02	99.99406
Dim.16	4.662991e-04	2.331495e-03	99.99639
Dim.17	3.219822e-04	1.609911e-03	99.99800
Dim.18	1.977546e-04	9.887731e-04	99.99899
Dim.19	1.481626e-04	7.408130e-04	99.99973
Dim.20	5.398663e-05	2.699331e-04	100.00000

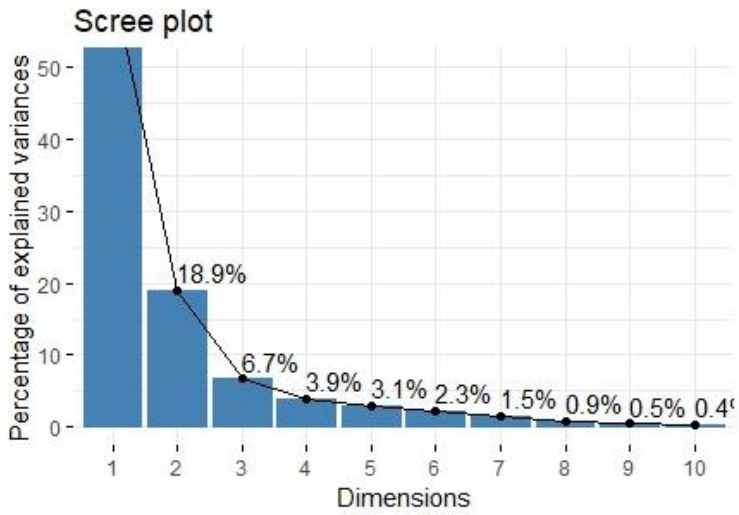

Figure(B) 13- Eigenvalues (top) and scree plot (down) for the dataset of a mixture of features extracted from PiB SUVr PET images of the group 4070 and PK BP and PK DVR PET images of group 4060.

$contrib

	Dim.1	Dim.2	Dim.3	Dim.4	Dim.5	Dim.6
PC_pibcer	6.829406	2.589983	0.58959619	1.789244229	2.069179788	1.61631486
PI_pibcer	7.018320	1.857339	0.13826738	0.325015071	1.355228105	8.00113841
PS_pibcer	7.046949	1.798434	0.25833474	0.128573525	0.390798238	8.59079979
Acing_pibcer	6.323395	2.952630	0.37395451	3.477037612	7.618943504	0.54464857
P_pibcer	7.198371	1.707255	0.66097919	0.002208558	0.130981101	5.55291933
B_pibcer	6.787061	2.518081	0.34515010	2.136780368	3.273275061	5.40145017
PC_pibwm	5.818722	3.583866	1.63741769	0.176679705	3.844341078	14.27758189
PI_pibwm	6.706461	2.519461	0.12930214	1.880306881	3.559816376	0.75725270
PS_pibwm	6.264858	2.305007	0.34997974	6.794661608	7.220616428	0.82840731
Acing_pibwm	5.280725	4.590666	0.99217372	0.066939040	0.002002035	20.61277077
P_pibwm	6.397127	2.192599	1.12580300	4.279216879	6.831539946	1.48643723
IPL_bpcer	3.751251	6.639323	4.83821851	23.472835904	3.190748917	1.13973841
SPL_bpcer	3.788210	9.868251	2.82560041	0.988007298	3.346123367	4.53301270
P_bpcer	4.012424	11.120497	0.05079115	1.183381512	5.615024248	0.32896718
IPL_bpsvca4	3.606855	4.646526	1.07750069	13.417707256	17.971583020	19.99847555
SPL_bpsvca4	2.930470	7.154969	20.55262157	2.533917731	2.867300529	0.32031833
P_bpsvca4	3.150046	7.769422	12.88641545	8.386444004	3.166777995	3.12130172
SFG_lmcer	1.974800	7.524641	32.32173902	1.429985653	0.344618283	2.49678989
P_lmcer	3.321209	11.459618	0.28194324	0.106245609	9.089997814	0.03610228
SFG_lmsvca4	1.793341	5.201434	18.56421156	27.424811555	18.111104168	0.35557291

Figure(B) 14- Contributions to the first six principal components of each variable (brain region).